

INVESTIGATIONS OF HEXAGONAL BORON NITRIDE: BULK CRYSTALS AND  
ATOMICALLY-THIN TWO DIMENSIONAL LAYERS

by

JARED L. SPERBER

B.S., Colorado State University - Pueblo, 2012

A THESIS

submitted in partial fulfillment of the requirements for the degree

MASTER OF SCIENCE

Department of Chemical Engineering  
College of Engineering

KANSAS STATE UNIVERSITY  
Manhattan, Kansas

2016

Approved by:

Major Professor  
Dr. J.H. Edgar

# **Copyright**

JARED L. SPERBER

2016

## Abstract

Hexagonal boron nitride has been used as an inert, refractory material with excellent resistance to thermal decomposition and oxidation for more than fifty years. In the past few years, hBN has been targeted for potential electrical and optical devices such as neutron detectors, ultraviolet light emitters, deep ultraviolet light detectors, and substrates for graphene and other atomically-thin two-dimensional materials. All of these potential applications benefit from high quality, single crystals, with thicknesses varying from nanometers to microns. This research was undertaken to investigate four aspects of hBN crystal growth and recovery. (1) In an effort to optimize hBN crystal growth from a nickel-chromium flux, a series of stepped cooling experiments were undertaken. The temperature profile was stepped in a way as to promote growth in both the  $a$  and  $c$  directions, at their optimal growth conditions. Crystals were found to be typically 100-500  $\mu\text{m}$  across and thickness of approximately 20-30  $\mu\text{m}$  with a pyramid-like crystal habit. (2) A method for the removal of hBN crystals prior to freezing of the metal flux was demonstrated using a specialized hot pressed boron nitride crucible capable of removing hBN crystals from the flux *in situ*. (3) Growth of isotopically pure hBN crystals was undertaken. By modifying the crucible material for solution growth, enrichment of hBN crystals over 90% was accomplished. (4) Exfoliation of hBN has many potential applications, specifically as graphene-hBN heterostructures where layers approaching thicknesses of single atoms are most effective surface to interact with graphene as an electronic device. Several methods were tested toward exfoliating a single crystal resulting in few-layered hexagonal boron nitride nanosheets. As a result of these investigations a greater understanding of hBN bulk growth, its isotopic enrichment, its recovery, and its exfoliation was obtained.

## Table of Contents

|  |     |
|--|-----|
| List of Figures .....                    | vii |
| List of Tables .....                     | ix  |
| Acknowledgements .....                   | x   |
| Dedication .....                         | xii |
| Chapter 1 - Introduction.....            | 1   |
| Chapter 2 - Literature Review.....       | 3   |
| Applications of hBN .....                | 6   |
| Lubrication .....                        | 6   |
| Electronics.....                         | 6   |
| Optics .....                             | 9   |
| Optimization of hBN Crystal Growth.....  | 10  |
| Melt Growth.....                         | 12  |
| CVD Growth.....                          | 13  |
| Solution Growth.....                     | 14  |
| Crystal Extraction .....                 | 23  |
| Isotope Enrichment of hBN Crystals ..... | 26  |
| Two Dimensional hBN .....                | 30  |
| Thermal Applications.....                | 34  |
| Magnetic Applications .....              | 35  |
| Wetting Applications .....               | 35  |
| Catalytic Properties.....                | 36  |
| Environmental Applications .....         | 36  |
| Electronic/Optical Applications.....     | 37  |
| Synthesis of Two Dimensional BN.....     | 38  |
| Mechanical Exfoliation.....              | 38  |
| Chemical Vapor Deposition.....           | 40  |
| Solid State Reactions .....              | 42  |
| Substitution Reaction .....              | 42  |
| High Energy Electron Irradiation.....    | 43  |

|   |    |
|---|----|
| Unzipping Boron Nitride Nanotubes .....   | 43 |
| Chemical Exfoliation .....  | 43 |
| Chapter 3 - Experiments and Analytical Tools.....   | 49 |
| Apparatuses .....   | 49 |
| Experiments .....   | 50 |
| Hexagonal Boron Nitride Crystal Growth Method.....  | 50 |
| Extraction of Hexagonal Boron Nitride Crystals from the Molten Metal Flux .....             | 51 |
| Boron Isotope Enrichment .....  | 53 |
| Exfoliation of Hexagonal Boron Nitride.....   | 54 |
| Adapted Hummers' Method .....   | 54 |
| Adapted Hummers' Method Acid Mixture.....   | 55 |
| Exfoliation by Methanesulfonic Acid (MSA).....  | 55 |
| Intercalation of Water Molecules.....   | 56 |
| Functionalization by ODA .....  | 56 |
| Analytical Tools .....  | 58 |
| Scanning Electron Microscopy (SEM) and Energy –Dispersive X-ray Spectroscopy<br>(EDS) ..... | 58 |
| X-ray Diffraction (XRD) .....   | 59 |
| Raman Microscopy .....  | 60 |
| Fourier transform infrared spectroscopy (FTIR) .....  | 61 |
| Chapter 4 - Results and Discussion .....  | 63 |
| Hexagonal Boron Nitride Crystal Growth Method.....  | 63 |
| Extraction of Hexagonal Boron Nitride from the Molten Metal Flux .....                      | 65 |
| Boron Isotope Enrichment .....  | 68 |
| Hexagonal Boron Nitride Exfoliation.....  | 71 |
| Adapted Hummers' Method .....   | 72 |
| Adapted Hummers' Method Acid Mixture.....   | 73 |
| Exfoliation by Methanesulfonic Acid (MSA).....  | 73 |
| Intercalation of Water Molecules.....   | 76 |
| Functionalization by Octedyclamine (ODA) .....  | 76 |
| Chapter 5 - Conclusion and Future Work .....  | 83 |

References..... 87

## List of Figures

|  |    |
|--|----|
| Figure 2-1 Crystal structure of hexagonal boron nitride.....   | 4  |
| Figure 2-2 Crystal structure of cubic boron nitride. ....  | 4  |
| Figure 2-3 Crystal structure of wurtzite boron nitride. ....   | 5  |
| Figure 2-4 BN phase diagram. (From Bundy and Wentorf [75]) .....   | 11 |
| Figure 2-5 Nucleation process for crystal growth.....  | 15 |
| Figure 2-6 Comparison of hBN grown at cooling rates of (a.) 10 °C/hr, (b.) 4 °C/hr, and (c.) 2 °C/hr after having soaked at 1500 °C for 24 hours. (From Hoffman [22]) .....  | 21 |
| Figure 2-7 X-ray diffraction spectra for hBN crystals growth with soak temperature of (a) 1550°C and (b) 1700°C. (From Hoffman [22]) .....   | 21 |
| Figure 2-8 Width (a.) and thickness (b.) of crystal grown at 1500 °C. Width (c.) and thickness (d.) of crystal grown at 1700 °C. (From Hoffman [22]) .....   | 22 |
| Figure 2-9 Diagram of (a) differences in crystal habit for hBN grown at low and high temperatures and (b) theoretical atomic arrangement for the high temperature, triangular hBN habit. (Adapted with permission from K.K. Kim, A. Hsu, X. Jia, S.M. Kim, Y. Shi, M. Hofmann, D. Nezich, J.F. Rodriguez-Nieva, M. Dresselhaus, T. Palacios, J. Kong, Nano Lett. 12 (2012) 161. Copyright 2012 American Chemical Society.) ..... | 23 |
| Figure 2-10 Structural models of (a and b) hBN sheets and (c and d) graphite sheets displaying the difference in their stacking sequence. Cross-sectional and plane view of (e) the pristine and (f) relaxed models of the bilayered h-BN edge. (From Pakdel [129]) .....  | 32 |
| Figure 2-11 A model illustrating the nucleation and two-stage growth of the BN nanosheets on the Si/SiO <sub>2</sub> substrate. (From Pakdel [137]).....   | 41 |
| Figure 3-1 Photo of the interior of the tungsten resistive element furnace with important features labeled. ....   | 49 |
| Figure 3-2 Illustration of chemical exfoliation apparatus.....   | 50 |
| Figure 3-3 Design of “nested” HPBN crucibles for crystal extraction. a) crucible 1 (top crucible). b) crucible 2 (bottom crucible). c) combined crucibles. ....  | 53 |
| Figure 3-4 Schematic of SEM.....   | 59 |
| Figure 4-1 Sample 1 from stepped temperature growth experiments. Crystals grown vertically, merging into each other to create pyramid like morphologies.....   | 64 |

|  |    |
|--|----|
| Figure 4-2 (a) Crucibles 1 (Top) and 2 (Bottom) after typical crystal extraction. (b) Magnification of crystal “halo”. (c) View of “halo” crystals and metal still attached to the bottom of crucible 1. ....                    | 65 |
| Figure 4-3 Close up of crystal “halo” with many different crystal geometries and orientations..  | 66 |
| Figure 4-4 Cracked crystals embedded in metal flux. ....   | 67 |
| Figure 4-5 Typical crystals grown from Ni-Cr solution method with enriched <sup>10</sup> B.....  | 68 |
| Figure 4-6 Crucibles before and after testing for enriched growth compatibility. (a) and (b), before and after alumina. (c) and (d), before and after yttria-stabilized zirconia. (e) and (f), before and after yttria.....      | 69 |
| Figure 4-7 Calibration curve relating boron enrichment to Raman shift in hBN crystals. (From Hoffman [117]) .....  | 70 |
| Figure 4-8 Raman Spectra of natural abundance boron in hBN crystals compared to blue shift of <sup>10</sup> B enriched hBN crystals.....   | 71 |
| Figure 4-9 Scheme for the exfoliation of hBN powder by modified Hummers’ method. (From Du [163]).....  | 72 |
| Figure 4-10 High magnification scanning electron microscope images of (a) exfoliation by adapted Hummers’ method, (b) pristine hBN, (c) exfoliation by acid adapted Hummers’ method, and (d) exfoliation by MSA protonation..... | 74 |
| Figure 4-11 High magnification SEM image of exfoliated hBN by MSA method.....  | 75 |
| Figure 4-12 High magnification scanning electron microscope images of (a) exfoliation by water freezing method, and (b) exfoliation by ODA functionalization.....  | 77 |
| Figure 4-13 FT-IR spectra of (a) pristine hBN powder and (b) ODA functionalized hBN powder. ....   | 79 |
| Figure 4-14 X-ray diffraction pattern comparison of ODA functionalized hBN powder (red) and pristine hBN powder (blue) (002) peaks.....  | 80 |
| Figure 4-15 ODA functionalized hBN that did not fully exfoliate.....   | 80 |
| Figure 4-16 X-ray diffraction pattern pure ODA powder.....   | 81 |
| Figure 4-17 Raman shift of exfoliated hBN powder (blue) from bulk hBN Raman signature (orange).....  | 82 |



## List of Tables

|  |    |
|--|----|
| Table 2-1 Selected properties of BN and carbon analogs at room temperature. ....     | 5  |
| Table 3-1 Furnace parameters for stepped temperature crystal growth.....             | 52 |
| Table 3-2 List the materials used in each experiment, their source, and purity. .... | 57 |

## Acknowledgements

I would like to first of all thank my committee members, Dr. James Edgar, Dr. John Schlup, and Dr. Placidus Amama for their support and insight both in this project and in the classroom. Dr. Edgar, thank you for your unwavering patience and optimistic attitude, for your tutelage in the lab and in the classroom, and for investing in me and my education. Special thanks to Dr. Schlup for his insight and advice concerning IR spectroscopy. A special thanks to Dr. Amama for the training and use of his Raman instrument as well as the use of his drying ovens. It has been a pleasure working with you all.

My research group, Song Liu, Clint Frye, Balabalaji Padavala, and Tim Hoffman, thank you all for your assistance, be it with equipment, advice, school work, or just good conversation. Special thanks to Tim Hoffman who also works with hBN for his collaboration and as a sounding board for ideas. I would like to thank Dr. Sean Tomlinson for taking a special interest in bringing me up to speed as a lab member and graduate student. To all my fellow graduate students in ChE, thank you for enhancing my experience at Kansas State University through learning about different cultures and people and for your collaboration, whether just borrowing a tool or being a sounding board for new ideas.

I would also like to recognize the entire department of chemical engineering, specifically the faculty who have been excellent instructors, always willing to help, and make the department very communal in their willingness to share resources and information. Thank you to Danita, Karen, and Cynthia who make the department run smoothly, eliminating many hurdles to conducting research that could be taken for granted. Finally, thanks to Dave Threewit for all of his help and work keeping the labs running.

Last but certainly not least, I would like to thank my family for their support and love, especially my Mom and Dad for always supporting their children and the pursuit of their passions. Thanks also to my soon to be wife, Christi, for her patience and support. I love you all and can't thank you enough.

# **Dedication**

To Christi and my Family

## Chapter 1 - Introduction

The intent of this research was to investigate the highly versatile compound boron nitride, specifically bulk single crystals of the low density crystal structure, hexagonal boron nitride (hBN) which is analogous to the hexagonal carbon structure, graphite. By far, the most common synthesis routes for hBN are chemical vapor deposition (CVD) [1-7] and solution growth [8-16]. A low pressure solution growth method to grow bulk single crystals developed by Edgar *et al.* [17] was optimized for growth in the lateral  $a$  and vertical  $c$  direction. From this information a new route to grow large crystals in both the  $a$  and  $c$  directions is proposed by using a stepped temperature cooling method.

Hexagonal boron nitride is being considered for several electronic and opto-electronic devices such as neutron detectors [18, 19], ultraviolet light emitters [20, 21] and deep ultraviolet light detectors [21]. Many of these applications are predicated on the characteristics of hBN as a III-V semiconductor. Boron is one of the few elements that strongly interacts with thermal neutrons, specifically due to the  $^{10}\text{B}$  isotope, making hBN crystals suitable for use as a solid state neutron detector.  $^{10}\text{B}$  is one of two stable isotopes, the other being  $^{11}\text{B}$ . Control of B enrichment in hBN crystals will improve essential properties which form the basis of the aforementioned applications. Therefore, control of B enrichment was studied.

The solution method presented by Hoffman *et al* [22] provides exceptional, large, single crystal hBN from a nickel and chromium flux. The resulting crystals from this flux can become embedded in the alloy created from the cooled flux. To obtain the largest most pristine crystals possible, crystals must be removed from the flux. Several methods to remove crystals have been broached including thermal release tape [22] and acid mixtures [23]. However, these methods have been found ineffective to a certain extent; they leave the crystals in the flux or cracked [23].

In order to fully realize crystal yields and avoid mechanical damage, an *in situ* method for removing hBN crystals from the metal flux is proposed.

There have been many studies focusing on two dimensional (2-D) layered materials since the discovery of graphene [24]. The attraction of 2-D BN lies in its ability to enhance and create new properties different from its bulk parent by its geometry and quantum effects observed at the nanoscale. There have been many routes taken to synthesize 2-D hBN such as CVD [1-3, 25-27], solid state reactions [28-30], substitution reactions [31], unzipping hBN nanotubes [169], electron irradiation [32, 33], and exfoliation [33-35]. Exfoliation of layered materials can be either mechanical or chemical in nature. Mechanical exfoliation typically involves mechanically peeling layers with tape until the desired number of layers remain. However, due to the nature of interlayer bonds this may result in cracking. A monolayer has not been reported by this route and as such this study was focused on the chemical exfoliation of hBN crystals to mono or few-layers for nano-optic and nano-electric applications.

## Chapter 2 - Literature Review

From the first, boron nitride (BN) has been an intriguing, versatile, and yet exacting material. W.H. Balmain first prepared BN in the 1840's by reacting boric oxide with potassium cyanide [36]. While its potential applications were perceived immediately, industrial production did not follow until nearly 100 years later [37, 38]. The microcrystalline powder form of BN has many uses as a lubricant or coating when chemical inertness at high temperatures is required. Boron nitride's thermal properties make it a good lubricant at both low and high temperatures even in an oxidizing atmosphere. Many mechanical parts can be produced by hot pressing BN. The hot-pressed form of boron nitride (HPBN) is especially useful as a refractory material. Properties such as its high thermal conductivity, high thermal shock resistance, and machining ease make HPBN invaluable in furnaces, reactors, as ceramics for high temperature processes, and as parts in high temperature equipment [38]; these parts can be used up to 3000 °C.

Boron nitride is considered the carbon of compounds, with its own equivalent of all the forms of carbon (C): graphite and hBN, diamond and cubic boron nitride (cBN), longsanite and wurtzite boron nitride (wBN), and graphene and hexagonal boron nitride nanosheets (hBNNS). The two most used forms of BN are its equivalents to graphite, hBN, and diamond, cBN.

Just as carbon has graphite, a layered hexagonal structure, boron nitride also has a layered structure, hBN. Hexagonal boron nitride is a soft, low density modification of BN and is composed of layers of flat six-atom  $sp^2$  hybridized hexagonal rings, (alternating three atoms boron and three atoms nitrogen) with the rings stacked perfectly atop each other in alternating fashion AA'AA' (boron atop nitrogen atop boron, etc.) (Figure 2-1). Both graphite and hBN sheets have a honeycomb lattice structure, however their different electronic properties and phonon band structure are a result of unequal stacking. A commonly encountered form of hBN

is pyrolytic BN (pBN) prepared by chemical vapor deposition (CVD); it adopts the layered hBN structure but is by no means single crystal since it has many grains and reduced long-range order.

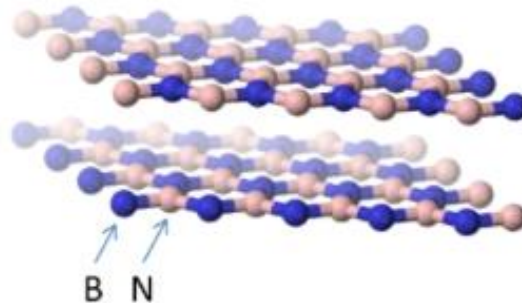


**Figure 2-1 Crystal structure of hexagonal boron nitride.**

The diamond-like (cBN) is produced from the basic hexagonal version, as diamond is from graphite, at extremely high pressures and temperatures. cBN is one of the hard, high density modifications of BN and adopts the zinc blende structure with a stacking sequence ABCABC. In this structure, every atom is bonded to four other atoms of the opposite element (boron to four nitrogens and nitrogen to four borons), giving it a  $sp^3$  hybridization structure (Figure 2-2). Table 2-1 lists some selected properties of hBN, cBN, graphite and diamond.

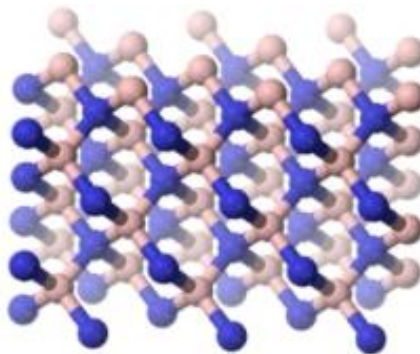


**Figure 2-2 Crystal structure of cubic boron nitride.**

One of the more extraordinary structures of BN is the wurtzite form (wBN), which has the same form as zinc oxide. Although the wurtzite structure is common among other group III-nitride compounds, wBN is a rare and metastable structure for BN. A high density BN



modification, the wurtzite unit cell is hexagonal but possesses  $sp^3$  hybridization bonding among the constituent atoms (Figure 2-3). Technically, wBN is even harder than the cubic form, though like the carbon structure, lonsdaleite, wBN has limited practical applications due to difficulties in synthesizing the material.

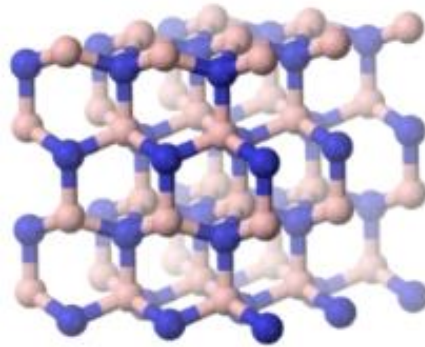


**Figure 2-3 Crystal structure of wurtzite boron nitride.**

**Table 2-1 Selected properties of BN and carbon analogs at room temperature.**

| Property                                       | hBN  | graphite   | cBN                        | diamond                |
|--|--|--|----------------------------|------------------------|
| Crystal structure                              | Hexagonal  | Hexagonal  | Cubic                      | Cubic                  |
| Lattice constant (Å)                           | a=2.504<br>c=6.661                                       | a=2.461<br>c=6.708                                       | 3.615                      | 3.567                  |
| Density (g/cm <sup>3</sup> )                   | 2.34   | 2.2  | 3.45                       | 3.515                  |
| Mohs hardness                                  | 1.5  | 1-2  | 9.5                        | 10                     |
| Band gap (eV)                                  | 5.971 (direct)   | 0 (semimetal)  | 6.4 (indirect)             | 5.4 (indirect)         |
| Electrical conductivity [(Ωcm) <sup>-1</sup> ] | a: <10 <sup>-15</sup><br>c: <10 <sup>-16</sup>           | a: 1.0 x 10 <sup>5</sup><br>c: 2.4 x 10 <sup>4</sup>     | ~10 <sup>-13</sup>         | ~10 <sup>-18</sup>     |
| Thermal conductivity (W/m/K)                   | a: 600<br>c: 30  | a: 250<br>c: 80  | ~400-700                   | ~2000                  |
| Linear thermal expansion (K <sup>-1</sup> )    | a: -2.9 x 10 <sup>-6</sup><br>c: 40.5 x 10 <sup>-6</sup> | a: -1.2 x 10 <sup>-6</sup><br>c: 25.9 x 10 <sup>-6</sup> | 1.2-1.9 x 10 <sup>-6</sup> | 0.8 x 10 <sup>-6</sup> |

## **Applications of hBN**

### **Lubrication**

Bulk hBN has presented many intriguing opportunities for some time due to its low density, electrical insulation, excellent oxidation resistance, high thermal conductivity, excellent inertness, and low friction coefficient. Like graphite, hBN makes a good lubricant, and its limited chemical reactivity and its brilliant white color means it has found its way into cosmetics. Currently, hBN is being used by all major cosmetic producers in foundations, eye shadows, lipsticks, and other skin care products [39]. Besides cosmetics, hBN is incorporated into high temperature ceramics, alloys, resins, plastics, rubbers, and other materials to give them self-lubricating properties; this is due to hBN's unique thermal properties and myriad of useful material properties making it an ideal solid lubricant. Hexagonal boron nitride lubricant is particularly useful in situations where the conductivity or chemical reactivity of graphite would be problematic. For example, hBN can even be an effective lubricant in a vacuum and does not require water or gas molecules trapped between layers, as graphene does. This makes hBN an ideal choice as a lubricant in space [40]. Hexagonal boron nitride has even made a foray into ammunition as bullet lubricant as an alternative to molybdenum disulfide, commonly referred to as "moly coating". This is claimed to increase the gun barrel life [41].

### **Electronics**

Hexagonal boron nitride's thermal stability is clearly essential in its application as a refractory material and industrial lubricant, however hBN's fascinating electronic and optical properties are of interest in this research. Hexagonal boron nitride may enable several electronic and optoelectronic devices including neutron detectors [18, 19], ultraviolet light emitters [21,

42], and deep ultraviolet light detectors [21], and as a substrate for graphene and other two dimensional atomically thin materials, such as MoS<sub>2</sub> [43, 44].

Hexagonal boron nitride can be a B diffusion source for Si, a protective coating to prevent chemical attack by other materials, or a gate insulator for field-effect transistors [45]. With excellent dielectric and thermal properties, hBN is used in electronics as a structural material for seals and microwave-transparent windows [45]. Unlike graphite, hBN is highly resistive, which is advantageous for some applications such as a substrate supporting semiconductor layers. Hexagonal boron nitride has been used as an electrical insulator in the development of van der Waals heterostructures. This is attributed to hBN's near atomic scale flatness, the absence of dangling surface bonds, and low phonon interactions between materials.

The near 2D sheets are likely to have wide applications in electronics where its insulating capability makes them a natural partner for graphene's conductivity. Recently, hBN has been employed as a dielectric in graphene devices [43] such as graphene field-effect transistors, hBN is an excellent gate dielectric and substrate that provides a smooth and flat surface necessary for maximum carrier mobility in graphene sheets [46]. The charge mobility of graphene on hBN is significantly higher than graphene on silica [43]. Graphene devices on standard silicon dioxide (SiO<sub>2</sub>) substrates are highly disordered, exhibiting characteristics that are inferior to those of pure graphene [47-56]. Carrier mobility is limited by scattering from surface charged states and impurities on SiO<sub>2</sub> substrates [48, 50, 52]. So far, efforts to engineer alternatives to SiO<sub>2</sub> have typically involved other oxides which have similar surface effect problems [57, 58]. Hexagonal boron nitride is an appealing substrate because of its strong in-plane ionic bonding which makes it relatively inert and free of surface charge traps and dangling bonds. The planar surface should

be key in suppressing rippling in graphene, conforming to both corrugated and flat substrates [53, 59]. Graphene can be transferred to hBN wrinkle free by polymethyl-methacrylate [60].

One of the most beneficial aspects of hBN as a substrate is the almost identical lattice constant (1.7% mismatch) to graphite as well as large optical phonon modes and electrical band gap [61]. Graphene devices on hBN substrates have carrier inhomogeneities and mobilities almost a full order of magnitude better than SiO<sub>2</sub>. Other advantageous qualities of these devices are improved chemical resistance, reduced roughness, and intrinsic doping. Dielectric properties of hBN compare favorably to those of SiO<sub>2</sub>, allowing the use of hBN as an alternative gate dielectric with no loss of functionality [62]. Surface optical phonon modes of hBN have energies two times larger than those of SiO<sub>2</sub> making hBN a superior option in high temperature and high electric field environments. The roughness of graphene on hBN is indistinguishable from hBN alone, making it three times smoother than on SiO<sub>2</sub>.

Electronic transport measurements of monolayered graphene transferred onto hBN show that the heterostructure is high quality; the mobility was always higher than graphene on SiO<sub>2</sub> [60]. The resistivity of the structure corresponding to the overall charge neutrality point is extremely narrow occurring at nearly zero gate voltage. The conductivity is strongly sublinear in carrier density indicating crossover from charge impurity dominated scattering to short-range impurity scattering at large carrier densities [49, 50, 55, 63]. The density independent mobility due to charge impurity long-range scattering of graphene on hBN is three times larger than graphene on SiO<sub>2</sub> and resistivity from short-range scattering is on par with values obtained for graphene on SiO<sub>2</sub> [63]. Transport measurements from bilayer graphene transferred to hBN show that the conductivity is linear with gate voltage up to large densities. The electron and hole Hall mobilities are  $6 \times 10^4 \text{ cm}^{-2} \text{ V}^{-1} \text{ s}^{-1}$  and  $8 \times 10^4 \text{ cm}^{-2} \text{ V}^{-1} \text{ s}^{-1}$  at  $T \approx 2 \text{ K}$  and  $4 \times 10^4 \text{ cm}^{-2} \text{ V}^{-1} \text{ s}^{-1}$  at

room temperature in air. High mobility in dual gated devices may be preserved by fabricating hBN-graphene-hBN stacks [62]. This leads to improved mobility, chemical stability, and field-effect transistor performance [64-68]. Atomically thin, multilayered BN nanosheet-graphene heterostructures with sandwich configurations (e.g. BN-C-BN) exhibit charge mobility as high as  $5 \times 10^5 \text{ cm}^{-2} \text{ V}^{-1} \text{ s}^{-1}$  [69]. The reverse heterostructure of (C-BN-C) has been utilized in field-effect tunneling transistor devices [70]. The electron tunnel current through BN nanosheets demonstrates that they are effective tunnel barriers down to a single atomic plane. The tunnel current is exponentially dependent on the BN barrier thickness [69]. The BN nanosheet can work as a barrier between graphene and a metal gate in the graphene tunnel junction [70]. It has been proposed that a band gap would be induced in graphene aligned to an hBN substrate, however, this has not been experimentally verified. The chemical reactivity of graphene on hBN is drastically different from that on  $\text{SiO}_2$ . Doping after annealing is non-existent compared to  $\text{SiO}_2$ . Magnetotransport measurements also bear out the superiority of hBN compared to  $\text{SiO}_2$  [71].

### **Optics**

As a III-V compound, BN is closely related to AlN and gallium arsenide (GaAs). III-V compounds have been extensively studied as semiconductors because of their superior electrical, thermal and structural properties compared to the ubiquitous Si semiconductor. For instance, while Si has an indirect band gap, many of the III-V compounds have direct band gaps that make optical applications like light-emitting diodes (LEDs) and lasers much more energy efficient.

Hexagonal boron nitride shows promise for ultraviolet (UV) optical applications because its quasi-2D excitation nature is expected to yield optical properties with large nonlinearities [20]. An UV laser using hBN was achieved by using an electron-beam excitation source. The

photoluminescence intensity of hBN is 100 times higher than aluminum nitride for the same input light stimulation, thus it is attractive as a deep ultraviolet (215-230 nm) emitter [21]. For example, Watanabe *et al.*[72] successfully demonstrated a deep UV hBN field emission device that generated a wavelength of 225 nm. However, the intrinsic optical properties of hBN, specifically luminescence properties, have a correlation with impurities and defects in the samples crystal structure. Poor crystalline quality has led to a wide variation in reported band gap properties, specifically excitation luminescence. Therefore, high purity hBN crystals are necessary to efficiently emit deep UV [48, 73]. Pure single crystals exhibit a dominant luminescence peak and a series of s-like excitation absorption bands at 215 nm. A lasing device with a p-n junction structure would require p and n-type doping control of hBN which has not been achieved. Because of hBN's thermal and chemical stability its threshold for UV damage should be high.

For all of these applications, hBN single crystals are preferred to achieve the best possible properties. In general, single crystals have the highest charge carrier mobilities, as they lack grain boundaries that cause scattering. Similarly, grain boundaries and other defects can create charge recombination centers that degrade luminescence efficiency. For substrate applications of hBN, a single crystal orientation is best, since the layer's properties change with its crystallographic orientation relative to the substrate; grain boundaries in the hBN substrate may affect the electrical properties of the graphene it supports [74].

### **Optimization of hBN Crystal Growth**

The unique and outstanding properties of hBN have been established, yet there is still significant work necessary to produce bulk crystals with the same control of defects and dimensions that now exists in the growth of single crystal Si.

Single crystals may be produced by the transport of crystal constituents in the solid, liquid, and vapor phase. Based on the phase transformation process, crystal growth techniques are classified as solid growth, vapor growth, melt growth, and solution growth. Choosing the appropriate growth technique plays a vital role in the impurities and defect concentrations of bulk crystals. Determining the best method for bulk crystal growth depends on the characteristics of the material being produced. A vital tool to help illuminate the best method of the material is its phase diagram. The BN phase diagram from Bundy and Wentorf [75], subsequently revised by Corrigan and Bundy [76], shows cBN to be the thermodynamically stable phase up to approximately 1500 °C (Figure 2-4).

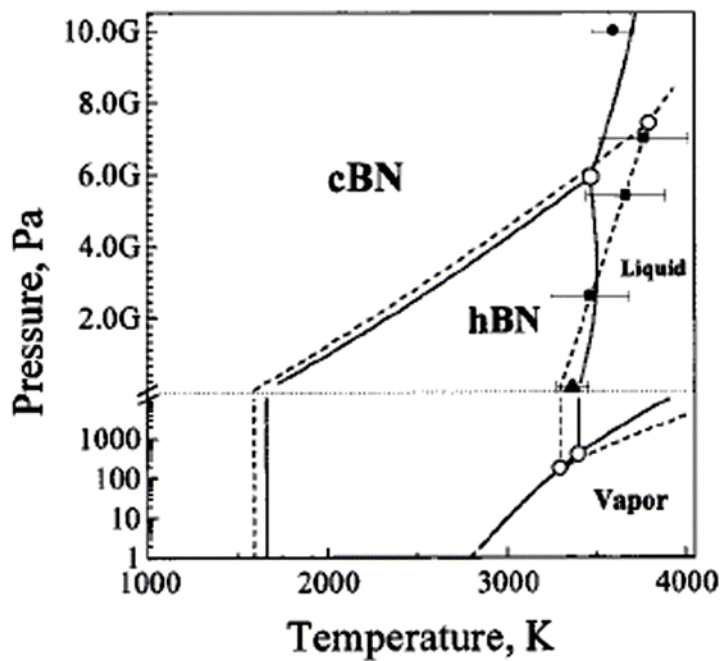


**Figure 2-4 BN phase diagram. (From Bundy and Wentorf [75])**

The relative stability of BN's main allotropes, cBN and hBN, has been unclear, and for many years it was believed that hBN was thermodynamically more stable than cBN at standard conditions. This was supported by the fact that the synthesis of BN normally results in the formation of hBN. Current analysis and measurements indicate the reverse, hBN is stable at zero

pressure and relatively high temperatures [77, 78]. The application of periodic local Meller-Plesset second order perturbation theory also favors the cubic phase. This indicates that long range electron correlation is the largest factor for the relative stability of the BN polymorphs [79]. Will *et al.* [78] demonstrated that kinetics is the decisive factor and the cBN to hBN transformation strongly depends on purity, grain size, and defect concentration. The findings of cubic phase BN at standard conditions is supported by most density functional theory (DFT) studies [80-84], however, there are still theoretical models that estimate hBN is more stable than cBN; these are the generalized gradient approximation and local density approximation calculations [85-87]. It has been suggested that the intrinsic deficiencies of the DFT method become critical for the small energy differences involved in the BN system which render this method incapable of providing a fully consistent and conclusive picture.

### **Melt Growth**

Growth from a melt by solidification is the most widely used method for the preparation of large single crystals. The Czochalski technique is widely adopted to grow many III-V semiconductors, which involves pulling a crystal from a melt [88]. In Czochralski method, the material to be grown is melted by induction or resistance heating under a controlled atmosphere in a suitable non-reacting container. By controlling the furnace temperature, the material is melted. A seed crystal is lowered to touch the molten charge. When the temperature of the seed is maintained very low compared to the temperature of the melt, by suitable water cooling arrangement, the molten charge in contact with the seed will solidify on the seed. Then the seed is pulled with simultaneous rotation of the seed rod and the crucible in order to grow perfect single crystals. Owing to the extremely high melting points of many of the borides, carbides, nitrides, etc., crystal growth by direct techniques (Czochralski, Bridgman, sublimation) at those



high temperatures is extremely difficult due to container problems and precise growth control [89-91]. Because of hBN's high melting temperature ( $>2950$  °C) [92] the growth of single crystals from a melt would be quite difficult.

### **CVD Growth**

Another possible method is vapor phase growth. By far, chemical vapor deposition (CVD) has been the most common method to synthesize hBN over the decades. In this process, chemical precursors containing boron and nitrogen flow through a reaction chamber where they are heated and deposited via chemical reaction onto a substrate. Some common precursors are trifluoroborane [1], trichloroborane [2] and diborane [3] with ammonia. The quality of hBN films made by CVD is dependent on temperature, pressure and molar flow rates of the precursors. Typically, these reactions are carried out at temperatures between  $1300^{\circ}\text{C}$  and  $1700^{\circ}\text{C}$  and pressures between 0.1 and 200 torr. The molar flow rates are then adjusted to ensure stoichiometric B-N deposition. More recently, CVD with a single precursory compound containing both boron and nitrogen such as borazine [4], ammonia-borane [93] or borane-amine organocomplexes [6] has gained appeal. Benefits of single-precursor over double-precursor CVD are lower reaction temperatures and elimination of precursor flow rate ratio optimization. However, contamination (especially carbon and oxygen) becomes an issue with complex precursors. The crystalline quality of pBN is less than desirable as the hBN layers exhibit stacking disorder [7]. CVD grown hBN can be limited by low growth rates, small grain sizes, lattice mismatches to substrates, strain, and cracking. Therefore, single crystal (and especially bulk crystal) hBN growth is unsatisfactory with CVD.

## **Solution Growth**

Solution growth of hBN single crystals is a viable option. Materials that have high solubility, which is strongly dependent on temperature, can be easily grown by solution method [88]. A solution is formed by the addition of a solid solute to a solvent. At a given temperature and pressure, there is a given amount of solvation. The amount of solute required to make a saturated solution at a given condition is called the solubility. Solution growth proceeds as follows: heat the container having a solvent and the solute to a temperature so that the solution mutually dissolves, this temperature is maintained for a soak period of several hours, and the temperature is lowered slowly resulting in crystallization. The driving force of the solution crystallization is supersaturation [94]. In order to relieve supersaturation and move towards equilibrium, the solute crystallizes. If crystallization occurs such that a stepped interface is formed in contact with a supersaturated solution, the growth process occurs in the following stages [94]:

1. Transport of solute to the vicinity of the crystal surface.
2. Diffusion through a boundary layer, adjacent to the surface for which a gradient in the solute concentration exists because of depletion of material at the crystal solution interface.
3. Adsorption on the crystal surface.
4. Diffusion over the surface.
5. Attachment to a step.
6. Diffusion along the step.
7. Integration into the crystal at a kink.

The sequence 1-7 is illustrated in Figure 2-5, where solute particles (black spheres) are surrounded in the solution by six solvent particles (white spheres) forming a regular octahedron for simplicity. Step 4.\* represents the ability of solution to desorb from the crystal surface.

There are many advantages to using a solution growth technique; probably the foremost being that crystal growth occurs at a lower temperature than that required for growth from a pure melt. Reducing the temperature is often beneficial if not essential especially for those materials that decompose before melting, resulting in crystallization of another phase and for highly refractory materials (i.e. BN) that require difficult techniques for crystallization from a melt.

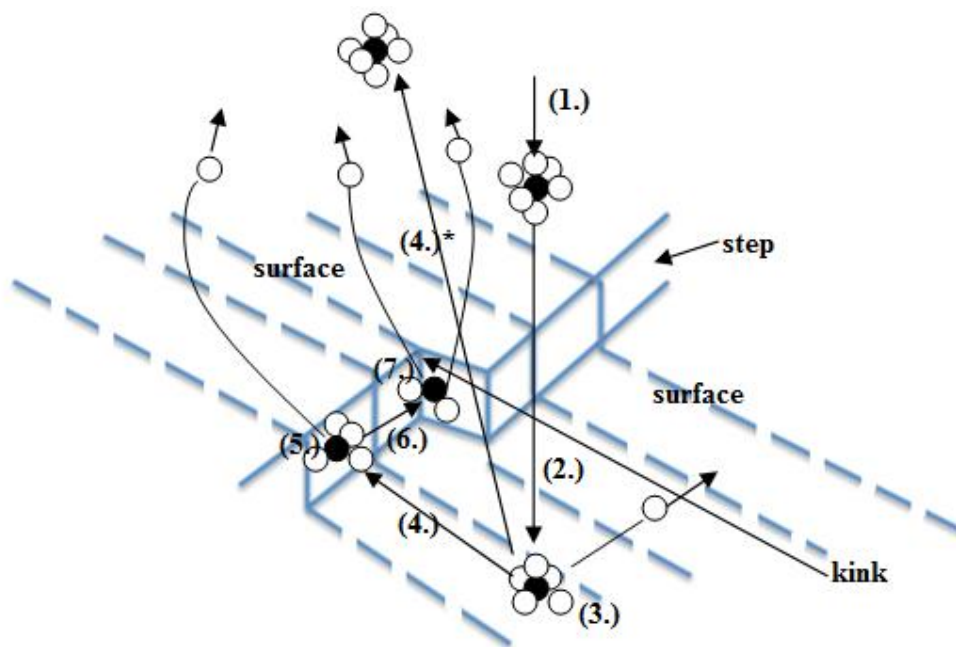


**Figure 2-5 Nucleation process for crystal growth.**

Further advantages of solution techniques for crystal growth are that the growing crystal can grow free from mechanical or thermal constraints into the solution allowing it to develop facets. Other advantages of relatively low growth temperature as compared to the melting point of the

solute, include decreasing point defects, dislocation densities, and low-angle grain boundaries improving crystal quality over those grown from their own melt. The disadvantages of the method are: substitution or interstitial incorporation of solvent ions into the crystal, microscopic or macroscopic inclusions of solvent or impurities, non-uniform doping, a slow growth rate, and container problems [94].

The solvent used in the solution method is of extreme importance. The type of solution and the solute-solvent interactions may play a decisive role in the crystal growth process. By selecting the proper solvent the tendency toward unstable growth may be reduced by increasing the width of the metastable region (i.e. supersaturation), thereby preventing inclusions and multinucleation. The choice of solvent also effects the degree of solvent-solute interaction and therefore the purity of the grown crystals [94]. The main requirements of a solvent are:

1. The ability to dissolve the components needed to form the crystal.
2. Low melting temperature.
3. Does not form intermediate compounds with the crystal components.
4. Low vapor pressure.
5. High purity to minimize contaminants.
6. Does not incorporate into the crystal.
7. Low viscosity.
8. The solubility changes significantly with temperature.

For crystal growth of borides compounds with very high melting points, transition metals which form compounds of relatively "low" melting point with B may act as solvents. For example,  $B_6P$  has been formed from Ni solution,  $AlB_2$  from Al solution, and BP and BAs from  $Cu_3P$  solution [94]. Many solvent choices that have been tested for hBN crystal growth such as

silicon [8], sodium [9], lithium bromide (LiBr) [95], copper [96], and BaF-LiN [11]. One of the first attempts to grow hBN single crystals was by Ishii and Sato [8] with boron dissolved in a silicon flux in a nitrogen atmosphere. After cooling from a temperature of 1850°C for two hours, their largest hBN crystal was reportedly two millimeters across and 20 μm thick. However, the hBN crystals were yellow in appearance due to carbon impurities and also contained nitrogen vacancies. Taniguchi and Watanabe [14] used a barium boron nitride to dissolve hot-pressed BN and powder BN at 4-5 GPa and 1500-1650°C for 20-80 hours. Since these conditions are close to cBN/hBN phase equilibrium, a mixture of the two phases was produced. Crystal size appeared to be less than one millimeter across, and the sensitivity of alkali and alkaline-earth metal solvents to air and moisture were significant disadvantages of this solvent. Kubota and Watanabe [15] performed another synthesis of cBN/hBN with a Ni solvent at 4.5-6 GPa and 1300-1900°C for 20 minutes. These crystals ranged from 5 μm (cBN) to 25 μm (hBN) across. While the crystals were small, the nickel solvent proved more stable and easier to work with. Since hBN is the predominant phase at low pressures, this suggests that it can be grown from similar cBN metal solvents at significantly lower pressures.

Yang *et al.* [16] synthesized hBN by dissolving 0.5 μm cBN crystals in a layer of molten nickel at 30 torr and about 1300°C. The hBN crystals they produced were only 2 μm across, most likely because nitrogen solubility in molten nickel is small (<0.01 wt% at 1550°C and 1 atm). The binary Ni-B and Ni-N phase diagrams show that 30 wt % B is in a liquid phase at 1550 °C [80], however the solubility of N in liquid Ni is only 0.0012 wt% at this temperature and 1 atm of N<sub>2</sub> [97]. The nitrogen solubility of a liquid Ni-Mo alloy increases with an increasing concentration of Mo reported by Kowanda and Speidel [98]. Kubota *et al.* [99] dissolved BN powder in a nickel solvent that contained 40 wt% molybdenum to increase

nitrogen solubility an order of magnitude over pure nickel [98]; the result was single hBN crystals that were 300  $\mu\text{m}$  across and 10  $\mu\text{m}$  thick. Their reported experimental conditions were 1350-1500°C for 12 hours followed by 4°C/hour cooling to 1200°C and quench cooling thereafter.

Since chromium dissolves nitrogen up to two orders of magnitude better than molybdenum [16, 98], Kubota *et al.* [99] mixed 53 wt% chromium with the nickel solvent under the same aforementioned conditions and obtained hBN crystals 500  $\mu\text{m}$  across and 60  $\mu\text{m}$  thick. The process employing a nickel-chromium flux developed by Kubota *et al.* [15] has perhaps been the most successful in its ability to produce good sized crystals (>500  $\mu\text{m}$ ) at modest temperature (1500 °C) with excellent optical properties.

For the systematic growth of large crystals and for the achievement of a high yield, the phase diagram has to be known to a sufficient degree. However, many high-temperature solutions contain three or more components, and the determination of a complete phase diagram in such cases is totally impractical. As stressed by Roy and White [100] the solution is treated as a pseudo-binary system with the phase to be crystallized as one component (solute) and the solvent as the other. The information required for crystal growth is the solubility curve of the phase to be crystallized and the stability field of this phase which is the range of composition and temperature over which it is stable. No Ni-Cr-B-N quaternary phase diagram is available, as such exact melting and solidification temperatures were unknown until Clubine [23] determined the Ni-Cr eutectic point of 1345°C at 53 wt% Cr. It was determined the Ni-Cr system was an appropriate solvent choice because the ratios of the boron-dissolving nickel and nitrogen-dissolving chromium were comparable, ensuring sufficient B and N were dissolved to precipitate hBN. When heating the Ni-Cr-B-N system, the melting temperature was not a concern because

it was sure to be below the Ni-Cr eutectic temperature of 1345°C since additional components tend to depress the initial melting temperature. However, the freezing temperature was important to know as it provides the lower temperature limit for crystal growth. Therefore Clubine used differential scanning calorimetry (DSC) finding the freezing range to be between 1175°C and 1215°C allowing crystal growth may occur in a 150 °C range. Hoffman *et al.* [22] grew bulk hBN crystals where Ni and Cr powders were mixed to a composition near 53 wt.% Cr, plus boron nitride powder, loaded at a 1:20 weight ratio to the Ni and Cr powders. These powders were loaded into boron nitride crucibles, dissolved, and crystals were produced using a slow cooling method.

The most common technique for producing supersaturation in flux growth is by slow cooling where generally a linear cooling rate is applied. The linear growth rate  $v$  (in cm/h) by slow cooling is related to the cooling [91] according to

$$v = \frac{V}{A\rho} \left( \frac{dn}{dT} \right) \left( \frac{dT}{dt} \right) \quad \text{Eq. 2-1}$$

where  $V$  is the volume of solution (cm<sup>3</sup>),  $A$  the area of the growing crystal (cm<sup>2</sup>),  $dn/dT$  the change in solubility per degree (g/cm<sup>3</sup>/°C), and  $dT/dt$  the cooling rate in °C/h. A constant linear growth rate and therefore a cubic decrease of temperature with time will cause unstable growth. Scheel and Elwell [101] have shown that the temperature regulation and the cooling rate have to be adjusted in such a way that the slope of the effective cooling can (including any oscillations or fluctuations) never exceed the slope of the calculated optimum cooling curve for stable growth at the corresponding temperature. The general rule is that the smaller the growth rate, the better and larger the crystals. However, one has to find a compromise between the slow cooling rate and the correspondingly long duration of an experiment. Also Laudise [102] stressed that cooling rates which are not at least comparable with the temperature fluctuations due to

inaccurate regulation are pointless. A very slow initial cooling rate is impractical for the (normal) case where the super-solubility curve is not known with sufficient accuracy and much time passes before nucleation starts.

The advantages of the slow cooling technique are:

1. That a closed container (sealed crucible) can be used thereby preventing evaporation of volatile solvent or solute constituents which are poisonous or corrosive and which cause uncontrolled supersaturation.
2. The technique is relatively simple for the growth of crystals up to 5- 10 mm size.
3. The slow cooling technique is suitable for exploratory materials research. It is usually simple to crystallize known crystals and also new phases in sizes from 2 to 5 mm, which are suitable for X-ray structure determinations and a number of physical measurements.

The slow cooling method of hBN crystal growth, employed by Hoffman *et al.* [22] involves 4 steps. First, the furnace temperature was increased from room temperature to the maximum or soak temperature. Second, the soak temperature was maintained for several hours so the Ni-Cr flux could saturate with boron and nitrogen. Third, samples were cooled at a controlled rate to 1200 °C, causing the hBN to precipitate and crystallize on the surface of the flux. Finally, after cooling to 1200 °C, the furnace was turned off, allowing it to cool to room temperature for analysis. They determined that the crystalline quality was directly related to the cooling rate where 4 °C/hr cooling marked the transition from polycrystalline hBN, at 10 °C/hr to single crystals with crystal grains greater than 500 μm (Figure 2-6) with crystals grown at 2 °C/hr being the highest quality. Their analysis showed the hBN crystals formed on the top of metal flux surface. The crystals were highly ordered, as determined by X-ray diffraction, where the (002), (004), and (006) planes exhibit strong, narrow peaks (Figure 2-7). Raman



spectroscopy of these crystals confirmed their quality with a single peak at  $1366\text{ cm}^{-1}$  and a FWHM of  $8.0\text{ cm}^{-1}$ .

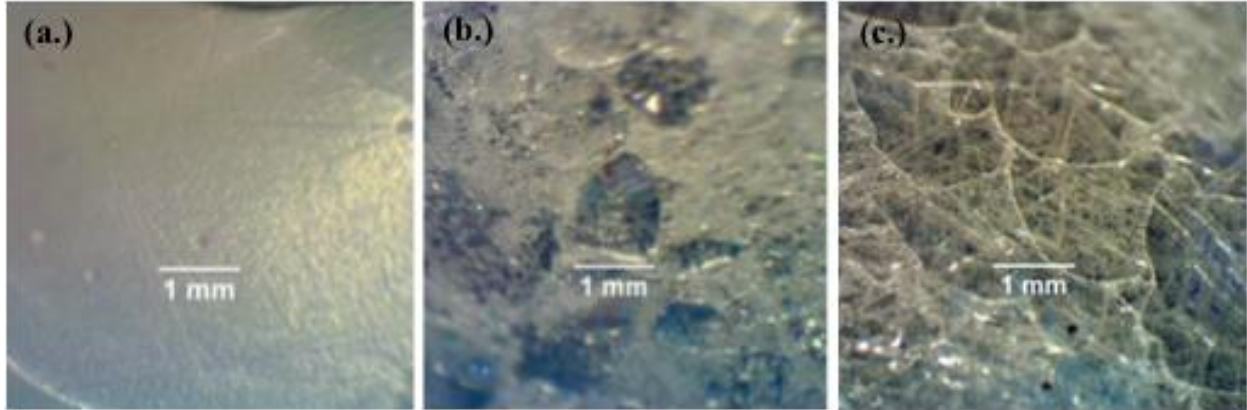


**Figure 2-6 Comparison of hBN grown at cooling rates of (a.)  $10\text{ }^{\circ}\text{C/hr}$ , (b.)  $4\text{ }^{\circ}\text{C/hr}$ , and (c.)  $2\text{ }^{\circ}\text{C/hr}$  after having soaked at  $1500\text{ }^{\circ}\text{C}$  for 24 hours. (From Hoffman [22])**

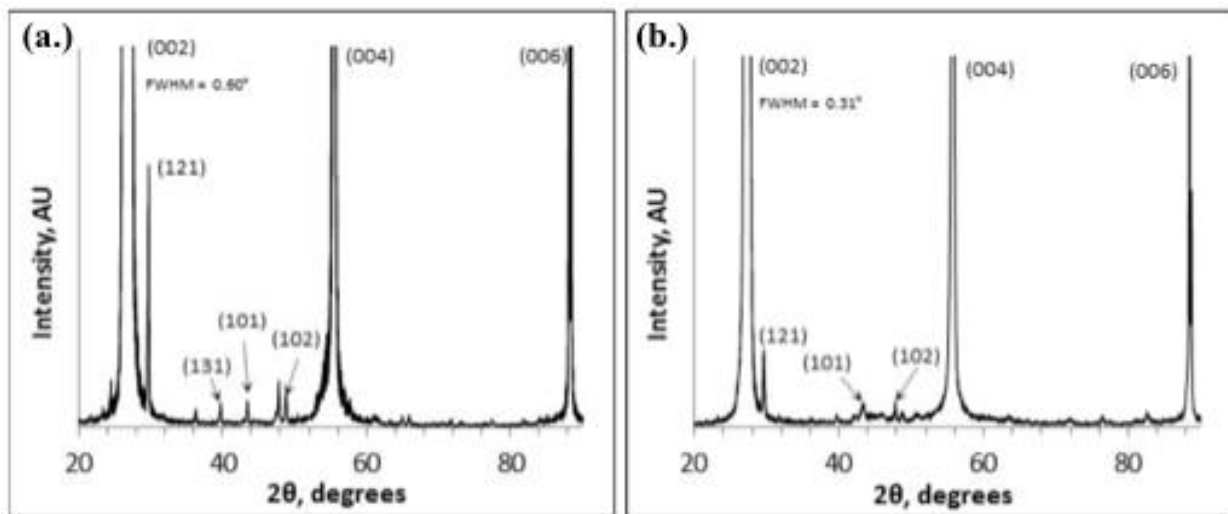


**Figure 2-7 X-ray diffraction spectra for hBN crystals growth with soak temperature of (a)  $1550\text{ }^{\circ}\text{C}$  and (b)  $1700\text{ }^{\circ}\text{C}$ . (From Hoffman [22])**

The maximum apparent crystal width formed increased with temperature from  $0.75\text{ mm}$  across at  $1450\text{ }^{\circ}\text{C}$  to  $5.0\text{ mm}$  across at  $1700\text{ }^{\circ}\text{C}$ , as shown in Figure 2-8. Crystal thickness showed an opposite trend, with crystal thickness as large as  $500\text{ }\mu\text{m}$  at  $1500\text{ }^{\circ}\text{C}$  and decreasing to  $40\text{ }\mu\text{m}$  at

1700 °C. Images of the crystal width and thickness of samples grown at 1500 and 1700 °C are shown in Figure 2-8. The morphology of the crystals formed also changed with the temperature. At higher temperatures, the crystals exhibited a more triangular habit and preferred to grow wider and thinner. At lower temperatures, the crystals exhibited a thicker, hexagonal shape, with growth rates roughly equal in the  $a$  and  $c$  directions. This is attributed to the preferential termination of the crystal edge with either N or B atoms, increasing crystal stability [93, 103]. Schematics of these two crystal habits and a diagram of an atomic layer of hBN preferentially terminating with N atoms are shown in Figure 2-9.

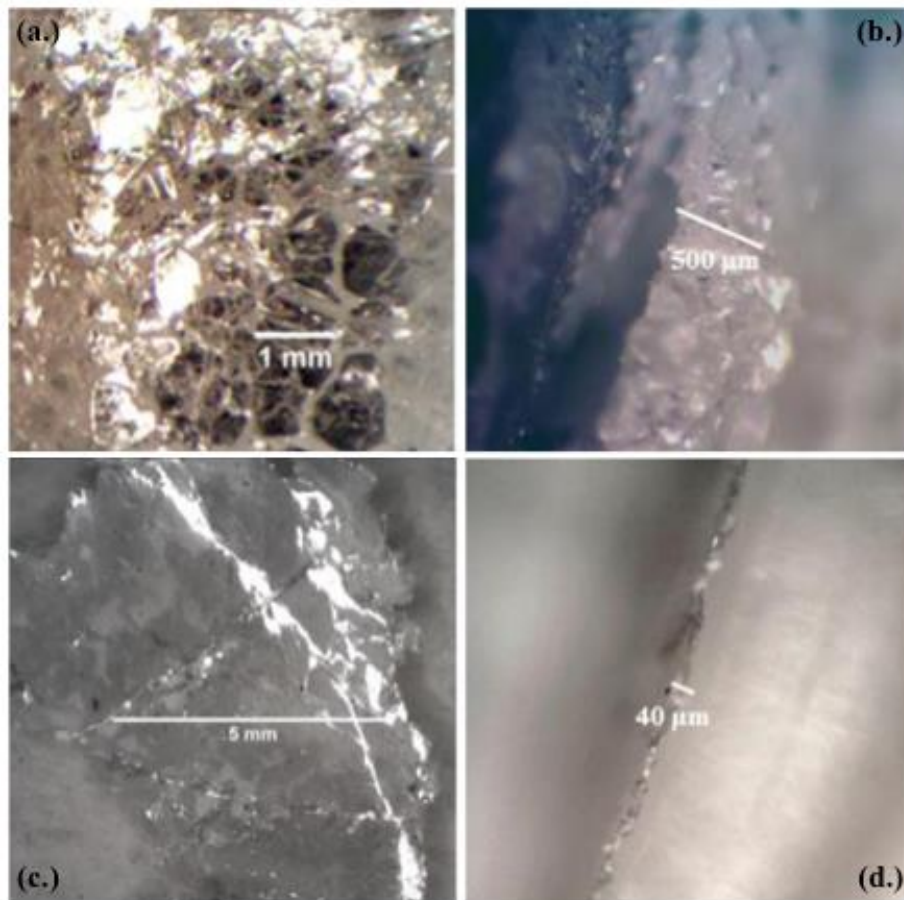


**Figure 2-8 Width (a.) and thickness (b.) of crystal grown at 1500 °C. Width (c.) and thickness (d.) of crystal grown at 1700 °C. (From Hoffman [22])**

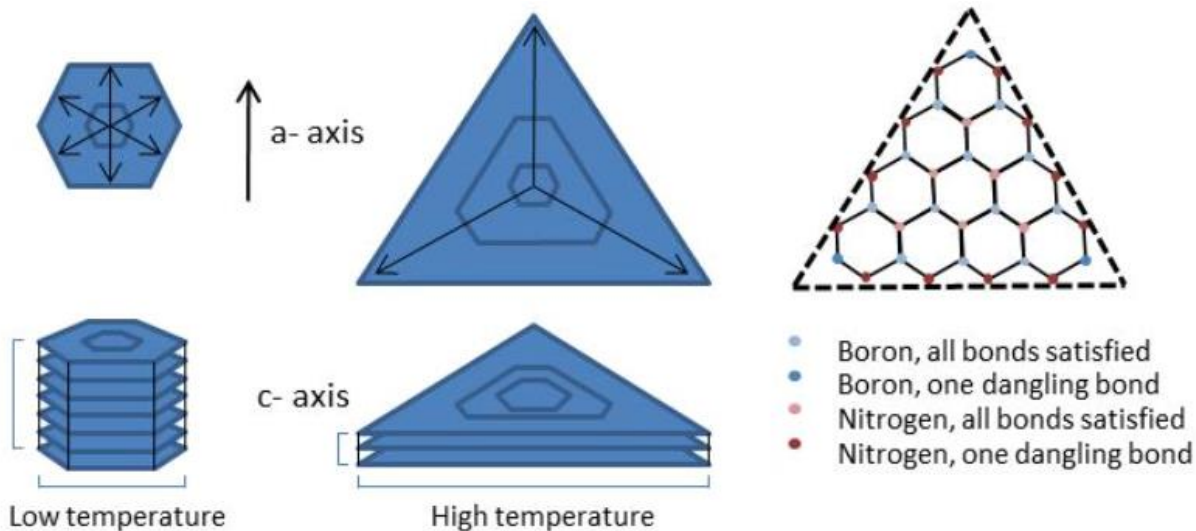


**Figure 2-9** Diagram of (a) differences in crystal habit for hBN grown at low and high temperatures and (b) theoretical atomic arrangement for the high temperature, triangular hBN habit. (Adapted with permission from K.K. Kim, A. Hsu, X. Jia, S.M. Kim, Y. Shi, M. Hofmann, D. Nezich, J.F. Rodriguez-Nieva, M. Dresselhaus, T. Palacios, J. Kong, *Nano Lett.* 12 (2012) 161. Copyright 2012 American Chemical Society.)

It is clear the solution method incorporating a Ni-Cr flux as the solvent is capable of producing highly ordered, large, thick hBN crystals. By modifying the slow cooling of the solution method by Hoffman *et al.* [22], it was proposed that crystals can be grown both larger and thicker (i.e. increased growth in the *a* and *c* direction).

## Crystal Extraction

Probably one of the more underappreciated components of solution growth is the separation of crystals from the solution immediately following crystal growth. Generally, crystallization from high-temperature solutions is terminated at a temperature above the eutectic point allowing for crystal separation from the solution or following relatively rapid cooling to room temperature. The former alternative is generally preferable when this is convenient, as in top-seeded growth where the crystal may normally be raised out of the solution by a motorized drive mechanism. However, if crystals are grown by spontaneous nucleation, it is necessary to

cool the crucible to room temperature prior to removal of the crystals. This is widely practiced because of its relative simplicity. The excess solution is then normally dissolved in some aqueous reagent, a process sometimes referred to as "leaching".

The leaching process relies on the differential solubility in this reagent of the crystal and the high-temperature solvent. It is clearly important for easy removal of the crystals that a suitable fast acting reagent exists. The disadvantage of removing the excess solution at or around room temperature is that the rate of dissolution may be extremely low. Warming the leachate promotes dissolution and the resulting saving in time can be dramatic, especially if leaching is performed at a temperature close to the boiling point of the aqueous reagent. Additionally, most rapid leaching rates require that the acid be replenished at frequent intervals depending on the volume of the container used. This results in considerable acid waste, which may require special disposal depending on the solution used.

Many experimentalist have simply poured off the excess solution by removing the crucible from the furnace with tongs and decanting the liquid after removing the crucible lid. This method is possible only when the lid fits loosely onto the crucible, since it is desirable that the crucible should be returned to the furnace as rapidly as possible in order to minimize thermal shock to the crystals. However, due to the extreme temperatures ( $1200\text{ }^{\circ}\text{C}$  >) and the sensitivities toward oxygen of the furnaces utilized this is not a viable option.

An alternative procedure has been suggested by Grodkiewicz *et al.* [104] who punctured the base of the crucible from below with a steel spike, to drain the solution without removing the crystal from the furnace. This is an intriguing solution, however the difficulty is finding a material that would be capable of puncturing a hole in the crucible with minimal force and capable of withstanding the high temperatures of the furnace ( $1450\text{ }^{\circ}\text{C}$  >).

The seeding technique of Bennett [105] and Tolksdorf [106] provides a particularly convenient means of removing the crystal from the residual solution by inversion of the crucible. Crucible inversion is applicable to sealed crucibles and may be used for unseeded growth if some mechanism is provided within the furnace. This mechanism may be extremely simple, for example, a wire attached to the base of the crucible, which is pulled vertically upwards, provided that the crucible is mounted on a suitable pivot. Completely sealed crucibles permit a greater degree of reproducibility in the crystal growth conditions but inversion and subsequent solidification of the residual solution presents problems in the removal of the lid and of access to the crystals.

An isothermal technique to remove excess solution has been used by Kawabe and Sawada [107] who, sucked up the still liquid flux through a nickel pipe by a rotary pump, and then cooled the furnace with the crucible to room temperature. In a similar manner for sealed crucibles, pressure from outside could be used to pump the excess solution out of the crucible.

Leaching was employed by Clubine [23] where hBN crystals were separated from the metal flux by immersing the entire sample in hot aqua regia, as hBN is unreactive with acids, to dissolve away enough of the metal to separate crystals. However, 1-2 days can be required to sufficiently dissolve the metal flux sufficiently, due to Cr and Ni being partially resistant to one or another of the component acids making up the aqua regia solution.

An alternative utilized by Hoffman *et al.* [22] involves mechanically peeling crystals from the metal flux with thermal release tape, eliminating the difficulty of dealing with acid waste and facilitating transfer to substrates. However, cooling of the crucible and crystals to room temperature while leaving the flux intact may cause cracking of the crystals. This was recognized by Edgar *et al.* [17]:

*“Frequently, the crystals were cracked, presumably due to contraction as the metal flux solidified, and the differences in the coefficients of thermal expansion of the hBN and the metal flux.”*

Additionally, the use of thermal release tape can crack or tear the crystals unevenly leaving layers of hBN still embedded in the metal flux, limiting the potential of the crystal thickness.

Zhidaglo *et al.* [108] was able to separate the hBN crystals from their high pressure solution method by heating the solution in a vacuum to evaporate and drive off the solvent. However, a drawback to this method is the high vapor pressure of the metal flux necessitating high temperatures to evaporate the Ni-Cr solvent and could result in dissolution of the hBN crystals [108].

A method for draining of the metal flux is here proposed for the solution growth of hBN single crystals, where the crystal pulling mechanism of a furnace is used to raise a custom made crucible, draining the solution *in situ* thereby alleviating crystal cracking due to the cooling of the metal flux and freeing the crystals unharmed. This is described in section 3.

### **Isotope Enrichment of hBN Crystals**

Boron has two stable isotopes,  $^{10}\text{B}$  and  $^{11}\text{B}$  where the natural abundance of B is 80.22%  $^{11}\text{B}$  and 19.78%  $^{10}\text{B}$ . Boron is one of the very few elements to absorb thermal neutrons. The neutron absorption property of B is mainly due to the presence of  $^{10}\text{B}$ , which undergoes the main capture reaction where thermal neutrons react with  $^{10}\text{B}$  to give off an alpha particle and energy while leaving a lithium ion:  $^{10}\text{B} + ^1_0\text{n} \rightarrow ^7\text{Li} + ^4_2\alpha + E$  where 94% of the time the  $^7\text{Li}$  particle is in an excited state and  $E = 2310$  keV, and 6% of the time the  $^7\text{Li}$  particle is formed in its ground state and  $E = 2790$  keV [109]. The lighter isotope has one of the highest thermal neutron

capture cross-sections of any element at about 3850 barns [109]. By using  $^{10}\text{B}$  as the boron source in hBN, many radioactive applications have been envisioned. For example hBN nanotubes have been proposed as radiation shields in future interplanetary missions [110]. Another feasible radioactive application of supreme interest to national security proposes hBN as a neutron detector. To defend its borders from nuclear attack, a country may inspect goods entering for radioactive material with gas-filled neutron detectors, mainly filled with  $^3\text{He}$ . However,  $^3\text{He}$  detectors are declining in popularity because of increasing prices. In the past,  $^3\text{He}$  was relatively abundant as it is created by decaying tritium in nuclear weapon stockpiles. With the conscious effort to halt the proliferation of nuclear weapons all around the world, the supply of  $^3\text{He}$  only met a third of demand in 2009 [111]. Therefore, a necessity exists to find replacement materials for neutron detection of which hBN is an exceptional option. Beyond a lack of  $^3\text{He}$ , an inherent disadvantage of gas-filled neutron detectors is their low efficiency [112]. Bulky, pressurized tubes are necessary to generate detectable electrical signals when a neutron interaction occurs, making the device delicate and expensive.

Solid-state neutron detectors offer higher efficiencies with a more sturdy and compact design, provided an appropriate material for neutron detection is incorporated into the device [112].  $^{10}\text{B}$ -enriched BN would reduce the material thickness required for completely capturing neutrons, making charge collection (and, hence, signal generation) in a material with low carrier mobilities easier [112]. Some other properties of boron nitride that are intriguing for neutron detection are its low effective atomic number (10.8 and 14 for natural boron and nitrogen, respectively) and high dielectric strength ( $>140$  eV/nm) [112]. The former property is useful for discriminating neutron emission from gamma radiation since low-Z nuclei are more transparent to gamma rays than heavier nuclei [112]. The latter property is important since high applied

voltages are typically necessary to operate the device with maximum charge- collection capability.

Conventional solid-state neutron detectors made of silicon and a neutron-capturing material have been around for decades [113] and are typically, composed of two regions. The first is the neutron-capturing layer (e.g. boron or boron compound) where an incident neutron strikes a  $^{10}\text{B}$  atom and ejects  $^7\text{Li}$  and an alpha particle. The alpha particle must then travel to the semiconductor layer (e.g. silicon) where it interacts with the silicon atoms to produce electron-hole pairs and, thus, a detectable electrical signal. The separated neutron-capture and charge-collection layers are responsible for the device's poor efficiency, and their thicknesses are critical; the boron layer must be thick enough to provide enough  $^{10}\text{B}$  centers for neutron capture, but thin enough to allow the generated alpha particles to escape the boron layer into the silicon layer where an electrical signal can be detected. Efforts to overcome the inefficiency of the layered devices have led to pillared devices where thin alternating layers of boron and silicon are stacked side-by-side to increase the likelihood of neutron capture and alpha particle-spawned electrical signals [114]. The efficiency of these devices is still below 50% [114]. The maximum theoretical efficiency is achieved if the neutron-capturing and charge- collection layers are integrated into a single layer. This implies the need for a material that is a semiconductor, and many such materials have been tested including boron carbide [115], boron phosphide [116] and pBN [18, 112]. While the efficiencies of the pBN devices tested by both Doty [112] and McGregor *et al.* [18] were quite low, this is most likely attributable to the polycrystalline nature of pBN. Bulk, single-crystal hBN should exhibit improved charge transport properties versus pBN. The use of a single hBN crystal as a neutron detector, in which it will serve as both neutron capture material and signal detector, requires a certain thickness to have appropriate



signal to noise ratios. The higher the enrichment of B as  $^{10}\text{B}$  in the compound, the thinner the crystal can be, while still maintaining a large neutron capture cross section. This would significantly boost efficiencies because its high Barnes cross-sectional capture paired with the charge transport properties of hBN. This highlights the need for a high quality,  $^{10}\text{B}$  enriched hBN single crystals.

Hoffman *et al.* [117] have successfully grown hBN single crystals enriched with  $^{10}\text{B}$  and  $^{11}\text{B}$  respectively using the solution method. Their method for growing hBN single crystals which used the crucible as the boron source was modified by adding a premelted flux of Ni and Cr as well as either a % by weight of 99%  $^{10}\text{B}$  or  $^{11}\text{B}$  included in the flux. This produced  $^{10}\text{B}$  % enriched and  $^{11}\text{B}$  % enriched hBN crystals. The specific B concentration was measured by secondary ion mass spectrometry (SIMS). From this, the researchers created a pseudo calibration curve, relating the atomic % B enrichment to the Raman shift, red for  $^{11}\text{B}$  and blue for  $^{10}\text{B}$  enrichment, from the  $1366\text{ cm}^{-1}$  signature peak of natural abundance hBN single crystals. It is proposed that by replacing the HPBN crucible used in the Ni-Cr flux method, with another material, one that does not contain boron, control of B enrichment will be increased.

Most experiments in crystal growth from high-temperature solutions are carried out in containers, either in crucibles or in ampoules. Thus crystal growers must choose a practical crucible material which is resistant to corrosion by the solvent, solute, and the atmosphere at the high growth temperatures. Further requirements are a high mechanical strength, ease of shaping and of cleaning, good thermal shock resistance, reasonably long lifetime (little recrystallization) and a low price. Corrosion is related to the wetting angle of the melt. The larger the difference in the type of bonding between crucible and melt, the smaller the wetting and the corrosion normally observed [94]. As a rule suitable crucible materials are those which have a type of

bonding different from that of the solvent and solute provided, that no decomposition reaction occurs. The difference in the chemical bond type generally leads to a sufficiently small solubility of the crucible material in the solvent, especially when this material has a relatively high melting point. Examples of the bonding difference rule are the use of platinum crucibles for ionic melts, of (ionic) oxide, and of covalent graphite and nitride crucibles for metallic melts [94]. For this reason, crucibles tested in the present study were limited to oxides as carbon inhibits hBN crystal growth and nitrides are too similar. As such three possible crucible replacements for the HPBN crucible were considered: alumina ( $\text{Al}_2\text{O}_3$ ), yttria-stabilized zirconia (Y-ZrO<sub>2</sub>), and yttria (Y<sub>2</sub>O<sub>3</sub>). As oxides, these materials are suitable for use with the metal solvent employed in the solution method. Also, because of the high temperatures necessary for hBN growth the crucible must have an extremely high melting temperature, which applies to all three materials. The interaction between BN, the Ni-Cr solvent, and the crucible materials was unknown however and so it was tested experimentally.

A successful crucible material will allow for higher enrichment of <sup>10</sup>B in hBN while not interacting with the solvent or solute. Boron 10 enrichment of hBN crystals near 100% will create optimal thermal neutron capture, allowing for thinner crystals, which in turn benefits detection of alpha particles. The resulting neutron detector, would be highly portable and far more rugged than current gas detectors as well as having much better efficiency than sandwiched devices layering B with Si.

## **Two Dimensional hBN**

With the explosive rise of graphene, beginning in 2004 [24], research began on the existence and stability of a 2D BN counterpart [118]. Hexagonal boron nitride nano-sheets (hBNNSs) were initially prepared in the form of so called nano-meshes [119]. The following

year, free standing 2D BN flakes were peeled off of hBN crystals [120]. Additionally, BN nano-ribbons, nano-sheets with variable lengths and narrow widths, were produced as hollow nano-strips in 2008 [121]. Today, the lightest group III-V compound is established as one of the most promising non-carbon nano-systems. 2D BN has many intriguing properties such as: high thermal conductivity, superb oxidation resistance, excellent chemical and thermal stability, electrical insulation, and mechanical robustness that have made them of supreme interest to material scientists. Various applications such as thermally robust catalytic and sensing substrates, highly durable field emitters, multifunctional fillers in composite materials, compact UV laser devices, and chemically inert super hydrophobic films have been envisioned. Boron nitride nano-sheets have promise as a “green” lubricant additive for water [122] and BN sheet polymer hybrid films can be a safe choice as protective coatings to prevent corrosion in marine environments [123]. Because of its isostructural relationship to graphene, these two materials can be combined to fine tune their composite properties [124, 125]. One example is as a 2D heterostructure with a BN substrate as an improved dielectric for graphene devices in order to enhance carrier mobility, and maintain a widened band gap. BN-C hybrid nano-sheets have great potential for fine tuning band gaps for use as fuel cells and transistors [69].

An hBN layer may be envisioned as a graphene layer, in which the carbon atoms are substituted by alternating boron and nitrogen atoms. Just like graphite, each hBN layer has atoms bound together by strong covalent bonds in the plane, while van der Waals forces hold the layers together. The crystallographic parameters of hBN and graphite are almost identical as shown in Table 2-1 [20, 37, 126, 127]. Unlike graphene monolayers, their corresponding 2D brethren, hBNNSs, have rarely been observed due to the unique stacking characteristics of hBN. The hexagons of neighboring planes in the hBN are superposed, B and N atoms are in succession

along the c axis (AA' stacking), while in graphite they are shifted by half a hexagon (AB stacking), as schematically depicted in Figure 2-10 [30]. Molecular dynamic simulations have been performed to evaluate the energy cost associated with a frustrated N-N or B-B bond as compared to a B-N bond. Starting from an isolated hBN sheet, if two neighboring B and N atoms are exchanged the energy cost associated with this antisite defect is 7.1 eV [128] after atomic relaxation. Due to the difference in electronegativity of B and N, the B - N bonds are partially ionic in contrast to the C - C bonds in graphite structures. This feature can lead to lip-lip interactions between neighboring layers in the BN nanostructures, forming “spot-welds” between the atoms of adjacent layers.

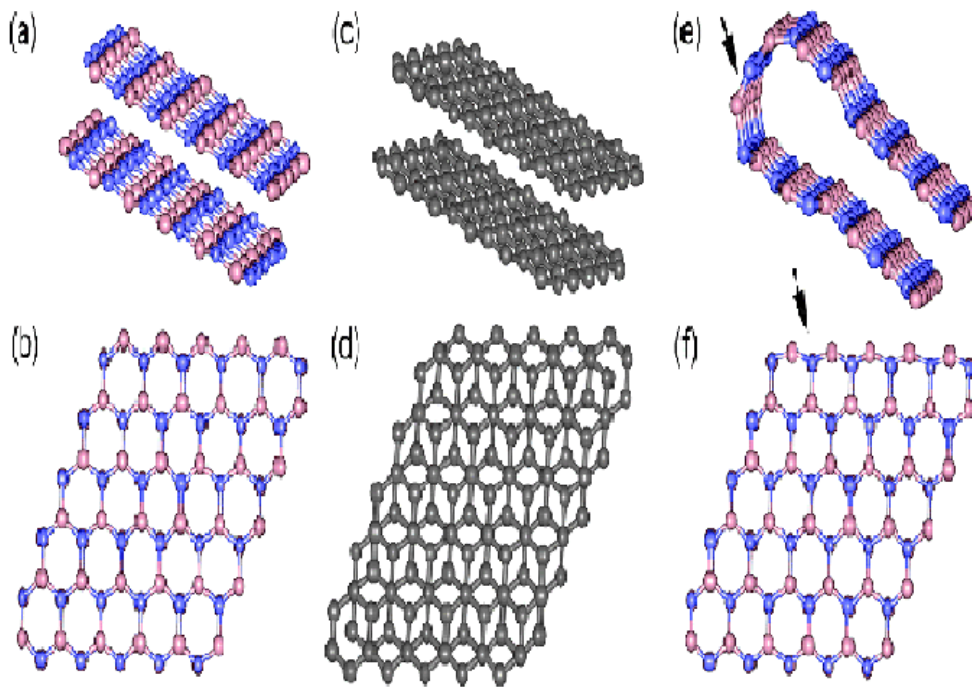


**Figure 2-10 Structural models of (a and b) hBN sheets and (c and d) graphite sheets displaying the difference in their stacking sequence. Cross-sectional and plane view of (e) the pristine and (f) relaxed models of the bilayered h-BN edge. (From Pakdel [129])**

In this way a metastable energy minimum is achieved by decreasing the number of dangling bonds at the edges and reducing the frustration effect of B - B bonds being formed or N - N

bonds instead of the more energetically favorable B - N bonds. Therefore, the formation of multilayered BN stabilizes the entire structure [128, 130-132]. Additionally, DFT studies suggest that covalent interlayer B - N bonds are spontaneously formed across the adjacent BN bilayers which results in a folded monolayered hBN as shown in Figure 2-10(e). By calculating the structural relaxations, interlayer covalent bonds form across the bilayered zigzag edge, leading to a closed edged termination. There is a calculated energy gain of -4.9 eV for each interlayer bond formed at the edge. These interlayer bonds in the out-of-plane direction have a covalent nature similar to the intralayer  $sp^2$  hybridized bonds within the bulk material, leading to the difficulty in isolating a monolayer of hBN [133]. Also, van der Waals corrected DFT calculations suggest that the adjacent BN layers might freely slide from AA' stacking to an AB stacking type with, N centered on B - N rings on adjacent layers, and along certain favorable directions, despite a band gap reduction of 0.6 eV. Furthermore, calculations suggest that the van der Waals forces role is to anchor the BN layers at a fixed distance, whereas the electrostatic forces dictate the optimal stacking mode and the interlayer sliding corrugation [134]. All this to say that extraction of a single sheet of hBN is highly unfavorable energetically as well as thermodynamically.

The attraction of hBNNSs lies in its ability to enhance and create new properties from its bulk parent by its geometry and quantum effects seen at the nano-scale. Thus, the ability to characterize its structure, in comparison to the bulk material, is necessary. Utilizing TEM, researchers have observed that typical multilayered nano-sheets have layers ordered with an interlayer distance of approximately 0.33-0.34 nm, characteristic of the interplanar spacing in bulk hBN (002) planes [135]. Spectroscopic signatures of hBN nano-sheets such as Raman and Fourier transform infrared (FT-IR) exhibit characteristic peaks that are quite similar to those of

bulk hBN crystals. The  $E_{2g}$  modes are Raman active, the  $A_{2u}$  and  $E_{1u}$  modes are IR active, and the  $B_{1g}$  modes are optically inactive. Both of the Raman active  $E_{2g}$  modes are due to in-plane atomic displacements; the low frequency mode is characterized by whole planes sliding against each other. The high frequency mode is due to B and N atoms moving against each other within a plane. High frequency interlayer  $E_{2g}$  vibration mode of the different BN structures is between  $1363\text{-}1374\text{ cm}^{-1}$  [136, 137]. Multilayered hBN has a red shift while single layered nano-sheets are observed to have a blue shift of approximately  $4\text{ cm}^{-1}$  attributed to hardening of the  $E_{2g}$  phonon mode due to slightly shorter BN bond in the isolated monolayers. The Raman peak frequency will shift higher or lower under compressive and tensile stresses [137, 138]. The typical absorption peak for FT - IR is at  $811\text{ cm}^{-1}$  and a broad absorption band with the bottom in the range of  $1350\text{-}1520\text{ cm}^{-1}$  which are ascribed to the B - N - B bending vibration mode parallel to the c-axis and B - N stretching vibration mode perpendicular to the c-axis modes of hBN, respectively [136].

### **Thermal Applications**

One of the largest and most successful applications of hBNNSs to date is as fillers in thermally conductive polymers [30, 139-141]. BN monolayers are predicted to have a larger thermal conductivity,  $k$ , value than their bulk counterparts. Out-of-plane vibrations contribute largely in the calculation of  $k$  value for hBNNSs, as well as reducing in phonon-phonon scattering in the 2D layer. This may explain the difference between a single layer and hBN bulk heat transport constant [142]. Consequently, BN monolayers will have one of highest room temperature thermal conductivities [142]. Previously, polymer materials have been embedded with  $\text{Si}_3\text{N}_4$ , AlN, and BN microparticles to improve their thermal conductivity. However, nano-materials are more effective fillers for such polymer matrix composites due to their higher

surface area [30]. Plastics with hBN additives have higher thermal conductivity and electrical resistivity as well as smaller thermal expansion. Unlike graphene, or other conductive fillers that may exhibit higher thermal conductivities [143], hBN nano-sheets eliminate possible electrical current leakage, compensating for lower dielectric constants and thermal conductivities.

Another application utilizing the high thermal conductivity of hBNNSs is as a 2D filler in mineral oil to form a Newtonian nanofluid. This nanofluid has a lower freezing point than pure mineral oil, excellent filler dispersion, high thermal conduction, and high electrical insulation [144]. These fluids may be the next generation of nanooils for lubrication, capable of efficient thermal management in heavy-duty machinery such as transformers.

### **Magnetic Applications**

The magnetic properties of 2D BN are confined to nanoribbons due to the edge effect [145]. However, DFT calculations have shown that by adding hydrogen (H) and fluorine (F) to hBNNSs they can become ferromagnetic, antiferromagnetic, or magnetically degenerate depending on how the surface is functionalized [146]. Vacancy defects in hBN monolayers may also induce magnetic properties [147, 148]. With the addition of iron oxide nanoparticles to hBN platelets, it is possible to orient the platelets in an epoxy matrix perpendicular to the substrate under a magnetic field, thus improving the thermal conductivity of the composite [149].

### **Wetting Applications**

Wetting is the ability of liquid to maintain contact with a solid surface, which is a result of intermolecular interactions at their interface. The degree to which a surface is wetted is determined by the adhesive forces between the solid and the liquid and the cohesive forces in the liquid. These are usually determined by the chemical composition and microstructural geometry. Water can wet bulk hBN surfaces relatively well, but hBNNS surfaces may repel water droplets.

A smooth hBN coating is relatively hydrophilic with an approximate contact angle of  $50^\circ$  whereas nano-rough hBN coatings made of vertically aligned nano-sheets can be hydrophobic with a contact angle up to  $150^\circ$  [135-137, 150-152]. These hBN nano-structure films may find use in water repelling, anti-fouling, self-cleaning, and anti-corrosion systems [137].

### **Catalytic Properties**

BN sheets have potential advantages for catalytic applications. DFT calculations predict that weak interactions between gold (Au) particles and hBN can lead to strong promotion of binding and catalytic activation of oxygen ( $O_2$ ) adsorbed on Au/hBN [153]. Au can be trapped effectively by nitrogen (N) or boron (B) vacancies and impurity point defects leading to strong adsorption accompanied by large transfer to and from the adsorbate. As a result, the excess of charge on the supported Au increases its catalytic activity [153]. Platinum has also been monodispersed along with Au on hBN nano-sheets and has been shown to be an effective catalyst in various reactions. In this way, the conversion of carbon monoxide (CO) is possible at lower temperatures and higher stability compared with other substrates such as aluminum oxide ( $Al_2O_3$ ) due to its high thermal conductivity, acid-base resistance, oxidation resistance, and hydrophobicity [154].

### **Environmental Applications**

Layered materials such as hBN have found many environmental applications. Recently, porous hBNNSs with high specific surface areas have shown high performance for the sorption of a wide range of solvents, dyes, and oils, and were proven effective for the removal of these contaminants from water [155]. A nanostructured material made from the sheets can absorb up to 33 times its own weight in oils and organic solvent, but also repels water. Once it has been saturated with the pollutant, the sheet can easily be cleaned by heating to burn off the pollutant.



Because of its unique thermal resistance properties, the hBN sheet is unharmed during the heating process and can be reused. Due to the interlayer space and flexibility of hBN it is feasible that it could accommodate various sized molecules such as proteins, viruses, pesticides, etc. However, the biocompatibility and toxicity levels of these nano-materials must still be studied. Nevertheless, it is easy to envision the possible applications in the biomedical fields [156].

### **Electronic/Optical Applications**

Of all the significant advances in nano-electronic materials and devices, semiconductors have seen the most dramatic changes as shown by Moore's Law where the number of field-effect transistors has doubled every 18-24 months. The effect of Moore's Law can easily be seen as the number of semiconductor chips being employed has seen an exponential increase. From the year 2000 to 2010 the industry nearly doubled in size. However, researchers have been hard pressed lately to keep up with Moore's Law, as devices become smaller and smaller, to the tens of nanometers size range, the benefits from new phenomena at the nano-scale are being diminished by increases in tunneling currents and the need for atomic-scale precision in fabrication, challenging the device's performance [157]. As such, new materials with fewer defects, tunable electrical properties, as well as superior thermal properties must be developed to further decrease device size.

In addition to the increased need for new nano-materials to continue to make progress in the semiconductor industry, nano-optics is a natural complement to nano-electronics and advances in the technology must also move forward. Nano-optic devices can perform optical functions in thin layers, often less than a micron thick. Due to their size being sub-wavelength in cases, the structures interact with light locally, involving quantum effects and can achieve optical

effects in an extremely short focal length compared with bulk optics [158]. Optical storage, photocatalysis, sterilization, ophthalmic surgery and nano-surgery are numerous applications requiring high transparency thin films with cathode luminescence in the deep ultraviolet range [20]. The optical properties of hBNNSs make it an enticing optical material for these applications. Hexagonal boron nitride nano-sheets do not exhibit optical absorption in the visible region of the spectrum. They exhibit high transparency as thin films or suspensions, and appear white when accumulated in bulk quantities [4, 35, 93, 159-161]. In the deep UV range hBNNSs show a sharp absorption peak at 210-220 nm. Boron nitride nano-sheets show a strong cathode luminescence emission in the deep ultraviolet range [93, 160, 162] making these 2D nano-materials appealing for compact emission in the deep ultraviolet range [93]. A single crystal provides better properties for these applications. As such, the exfoliation of a single crystal hBN into hBNNSs is proposed.

### **Synthesis of Two Dimensional BN**

There are currently many routes being employed in the synthesis of 2D BN nanostructures. Most are variations adopted from the procedures used to produce graphene sheets and ribbons. Some of the current methods being developed include: mechanical exfoliation [33-35], chemical vapor deposition [1-3, 25-27], solid state reactions [28-30], substitution reaction [31], high energy electron irradiation [32, 33], unzipping BN nanotubes [169], and chemical exfoliation [163-167].

#### ***Mechanical Exfoliation***

The first effort to obtain atomic sheets of hBN was the mechanical exfoliation technique, in which the BN layer is mechanically peeled or cleaved. This method was initially used to isolate graphene in 2004 [24] and has since been applied to many other layered materials such as

hBN and molybdenum disulfide ( $\text{MoS}_2$ ) [120]. Layers of hBN can be peeled off with an adhesive tape, attached to a substrate, and identified with an optical microscope. This method has characteristic traits of thickness and larger lateral size, which make them easier to work with for studies in physics and optoelectronics [33-35]. This route has been quite successful in the synthesis of graphene but cannot produce hBN monolayers. This method results in hBNNSs with approximately 10 layers or 3.5 nm thick. As stated above, this could be due to the strong lip-lip interactions between hBN basal planes because this interaction is essentially a chemical bond between adjacent layers decreasing the number of dangling bonds at the edges [130, 168]. Another route to mechanical exfoliation of hBN is to use shear forces instead of the direct force of pulling. This is done through mild wet ball-milling processes. Under a nitrogen atmosphere ( $\text{N}_2$ ), an hBN powder precursor gently shears the layers, and benzyl benzoate is used as the milling agent to reduce ball impact and contamination [169]. This produced improved yields over peeling with adhesive tape, producing layers of less than 10nm in thickness, but the process is incompatible with hBN single crystals.

Another method that shows promise of high throughput and large scale production of few layered hBN nano-sheets is the high pressure microfluidization process. A combination of DMF and chloroform are combined with hBN powder and inserted inside a microfluidizer processor and kept at a constant pump pressure of 207 MPa. This accelerates the product into the interaction chamber, and inside the chamber, the product stream separates into micro channels of various geometries and is forced to collide upon itself creating incredible forces of impact and shear stress. These forces are several orders of magnitude greater than those created by sonication. This results in hBN with a reported yield efficiency of 45% with hBNNSs between 20-30 layers and 500 nm lateral dimensions [170]. While this provides an impressive yield, the

violent shearing forces render hBNNSs bent and out of shape where as it is desirable to preserve the original lateral dimensions of the hBN following treatment.

### ***Chemical Vapor Deposition***

Chemical vapor deposition of hBNNSs is possible through various precursors and substrates. In 1964, Malcolm Basche deposited BN coatings onto a surface by the thermal decomposition of ammonia ( $\text{NH}_3$ ) with boron trichloride ( $\text{BCl}_3$ ) at 1450-2300 °C [171]. Other experiments have used  $\text{NH}_3$  and diborane ( $\text{B}_2\text{H}_6$ ) as precursors to deposit amorphous BN films less than 600 nm thick on Si, germanium (Ge), molybdenum (Mo), and tantalum (Ta) at temperatures ranging from 600 to 1000 °C [172]. Currently, researchers are working with precursors such as borane ( $\text{BH}_3$ ), trichloroborazine ( $\text{H}_3\text{B}_3\text{Cl}_3\text{N}_3$ ), hexachloroborazine,  $\text{BF}_3\text{-NH}_3$ ,  $\text{BCl}_3\text{-NH}_3$ , and  $\text{B}_2\text{H}_6\text{-NH}_3$  [1-3, 25-27].

The first hBN monolayer film was grown by the adsorption and decomposition of  $\text{B}_3\text{N}_3\text{H}_6$  on Pt(111) and Ru(0001) surfaces in 1990 [173].  $\text{B}_3\text{N}_3\text{H}_6$  can be compared to benzene in which the C atoms are substituted with alternate B and N atoms in a natural BN stoichiometry of 1:1. Therefore, there is no need for two or more gasses to grow hBN layers [1]. Vertically aligned hBN nano-sheets on Si substrate were grown at 800 °C from a mixture of  $\text{BF}_3\text{-N}_2\text{-H}_2$  gases using a microwave plasma CVD technique [136]. This produced protruding BN nano-sheets rather than uniform granular films. This was attributed to the strong etching effect of fluorine and the electrical field generated in the plasma. By manipulating the ratio and flow rates of  $\text{BF}_3$  and  $\text{H}_2$  the morphology and thickness of the hBNNSs could be controlled. Lateral dimensions varied between 80 nm to 2.9  $\mu\text{m}$  and thicknesses of approximately 60 layers. By decreasing the ratio of  $\text{BF}_3$  to  $\text{H}_2$ , to 2:30 the thickness of the nano-sheets was decreased by a factor of four. The control of the  $a$  direction growth is impressive, and would be particularly

useful in nano-electronic and nano-optic applications, however, the thickness of hBN sheets are no where near a monolayer.

Alternatively, a thermal CVD technique was developed in which B, magnesium oxide (MgO), and iron oxide (FeO) powders were heated up to 1300 °C in a tube furnace under NH<sub>3</sub> flow [135, 150]. As a result, vertically standing hBNSS were grown on Si/SiO<sub>2</sub> substrates with different sizes and morphologies, depending on synthesis temperature. As the temperature was increased from 1000 to 1200 °C, the nano-sheets increased in lateral size. As the temperature approached 1300 °C branching of the nano-sheets occurred on the main nano-sheet surface. Nano-sheets grown at higher temperatures had higher degrees of crystallinity. hBNSSs produced by this method had typical thicknesses of 5nm, and were polycrystalline in nature. Figure 2-11 illustrates the proposed model for two stage growth of hBNSSs.

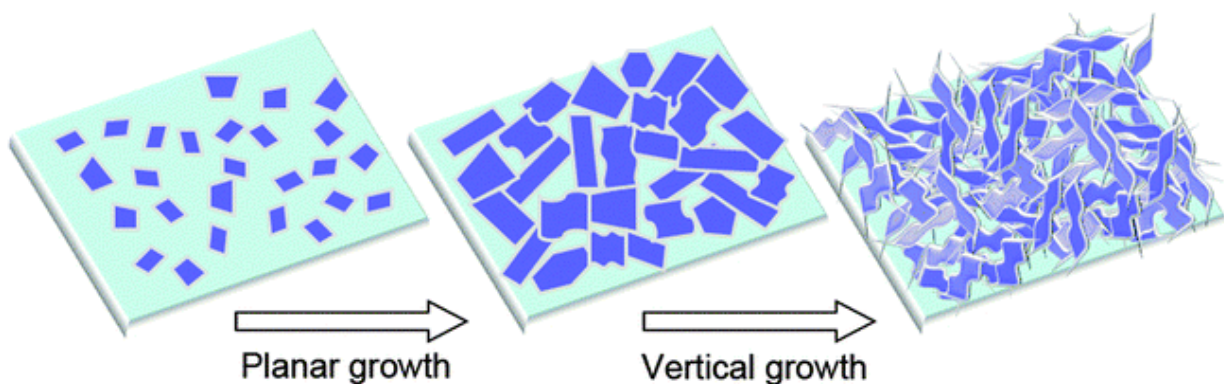


**Figure 2-11 A model illustrating the nucleation and two-stage growth of the BN nanosheets on the Si/SiO<sub>2</sub> substrate. (From Pakdel [137])**

As seen in Figure 2-11, first there is a stage of growth in which the base layers are parallel to the substrate. As the grain boundaries expand, sufficient levels of force curl the edges of the top layers upward producing vertically oriented nano-sheets. At these higher temperatures, adsorbed B and N atoms have a high mobility and can move along the surface towards the edge of the nano-sheet and then covalently bond with the edge of the hBN sheet, growing taller instead of

thicker [137, 150]. CVD methods are excellent in regard to controlling the thickness of hBNNSs, however, these methods are far better suited to thin film applications and can lack the structural integrity of hBN layers from a single crystal.

### ***Solid State Reactions***

Lian *et al.* [28] produced hBNNSs by a solid state reaction:  $NaBF_4 + 3NH_3 + 3NaN_3 \rightarrow BN + NaF + 3NaCl + 4N_2 + 3NH_3 + 3HF$ . The powders were mixed and pressed into pellets, then heated in an autoclave for 20 hours at 300 °C producing nanoflower-like nanoflakes. hBNNSs produced by this process measured only 300-400 nm laterally, with thicknesses of approximately 20 layers.

Few-layered hBNNSs with lateral dimensions over 100 μm have been produced by a chemical blowing technique that does not require a substrate or catalyst. Instead,  $NH_3BH_3$  is heated to 80 °C and then to 110 °C to begin the blowing process by dehydrogenization, and then the reaction mixture was raised to 400 °C to dehydrogenate. Hydrogen is rapidly released from the soft and swollen B-N-H compound. This is then heated to 1400 °C for three hours to crystallize the layers into the nano-sheet. Subsequent ultrasonication and centrifugation to remove bulky BN from the suspension yielded few layered polycrystalline hBN [29, 30].

### ***Substitution Reaction***

Substitution reactions have also been used in the synthesis of BN nano-sheets. This involves replacing an atom or functional group with another functional group or atom. One series of experiments utilizing this method involves heating  $B_2O_3$  powder to 1,650 °C in an open graphite crucible covered by  $MoO_2$  and graphene sheets under continuous flow of  $N_2$ . This product was collected from the graphene sheets and heated in air at 650 °C for 30 minutes to remove any residual C layers [31] producing hBNNSs between 15 and 4 layers with lateral

dimensions in the nanometer range. The layers are also polycrystalline with Raman FWHM greater than  $20 \text{ cm}^{-1}$ .

### ***High Energy Electron Irradiation***

High energy electron irradiation can be used to sputter layers off of layered materials inside a TEM. In this way, few layered nano-sheets, produced by mechanical cleavage of hBN powders, are thinned down to monolayers by carefully burning layer by layer with the electron beam [32, 33]. This has proved an excellent way to study hBN monolayers, but is tedious and unscalable as a means of producing hBNNSs.

### ***Unzipping Boron Nitride Nanotubes***

Nanotubes have been successfully unzipped to produce hBNNSs [174]. This process was inspired by the unzipping of carbon nanotubes. Argon etching was used to unwrap multiwalled hBN nanotubes [175]. Nanotubes were first deposited on a Si substrate and coated with a thin film of PMMA. This film was pulled off the substrate, taking hBN nanotubes with it. The bottom of the film was subject to Ar plasma etching for 100 seconds. One side of the hBN nanotube was protected by the polymer while the other side was cut in half by the plasma. The PMMA was removed by soaking the nanosheet in acetone ( $(\text{CH}_3)_2\text{CO}$ ). The resulting nanosheets were heated for 6 hours at  $600 \text{ }^\circ\text{C}$  in order to remove any residue or C contaminates. To further apply this technology progress must be made in the ability to control size, edge structure, layer number, and yields of hBN nanosheets. This method successfully created monlayer hBN, however the width of the sheets are typically only 15 nm, also the plasma cutting causes many defects.

### ***Chemical Exfoliation***

The prior methods suffer from low yields, production rates that are not technologically scalable

in their current form, poor crystallinity, the inability to produce a monolayer, damage and defect introduction, or extremely small lateral sizes. One possible solution is the exfoliation of layered compounds in liquids to give large quantities of dispersed nanosheets. This should allow for methods to obtain sizable quantities of 2D materials that can be processed by using existing industrial techniques. There are a number of methods to do this that involve oxidation, ion intercalation/exchange, or surface passivation by solvents. All result in liquid dispersions containing large quantities of nanosheets. This brings considerable advantages: liquid exfoliation allows the formation of thin films and composites, is potentially scalable, and may facilitate processing by using standard technologies such as reel-to-reel manufacturing.

Preparation of mono and few layered nanosheets from polycrystalline hBN by chemical solution was first accomplished in 2008 [176]. The hBN was placed in 5 mL of 1,2-dichloroethane solution of poly(*m*-phenyl-enevinylene-co-2,5-dictoxy-*p*-phenylenvinylene) in a 1.2mg/10mL ratio and sonicated for one hour to disperse and break up the hBN powder into few layered hBN. Since then, many solvents have been tested in order to increase nanosheet formation. One of these is N,N-dimethylformamide (DMF), a highly polar solvent, to interact with hBN surfaces. This yielded only milligram levels of pure nanosheets with thicknesses between 2 and 10 nm. Other organic solvents such as chloroform and 1,2-dichlorethane have been used which ensures simple and quick removal of the solvent [177].

Molten hydroxides have also been used to chemically exfoliate hBN. Sodium hydroxide, potassium hydroxide, and hBN powders were ground and then transferred to a polytetrafluorethylene lined stainless steel autoclave and heated at 180 °C for two hours. The exfoliation process is assumed to follow the following steps: 1.) cations adsorbing at the edges of the hBN surface resulting in self curling of the sheets, 2.) anions and cations enter the



interlayer space causing continuous curling of the BN layer, and 3.) direct peeling away from the bulk material caused by the surface reaction with hydroxides producing layers between 2-4 nm thick. This method has the advantage of being low cost, simple, and easily transferable to common solvents such as water and ethanol [178]. However, this method is ill-adapted toward the exfoliation of single crystal hBN.

The following methods reported for the chemical exfoliation of hBN were selected for further study as a way of exfoliating single crystals based on their ease of use, high yields, clean processing, and success in producing monolayers.

A low cost, facile method for chemical exfoliation of hBN was reported by Du *et al.* [163]. This method was adapted from Hummers' method of oxidation and exfoliation of graphite to graphene [179]. The exfoliation of hBN to few to single layer BNNSs was undertaken by combining hBN powder with  $\text{H}_2\text{SO}_4$  and  $\text{KMnO}_4$  while heating and the subsequent addition of  $\text{H}_2\text{O}_2$ . The proposed mechanism of exfoliation proceeds as: 1.) hydrogen ions from  $\text{H}_2\text{SO}_4$  intercalate into the layers of the hBN powder, enlarging the spacing between layers. 2.)  $\text{KMnO}_4$  reacts with  $\text{H}_2\text{SO}_4$ , forming  $\text{MnO}_2$  nanoparticles, now able to intercalate because of the enlarged layer spacing. These nanoparticles help to push apart and exfoliate the layers. 3.) Finally,  $\text{MnO}_2$  particles are removed by the addition of  $\text{H}_2\text{O}_2$ . The oxygen generated from the reaction may also contribute to the exfoliation by creating an outward pushing force. The resulting hBNNSs were small and transparent when compared to the original bulk hBN powder but the lateral dimensions remained in micro size as well as highly bending and scrolling. The thinnest observed BNNS was measured at approximately 1.44 nm by atomic force microscopy, corresponding to two layers of hBN. Advantageous aspects of this process are its facile nature, where high pressures, vacuum, or high temperatures are not necessary, as well as

wet chemical processing provides for easy scale up of the method.

Bhimanapati *et al.* [164] have implemented a similar method towards the chemical exfoliation of hBN. Where Du *et al.* [163] employed  $\text{H}_2\text{SO}_4$  as the acid in a modified Hummers' method, Bhimanapati utilized a 9 to 1 acid mixture of sulfuric and phosphoric acids. By employing an acid mixture of phosphoric and sulfuric acid instead of solely sulfuric acid, the reaction does not result in a large exotherm and produces no toxic gas [180]. Also, the addition of phosphoric acid increased the yield of hBNNSs over the previous method. Additionally, the acid mixture increases the hydrophobicity of hBN, creating improved stability and transparency in deionized water [180]. However, how the mechanism of exfoliation takes place is not postulated by the author. Further stated advantages of this method are lateral dimensions are maintained from the original hBN powder prior to exfoliation, as well as exfoliation efficiency up to 25% resulting in BNNSs between 1-4 layers thick. Reported drawbacks for this method are: bending and folding of hBN layers, as well as functionalization of the hBN with sulfur, requiring heat treatment for removal of the functional molecules.

Methanesulfonic acid (MSA) has been used as solvent for the liquid-phase exfoliation of hBN by Wang *et al.* [165]. Hexagonal boron nitride was dispersed in MSA for 8 hours under low power sonication, followed by centrifugation, and the resulting supernatant was removed. It is hypothesized that the repulsion between layers necessary to exfoliate the powder is due to the protonation of the hBN nanosheet edges and surfaces by the organic acid. The product was orange in color, which may be the result of charge transfer between the acid molecules and nanosheets [181]. As a result, the final concentration of hBNNS in MSA can be as high as 0.3 mg/ml after mild sonication. The hBNNSs collected from the hBNNS/MSA solution can be readily redispersed in a number of organic solvents. Once again, the lateral sizes of the

hBNNSs were reduced as compared to the original powder sizes. The authors report that the lateral size of the hBNNSs are typically less than 500 nm. Layers were also mechanically damaged by folding edges.

Liquid-phase exfoliation methods often employ chemical reagents that are harmful to the environment. Therefore, Li *et al.* [166] proposed a facile, eco-friendly exfoliation method, on the basis of the natural phenomena of freezing and thawing of soil. In the seasonal cycle, when spring comes after winter, the topsoil tends to become spongy because of the alternate freezing and thawing cycles. Water exhibits a minimum volume at 4 °C and will freeze below 0 °C during which the water molecules exhibit a honeycomb structure maximizing the volume of water thereby increasing the volume of soil. However, when the ice melts, the soil does not return to its original condition. By modeling this process, the exfoliation of hBN powder was demonstrated by utilizing the force of water expanding and contracting between layers of hBN. This was accomplished by cyclically freezing and thawing of hBN powder 4-12 times resulting in a yield of 0.120% of hBNNSs, The lateral sizes of hBNNSs average approximately 2 μm, where the thickness was determined to be 7 layers with a rough, bumpy morphology.

Lewis bases can be utilized to obtain water soluble hBN nanosheets. Lin *et al.* [167] have functionalized hBN powder with octadecylamine (ODA, CH<sub>3</sub>(CH<sub>2</sub>)<sub>17</sub>NH<sub>2</sub>), a long chain amine, forming complexes with the electron deficient B atoms of hBN. The reaction mixture is heated for 4-6 days under a N<sub>2</sub> atmosphere. After complexation, a solvent is added to the reaction mixture followed by sonication and centrifugation to separate the supernatant dispersion from the residue [182]. The authors claim that exfoliation efficiencies of this method are 10-20%. They report aggregation of the nanosheets as well as the eventual decomplexation of the amine. As such, the identification of free standing monolayers was difficult. Typical lateral

dimension was less than 100 nm, where the exfoliated sheets ranged from a few tens of nm to as large as over 1  $\mu\text{m}$ . Due to the excellent thermal stability and oxidation resistivity of hBN the functional groups were removed by heating the exfoliated sheets to 1000  $^{\circ}\text{C}$  in an inert atmosphere. The suspected mechanism of exfoliation involves complexation of the amine molecules and the hBN surface with partial intercalation; subsequent sonication in THF produced the force necessary to exfoliate the layers.

As a monolayer material, hBN exhibits many additional optical and electric properties that deviate from the bulk, which makes it attractive as a substrate in nanoelectronic device. Many methods have been discovered to produce few to monolayered hBN, however, many of these are actually pBN monolayers in the case of CVD growth, or come from hBN polycrystalline powders with small domains as with many of the chemical exfoliation methods listed above. Mechanical exfoliation is currently the best option for exfoliating a bulk crystal. Unfortunately, due to the chemical and structural nature of hBN (i.e lip-lip interactions, mechanically weak compared to graphene, etc.) mechanical exfoliation is physically limited and unable to produce monolayered hBN. Thus, a technique to exfoliate large domain, quality single crystals is desired in order to reach hBN nanosheet's full potential in electronic and optical nanodevices.

## Chapter 3 - Experiments and Analytical Tools

This chapter describes the apparatuses and procedures of each experiment followed by descriptions of the analytical tools used to characterize the results.

### Apparatuses

Boron nitride dissolution/precipitation experiments were conducted in a vertical resistively- heated tungsten furnace (Figure 3-1). This furnace was employed to reduce the potential for carbon contamination. The furnace, manufactured by Centorr Vacuum Industries, is water-cooled with maximum temperatures above 2000°C. It is equipped with both mechanical and diffusion vacuum pumps and a pyrometer temperature sensor. A programmable thermostat allowed for smooth control of set points and ramps.

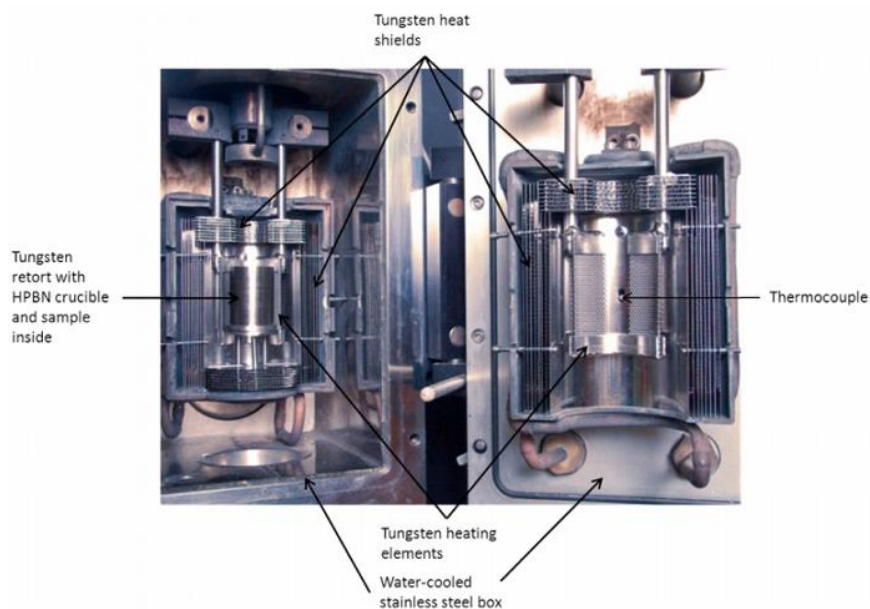


**Figure 3-1 Photo of the interior of the tungsten resistive element furnace with important features labeled.**

For the chemical exfoliation of hBN by functionalization of ODA, hBN powder and ODA was refluxed under  $N_2$  atmosphere. The solution was heated with reflux due to the extended period of time the solution was heated (4-6 days) so as to keep from losing ODA from

evaporation. Reflux of the solution required a special apparatus that consisted of a round bottom flask on a heater/stirrer, with N<sub>2</sub> gas flowing into the flask and out through a water-jacketed condenser. Figure 3-2 illustrates this apparatus.

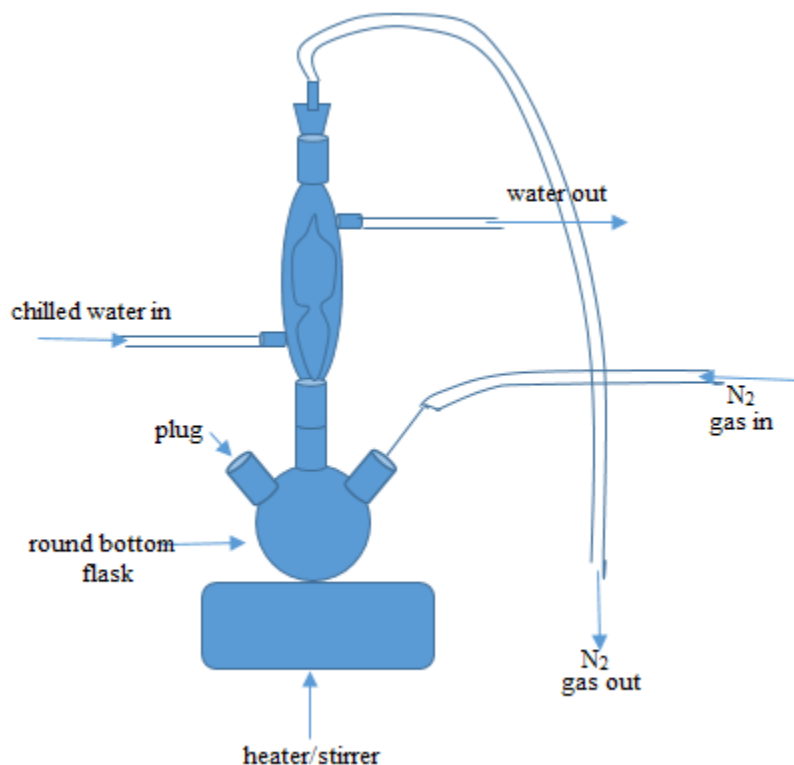


**Figure 3-2 Illustration of chemical exfoliation apparatus.**

## **Experiments**

### **Hexagonal Boron Nitride Crystal Growth Method**

In previous experiments, Hoffman *et al.* [22] showed that the largest hBN crystals are produced when the flux is prepared first, before attempting crystal growth. Hot pressed hBN crucibles (Momentive, HBC grade) were cleaned by sanding and polishing. Nickel and Cr powders were weighed out and mixed together in each crucible. The crucibles were placed into a large tungsten retort and loaded into the tungsten crystal furnace. The furnace chamber was pumped down to a pressure less than 1E-6 torr and back filled with nitrogen no less than four

times. The furnace was heated over six hours to approximately 1420 °C as read by an optical pyrometer. The temperature was held constant for 24 hours at a pressure of approximately 800 torr. Over 6 hours, the furnace was gradually cooled to room temperature, and the crucibles were removed and weighed. Next the flux was prepared for crystal growth. The resulting metal lumps were sanded and polished and any small residual metal balls were discarded. The crucibles were also sanded and polished before replacing the metal lumps and weighed once again. The purging process, as described above, was repeated. The stepped temperature process of each sample is described by Table 3-1 with the pressure at approximately 800 torr. Each experiment consisted of four steps. A step is defined by a ramp rate (hr), the time to reach a soak temperature (°C), and a soak time (hr) denoting the duration the furnace was held at the soak temperature. Each sample underwent the same first step, consisting of a ramp rate of 6 hr. to a soak temperature of 1410 °C and a soak time of 24 hr. Step two varied for each sample (Table 3-1). The ramp rate was varied from 1-7 hr. down to a soak temperature of between 1320 °C and 1394 °C for a soak time of 24 hr. Step three is consisted of a ramp rate of 0.5-1 hr. to a soak temperature between 1010 °C and 1050 °C and between 0-4 hr. In step four, each sample was ramped over 4 hr. to 20 °C and quenched.

### **Extraction of Hexagonal Boron Nitride Crystals from the Molten Metal Flux**

The goal of these experiments was to remove the metal flux from the crystals by separating the crystals from the liquid flux. A specialized crucible was created from a 1.5 inch diameter HPBN rod from Momentive (Figure 3-3). The crucible consisted of two pieces with one piece (1) nested inside of a larger piece (2). Crucible 1 was affixed to an elevator assembly that can move vertically in and out of the furnace hot zone, secured to the elevator with a length of molybdenum wire. A premelted metal flux was placed in crucible 1, which would fit inside

crucible 2, and both were placed in a tungsten retort. The tungsten resistive heating furnace was heated to maximum temperatures between 1500 and 1600 °C. The metal flux was slowly cooled to just above its eutectic point, approximately 1350 °C, at which point the elevator was activated and crucible1 was raised out of the heating zone and the melt, still in liquid phase, was drained away from the crystals into crucible.

**Table 3-1 Furnace parameters for stepped temperature crystal growth.**

| Step | Action                | Sample |      |      |      |      |
|------|-----------------------|--------|------|------|------|------|
|      |                       | 1      | 2    | 3    | 4    | 5    |
| 1    | Ramp Rate (hr.)       | 6      | 6    | 6    | 6    | 6    |
|      | Soak Temperature (°C) | 1410   | 1410 | 1410 | 1410 | 1410 |
|      | Soak Time (hr.)       | 24     | 24   | 24   | 24   | 24   |
| 2    | Ramp Rate (hr.)       | 1      | 7    | 4    | 3.5  | 5.25 |
|      | Soak Temperature (°C) | 1320   | 1375 | 1394 | 1375 | 1375 |
|      | Soak Time (hr.)       | 24     | 24   | 24   | 24   | 24   |
| 3    | Ramp Rate (hr.)       | 0.5    | 1    | 1    | 1    | 1    |
|      | Soak Temperature (°C) | 1010   | 1040 | 1050 | 1050 | 1050 |
|      | Soak Time (hr.)       | 4      | 0    | 0    | 0    | 0    |
| 4    | Ramp Rate (hr.)       | 4      | 4    | 4    | 4    | 4    |
|      | Soak Temperature (°C) | 20     | 20   | 20   | 20   | 20   |
|      | Soak Time (hr.)       | 0      | 0    | 0    | 0    | 0    |



The furnace was cooled to room temperature and crucible1 was removed from the elevator assembly.

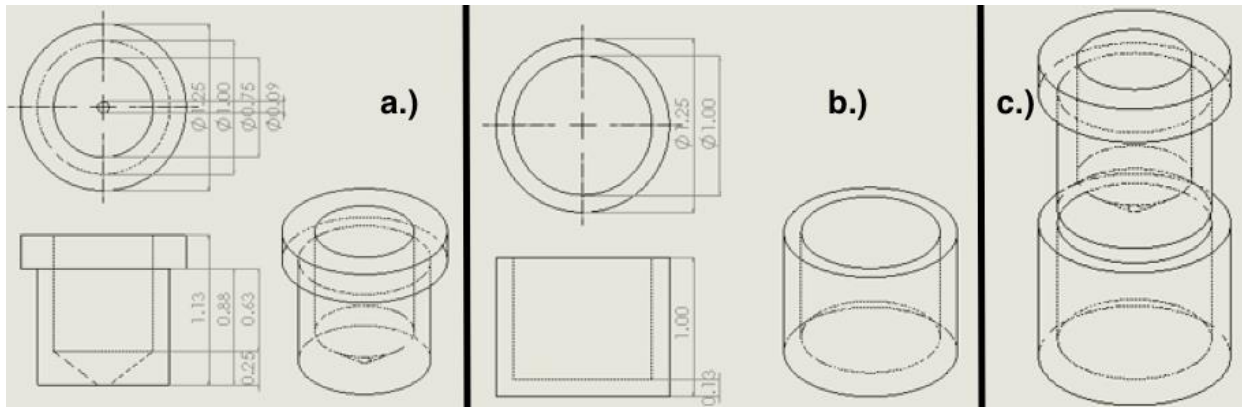


**Figure 3-3 Design of “nested” HPBN crucibles for crystal extraction. a) crucible 1 (top crucible). b) crucible 2 (bottom crucible). c) combined crucibles.**

### **Boron Isotope Enrichment**

The typical process used to grow hBN crystals utilizes hot pressed boron nitride as a crucible. During crystal growth, a portion of the hBN crucible dissolves into the metal flux since the HPBN is the B source, with a natural abundance, producing hBN crystals which contain both  $^{10}\text{B}$  and  $^{11}\text{B}$  isotopes. To eliminate this isotope dilution, different materials were tested as crucibles for enriched growth. Materials tested were yttria, yttria-stabilized zirconia, and alumina. The reactivity of these material with the metal flux were tested by filling the crucibles with premelted mixtures of nickel, chromium, and boron. This was heated in a horizontal tube furnace to 1500 °C at 200 °C/hr and maintained for 12 hours followed by cooling to room temperature at 200 °C/hr. The solid metal flux was removed from the crucible, and Raman spectroscopy was performed on each crucible and compared to its pristine spectra.

hBN crystals with  $^{10}\text{B}$  enrichment were grown from a metal flux of 48% Ni, 48% Cr, and 4%  $\text{B}^{10}$  by weight respectively. The reaction vessel was an alumina crucible from Almath

Crucibles. The reaction was performed in a Centorr model M60 resistance heating, 2"x3" hot zone furnace under nitrogen atmosphere.

Before heating, three cycles of evacuations and nitrogen purges were performed, with all three evacuations being  $< 1 \mu\text{Torr}$ . The furnace was operated slightly above atmospheric pressure (780 to 800 torr). Each sample was heated for over six hours and held at a maximum temperature of  $1580^\circ\text{C}$  for 24 hours. This temperature is higher than was typically used with HPBN crucibles was as the B source. The reaction mixture was subsequently cooled to  $1340^\circ\text{C}$  at a rate of  $4^\circ\text{C/hr}$  at which point the furnace was cooled to room temperature over 6 hrs. Crystals from each sample were transferred from the metal flux using thermal release tape. These were heated on a hot plate at  $200^\circ\text{C}$  for approximately 15-20 minutes with subsequent sonication in acetone. The tape was then rinsed with acetone and removed while the crystals were filtered from the acetone. Crystals were brushed off the filter paper into an alumina crucible using a paint brush and the crystals were heated in air for 30 minutes at  $500^\circ\text{C}$  to remove any remaining adhesive or solvent. Raman spectroscopy was conducted on each sample.

### **Exfoliation of Hexagonal Boron Nitride**

Several different methods, from the literature were tested on hBN powder in order to find an appropriate method for the exfoliation of a single crystal.

#### ***Adapted Hummers' Method***

In a typical experiment, 1 g of BN powder, and 25 mL of concentrated sulfuric acid ( $\text{H}_2\text{SO}_4$ ) were mixed and stirred. Then, 0.5 g of potassium permanganate ( $\text{KMnO}_4$ ) was added slowly to the solution with stirring and the reaction vessel was immersed in an ice bath. After this, the suspended solution was stirred continuously for 12 h. Subsequently, 10 mL of hydrogen peroxide ( $\text{H}_2\text{O}_2$ ) (30%, w/w) was added into the suspension. Finally, the resulting suspension

was centrifuged at 3450 rpm for 10 min in order to remove unexfoliated hBN. The supernatant was filtered and washed with deionized water (DI water) to remove metal ions until the pH value of the filtrate was 7. The final products were dried in a vacuum oven at 100 °C for 24 h.

#### ***Adapted Hummers' Method Acid Mixture***

To synthesize mono- and few-layer hBN, 1 g of hBN powder was mixed with 6 g of  $\text{KMnO}_4$  in a 1 L glass beaker. An acid mixture of 135 mL was prepared separately by mixing phosphoric acid ( $\text{H}_3\text{PO}_4$ ) and  $\text{H}_2\text{SO}_4$  in the 1: 8 ratio and was added to the hBN powder. The resultant reaction is slightly exothermic, leading to a temperature rise in the solution to 40 °C. The solution was then heated on a hot plate to 75 °C under constant mixing for 12 hours. Subsequently, 6 mL of  $\text{H}_2\text{O}_2$  and 120 mL DI water were added to this mixture to halt the oxidation. The resultant suspension was cooled to room temperature and centrifuged at 3450 rpm for 45 minutes, and the supernatant was pipetted out from the solution. Subsequently, 45 mL DI water was added to this solution and centrifuged again at 3450 rpm. The non-exfoliated material was removed during the centrifugation and the supernatant solution was then subjected to a series of washing and centrifugation stages with DI water, ethanol and HCl. These washings were performed until a pH >3 was reached, which ensures the complete removal of the metal ions. The supernatant solution was then drop-cast on Si wafers and dried to obtain the exfoliated and functionalized hBN sheets.

#### ***Exfoliation by Methanesulfonic Acid (MSA)***

The hBN powder (0.2 g) was dispersed in 100 ml of MSA in a sealed bottle at an initial concentration of 2 mg/mL. The mixture was then subjected to sonication for 8 hr, followed by centrifugation at 3450 rpm for 90 min resulting in an orange supernatant. The sediments, after centrifugation, were washed with water several times, and collected by filtration.

### ***Intercalation of Water Molecules***

One gram of hBN powder was added to a plastic container and the residual volume of the container was filled with distilled water. The dispersion was shaken well, to ensure the effective blending of hBN powder with the added water. The sample was then refrigerated at 4 °C for 24 h. Following that, the sample was immediately transferred to a freezer with a temperature less than -20 °C. The system was maintained at this temperature for 24 h and then restored to 4 °C naturally. This process was repeated four times. Subsequently, the as-obtained samples were sonicated for 10 min. The suspension of exfoliated hBN nanosheets was finally obtained after equilibration for 24 h to allowing the unexfoliated hBN powder to fall out of solution.

### ***Functionalization by ODA***

In a typical experiment using octadecylamine (ODA) to functionalize and exfoliate hBN, the hBN powder (1 g) and ODA (10 g) were mixed in a round-bottom flask and heated to ~160-180 °C for 4-6 days under a steady nitrogen flow. After cooling the reaction mixture to room temperature, THF (~100 mL) was added. The slurry was briefly sonicated and centrifuged (3450 rpm, 10 min), and the supernatant was collected. The extraction cycle was repeated 5 to 8 times on the residue from the centrifugation, and the supernatants were combined as the THF dispersion of the final product ODA-functionalized hBN (or ODA-BN).

**Table 3-2 List the materials used in each experiment, their source, and purity.**

| Experiment  | Materials                      | Source                     | Purity    | Misc.       |
|---|--------------------------------|----------------------------|-----------|-------------|
| Hexagonal Boron Nitride                               | HPBN Crucible                  | Momentive                  | HBC Grade | -           |
| Crystal Growth Method                                 | Ni Powder                      | Alfa Aesar                 | 99.7%     | 50+100 Mesh |
|   | Cr Powder                      | Alfa Aesar                 | 99%       | -100 Mesh   |
|   | N <sub>2</sub> (g)             | Matheson TRIGAS            | UHP       | -           |
| Exfoliation of Hexagonal Boron Nitride                | BN Powder                      | Momentive                  | Nx1       | -           |
|   | KMnO <sub>4</sub>              | Fisher Scientific          | 99.2%     | -           |
|   | H <sub>2</sub> SO <sub>4</sub> | Macron Chemicals           | 95%       | -           |
|   | H <sub>3</sub> PO <sub>4</sub> | Fisher Scientific          | 85%       | -           |
|   | H <sub>2</sub> O <sub>2</sub>  | Fisher Scientific          | 30%       | -           |
|   | MSA                            | Acros Organics             | 99%       | -           |
|   | ODA                            | Acros Organics             | 90%       | -           |
|   | THF                            | Acros Organics             | 99.5%     | -           |
| Extraction of Hexagonal Boron Nitride From Metal Flux | HPBN Crucible                  | Momentive                  | HBC Grade | -           |
|   | Ni Powder                      | Alfa Aesar                 | 99.7%     | 50+100 Mesh |
|   | Cr Powder                      | Alfa Aesar                 | 99%       | -100 Mesh   |
|   | N <sub>2</sub> (g)             | Matheson TRIGAS            | UHP       | -           |
|   | Mo Wire                        | ESPI Metals                | 3N8       | -           |
| Boron Isotope Enrichment                              | Alumina                        | Almath Crucibles           | 99.8%     |             |
|   | Ni Powder                      | Alfa Aesar                 | 99.7%     |             |
|   | Cr Powder                      | Alfa Aesar                 | 99%       |             |
|   | N <sub>2</sub> (g)             | Alfa Aesar Matheson TRIGAS | UHP       |             |
|   | <sup>10</sup> B                | 3M Ceradyne                | 99.14%    | 99.22 At%   |

## **Analytical Tools**

### **Scanning Electron Microscopy (SEM) and Energy –Dispersive X-ray Spectroscopy (EDS)**

Scanning electron microscopy (SEM) generates high-resolution images by directing an electron beam towards a sample and resolving an image by detecting electrons emitted from the sample [183]. SEM has a bevy of quantitative and qualitative analytical tools, as well as a higher resolution than is possible with an optical microscope. Two primary types of electrons are detected from a sample: secondary and backscattered electrons. Secondary electrons are utilized for fine topographical imaging at the sample's surface. Backscattered electrons can be used to distinguish regions with different compositions; these electrons scatter in proportion to an atom's atomic number providing contrast in light and heavy atoms. Figure 3-4 presents the important features of SEM. The electron beam, accelerating at up to 30 kV, is directed at a sample causing electrons in the inner shell of the sample atoms to be detected. As a result, electrons from the outer (high energy) shells replaces the electron ejected from the inner shell (low energy). A characteristic X-ray is emitted when this happens. Each element has a unique energy associated with it and this can be measured by energy-dispersive X-ray spectrometry (EDS) to determine the abundance and type of elements in the sample. This research was conducted with a FEI Nova NanoSEM 430 with Oxford X-Max Large Area Analytical EDS silicon drifter detector (SDD) (80 mm<sup>2</sup>). This instrument is capable of accelerating voltages between 1-30 kV with a resolution of 0.8 nm at 30 kV. Detectors included with this instrument are: Everhart-Thornley detector (ETD), through the lens detector (TLD), low voltage high contrast detector (vCD), and low vacuum detector (LVD). ETD and TLD detectors are standard detectors in SEM systems, however, when samples do not conduct electrons well, vCD and LVD detectors may be

necessary. Because of its large bandgap, hBN tends to build up charge due to continuous electron bombardment. In this case, a small amount of water vapor can be used to dissipate the charge and the LVD detector must be used.

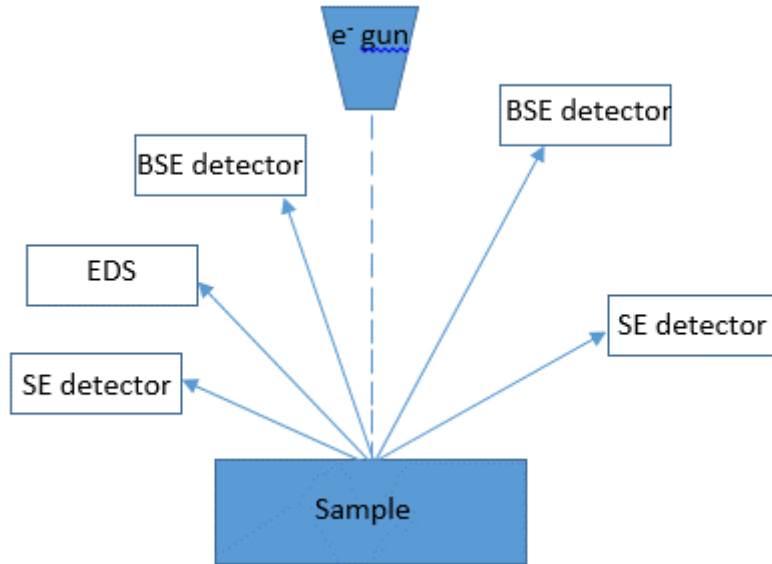


**Figure 3-4 Schematic of SEM**

### **X-ray Diffraction (XRD)**

X-ray diffraction (XRD) is the preliminary nondestructive technique in the investigation of crystal structures [184]. XRD was used to determine the phase of BN present in samples. This technique involves directing x-rays onto a sample and detecting diffracted x-rays exiting the sample. X-rays reflect off individual atoms from different atomic planes and some incident angle  $\theta$ . When x-rays travel an integer multiple of the wavelength between planes, constructive interference results in a high x-ray intensity that appears as a peak in the XRD spectrum. The angle,  $\theta$ , at which this interference occurs along with the x-ray wavelength,  $\lambda$ , and spacing,  $d$ , between the planes of atoms are related by Bragg's law,  $n\lambda=2d\sin\theta$ . Here,  $n$  is the order of the diffraction but is typically included in reported  $d$ -spacings. By changing the angle between the

sample and the x-ray source for which the wavelength is known, the angles of the peaks in the spectrum correspond to ordered planes of the material with atomic spacing,  $d$ , calculated by Bragg's law. XRD spectra for this research came from a Rigaku MiniFlex II powder x-ray diffractometer with a Cu K $\alpha$  x-ray source ( $\lambda=0.154056$  nm). Raw data obtained was analyzed by PDXL x-ray diffraction software to identify diffraction peaks and match to ICDD PDF card data.

### **Raman Microscopy**

Raman microscopy elucidates chemical information of a sample from its lattice vibrations. A sample is hit with incident single wavelength light from a laser, and the light given off by the sample is detected. Light incident on a solid is mostly reflected without a change in frequency,  $\nu_0$ , however a small amount of light will be scattered at a slightly different frequency,  $\nu_0 \pm \nu$  [185]. This change in frequency is known as Raman scattering. Vibrational modes in a solid give off a characteristic Raman scattering. The shift in frequency resulting from Raman scattering is only detected when the incident light induces a change in the polarizability of the solid. Any vibrational mode, not associated with this change in polarizability will not be detected and is hence Raman inactive. Raman spectra are unique to each compound and as such can be used to distinguish the structure of a material. Hexagonal boron nitride can thus be distinguishable from cBN by its Raman spectra by peak position. Furthermore, the quality of a crystal sample is indicated by the full-width half-maximum (FWHM) of a Raman peak. FWHM of pBN is approximately  $20 \text{ cm}^{-1}$  where single crystal hBN is less than  $10 \text{ cm}^{-1}$ . Defects in a crystal cause bonds to be either compressed or stretched which leads a widening of a peak meaning the sharper a Raman peak, the more pristine the crystal sample. A Raman shift of  $1366 \text{ cm}^{-1}$  is widely reported as the fundamental  $E_{2g}$  vibrational mode of a hBN and is the only observable Raman-active mode in hBN.



## **Fourier transform infrared spectroscopy (FTIR)**

Fourier transform infrared spectroscopy (FT-IR) obtains an infrared spectrum of absorption or emission of a solid, liquid or gas. FT-IR was used in this research to determine chemical composition of chemically exfoliated hBN. An FT-IR spectrometer simultaneously collects high spectral resolution data over a wide spectral range.

Fourier transform spectroscopy is a faster, more sensitive method to collect IR spectra. Rather than using a monochromatic beam of light, light containing many frequencies is incident on the sample and measures how much of that beam is absorbed. Next, the beam is modified to contain a different combination of frequencies, giving a second data point. This process is repeated many times. Afterwards, a computer takes all these data and works backwards to infer the absorption at each wavelength. The beam described above is generated by starting with a broadband light source, one containing the full spectrum of wavelengths to be measured. The light shines into an interferometer, a certain configuration of mirrors, one of which is moved by a motor. As this mirror moves, each wavelength of light in the beam is periodically blocked, transmitted, blocked, transmitted, by the interferometer, due to wave interference. Different wavelengths are modulated at different rates, so that at each moment, the beam coming out of the interferometer has a different spectrum. The processing required turns out to be a common algorithm called the Fourier transformation. The raw data is sometimes called an "interferogram".

The interferogram has to be measured from a zero path difference to a maximum length that depends on the resolution required. The interferogram is converted to a spectrum by Fourier transformation. This requires the interferogram to be stored in digital form as a series of values at equal intervals of the path difference between the two beams. To measure the path difference

a laser beam is sent through the interferometer, generating a sinusoidal signal where the separation between successive maxima is equal to the wavelength. The result of Fourier transformation is a spectrum of the signal at a series of discrete wavelengths. The range of wavelengths that can be used in the calculation is limited by the separation of the data points in the interferogram [185].

A Thermo Nicolet Nexus 670 FT-IR was employed in this study with an EverGlo source operating in the mid IR region (5000-400  $\text{cm}^{-1}$ ).

## Chapter 4 - Results and Discussion

### Hexagonal Boron Nitride Crystal Growth Method

A stepped cooling process was studied with the goal of optimizing hBN single crystal growth in the lateral,  $a$ , and perpendicular plane,  $c$ , directions. The set of five experiments produced triangular crystals which differed in the quality, quantity, and geometry of crystals. Besides hBN crystals, all samples exhibited pink crystals, which were chromium oxide, as determined by EDS. All samples exhibited pyramid-like crystal growth (Figure 4-1). The top side of the cooled metal flux had mostly amorphous hBN with some flat hBN crystals of varying size on top. Most of the pyramid-like hBN crystal were formed on the sides of the metal flux. It is hypothesized that in solution growth of hBN single crystals, the lateral size of the crystals is a strong function of the soak temperature. The higher the dwell temperature, the larger the crystal width [22], however there is a trade off in the thickness of the crystals. The crystal thickness is believed to be strongly dependent on the cooling rate [22]. However, it is hypothesized that by slowly cooling the solution from a high temperature ( $>1400$  °C) and cooling slowly ( $4-90$  °C/hr) over a small time period of time, followed by dwelling at that temperature for an extended period of time, would allow for large growth in both the  $a$  and  $c$  directions of the crystal structure. Table 3-1 summarizes the growth conditions for each sample in the four step process. The largest average crystal width was  $174.0$   $\mu\text{m}$  produced by sample 3. The conditions from which these crystals were grown was a step two soak rate of 4 hr to  $1394$  °C and a step 3 soak rate of 1 hr to  $1050$  °C. A minor trend occurred where the crystal width increased with increasing soak temperature in step two. The largest average crystal thickness was  $17.4$   $\mu\text{m}$ , produced by sample 3. The trend in crystal thickness did not follow the trend in lateral thickness. The thickest average crystals were grown with a median step two soak temperature. A trend did appear in

crystal thickness where the slowest cooling rate produced the largest average crystal thickness. These trends, coupled with the fact that the thickest and widest crystals on average came from sample three suggests that a stepped temperature growth may allow the crystals to be grown with large lateral dimensions while maintaining crystal thickness. However, while the average crystal thickness and width were maximized by the stepped temperature process, crystals grown in this series of experiments were not larger overall than those reported by others who employed the Ni-Cr solution method. Hoffman *et al.* [22] have reported crystals of 1-5 mm in the *a* direction and thicknesses of approximately 500  $\mu\text{m}$ . The stepped temperature process employed here yielded crystals on the order of 100-500  $\mu\text{m}$  across with typical thicknesses of approximately 10-30  $\mu\text{m}$ , as measured by SEM. However, the strange geometries present in crystals grown from this method are intriguing. Apparently, the high temperature growth produced large lateral sized crystals, but the nonlinear cooling of the stepped temperature growth procedure induced crystal orientations with the *a* direction growing mostly vertical at angles merging into each other producing the pyramid-like geometries observed in Figure 4-1.



**Figure 4-1** Sample 1 from stepped temperature growth experiments. Crystals grown vertically, merging into each other to create pyramid like morphologies.

## Extraction of Hexagonal Boron Nitride from the Molten Metal Flux

The solution growth of hBN in the Ni-Cr solvent system occurs with the supersaturation of dissolved hBN. The low density, solid hBN floats to the top of the liquid solvent system, where it nucleates and continues to grow. It was the intent of this experiment to allow crystals to form and grow on top of the liquid solvent. After an appropriate growth period, the solvent is removed, thus leaving the crystals free and undamaged. This process has proved promising for the extraction of crystals from the metal solvent, which eliminates the problem of mechanical breakage by the cooling metal or by extraction with thermal release tape. Figure 4-2(a) shows the result of a typical process of crystal growth and extraction. A premelted metal flux of hBN-Ni-Cr was heated to between 1500 and 1600 °C and soaked for 24 hr. This was followed by slow cooling at 4 °C/hr to a temperature of 1350 °C and dwelling at this temperature for 12-24 hr at which time the crystal pulling mechanism of the furnace was activated pulling up crucible 1, draining the molten metal flux into crucible 2. At this point, the furnace was cooled to room temperature over 6 hr.

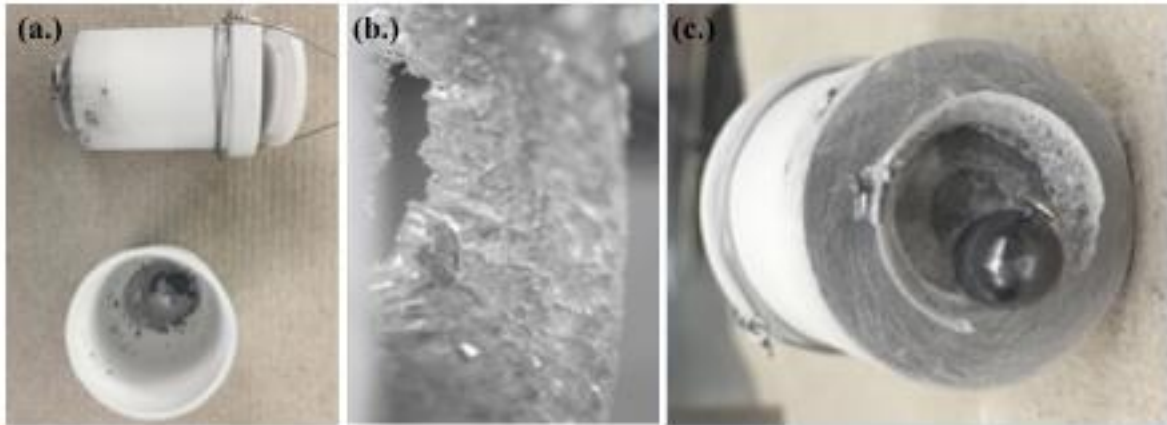


**Figure 4-2 (a) Crucibles 1 (Top) and 2 (Bottom) after typical crystal extraction. (b) Magnification of crystal “halo”. (c) View of “halo” crystals and metal still attached to the bottom of crucible 1.**

Clearly, the metal flux was transported to the bottom crucible 2 by raising the top crucible 1. Above crucible 2, the top crucible, crucible 1 can be seen. At the bottom of 1, a “halo” of hBN crystals formed, with a small amount of metal solution inside of the crystal “halo”

Figure 4-2(b) is a macro photograph of the hBN crystal “halo”. It consists of a large number of crystals with many different orientations and grain sizes. These crystals have unique geometries, slightly resembling a circuit board (Figure 4-3). In addition to the equilateral triangles, the crystals have rhombus-shaped patterned pits. Most importantly, the crystals were not cracked. Therefore, it can be inferred that by removing the crystals from the metal solvent system before the metal solidified, mechanical stresses that often damages the crystals may be avoided.

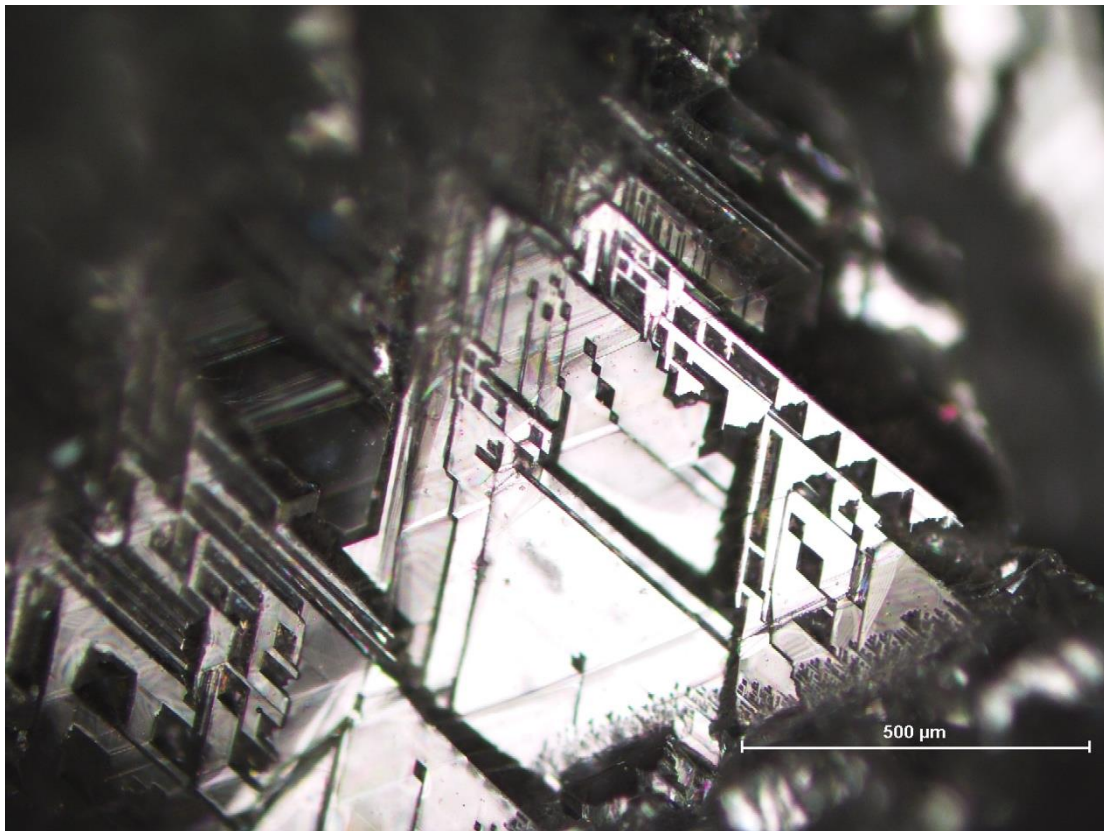


**Figure 4-3 Close up of crystal “halo” with many different crystal geometries and orientations.**



These results are encouraging: the basic process of separating the liquid melt from hBN crystals *in situ* diminishes crystal cracking due to the differences in thermal expansion of the metal flux and hBN and from mechanical stresses by removal with thermal release tape. However, this process is not without problems. The hBN crystals were connected to the bottom of crucible 1 in a concave shape (Figure 4-2(c)), whereas the ideal outcome would be a flat sheet of crystals inside of crucible 1. The presence of the crystals on the bottom of crucible 1 suggests that the liquid metal is behaving in one of two ways during the process. While the solution is dwelling in the furnace, metal solvent is leaking in between the two crucibles and forming crystals on the bottom of crucible 1; or the metal solvent has a high affinity toward the HPBN and when the top crucible is raised, the metal solvent does not drain, and the crystals form on top of the metal while it cools as it leaves the heating zone. Due to the absence of cracking in the crystals that is normally seen when the system is cooled with crystals on the metal, especially on curved metal surfaces (Figure 4-4), the former option seems most probable.

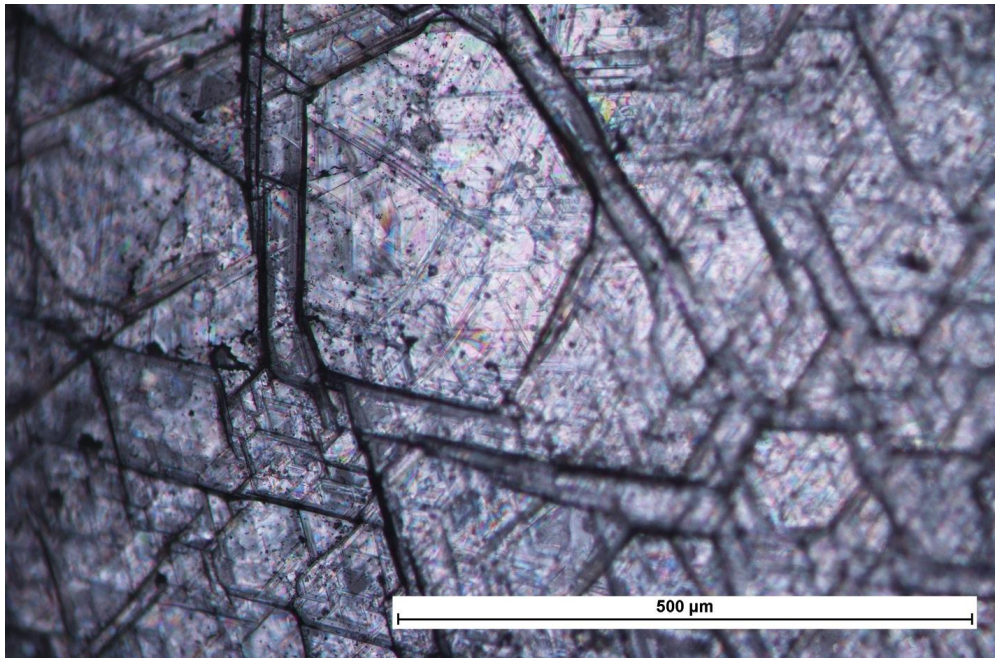


**Figure 4-4 Cracked crystals embedded in metal flux.**

## Boron Isotope Enrichment

Hexagonal boron nitride crystals were grown with enriched B concentrations of  $^{10}\text{B}$ . The observed crystals were optically transparent and water clear. The crystals were grown by premelting a mixture of Ni, Cr, and B powders at a wt % of 48, 48, and 4 %, respectively, where the B powder contained 99.14 wt %  $^{10}\text{B}$ . The premelt was performed by heating the powder mixture in an alumina crucible to 1600 °C over 6 hr and soaking for 24 hr in an  $\text{N}_2$  atmosphere, followed by cooling over 6 hr to room temperature. The resulting solid flux was polished and returned to a clean alumina crucible. The furnace was heated to 1600 °C and soaked at this temperature for 24 hr. and cooled to 1400 °C at a cooling rate of 4 °C/hr, followed by cooling to room temperature over 6 hr. The geometries of the crystals were similar to those typically seen from the Ni-Cr solution method, however grain sizes were between tens to hundreds of microns as seen in Figure 4-5 where typical crystals from the Ni-Cr solution method are the order of hundreds to thousands of microns.

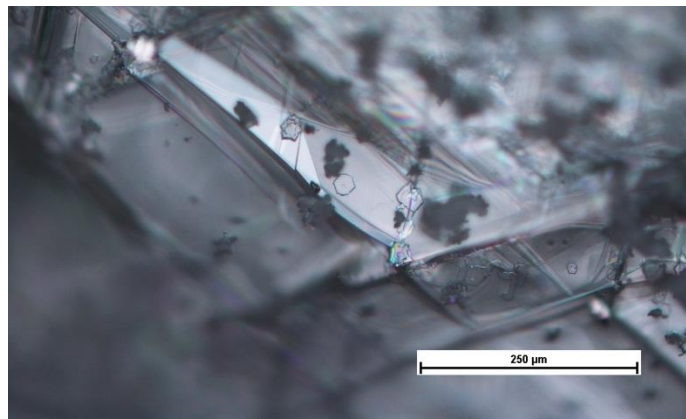


**Figure 4-5 Typical crystals grown from Ni-Cr solution method with enriched  $^{10}\text{B}$ .**

The typical process used to grow hBN crystals utilizes hot pressed boron nitride as a crucible as well as the hBN source. Since HPBN is only available with a natural distribution of boron it cannot be used to produce hBN that is isotopically pure. As the crucible dissolves, it



dilutes the boron in the flux with both  $^{10}\text{B}$  and  $^{11}\text{B}$ . To control the boron isotope content, different materials were tested as crucibles for enriched growth. Materials tested were yttria, yttria-stabilized zirconia, and alumina. Crucibles were tested for reactivity with the metal flux by melting the flux at the same conditions hBN crystals were grown using HPBN crucibles. The crucibles were filled with premelted metal flux of BN-Ni-Cr. This were heated in  $\text{N}_2$  atmosphere to  $1500\text{ }^\circ\text{C}$  at a rate of  $200\text{ }^\circ\text{C/hr}$  and held constant for 12 hr followed by cooling at  $200\text{ }^\circ\text{C/hr}$  to room temperature. All crucibles experienced a color change of some kind (Figure 4-6) but did not show any structural damage or wetting by the metal solution. Raman spectra revealed that alumina and yttria did not affect the boron composition. Due to its ease of use and relatively low cost, alumina was chosen as the crucible materials.

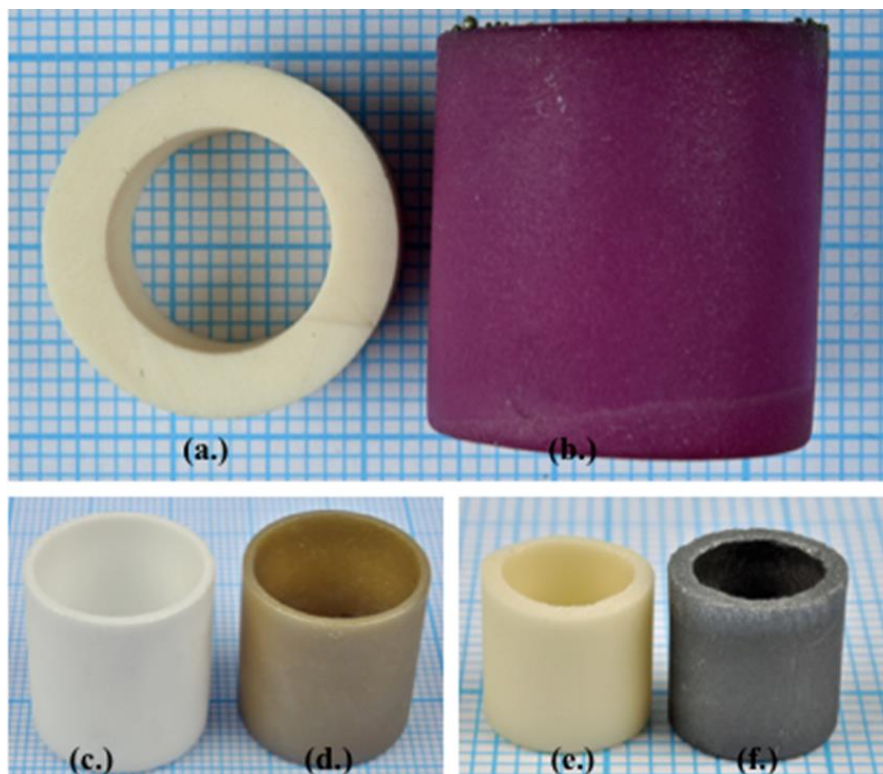


**Figure 4-6 Crucibles before and after testing for enriched growth compatibility. (a) and (b), before and after alumina. (c) and (d), before and after yttria-stabilized zirconia. (e) and (f), before and after yttria.**

Hexagonal boron nitride crystals were produced with boron concentrations of  $^{10}\text{B}$  enrichment above 96% respectively according to Raman spectroscopy measurements. An hBN crystal with natural abundance B will have a Raman signature at approximately  $1366\text{ cm}^{-1}$ . By increasing the atomic percent of  $^{11}\text{B}$  above that of naturally occurring boron in hBN a red shift is seen in the Raman spectra. The red shift is due to an increase of mass in the crystal lattice by the addition of  $^{11}\text{B}$  atoms. On the other hand, the Raman peak will blue shift when the atomic percent of  $^{10}\text{B}$  is increased above natural abundance in the hBN crystal.  $^{10}\text{B}$  atoms replacing  $^{11}\text{B}$  in the lattice structure induces a larger frequency leading to an increase in Raman shift. The atomic composition of enriched crystals was measured by SIMS. By correlating the isotope concentration from SIMS data with the Raman peak position a calibration curve was created (Figure 4-7).

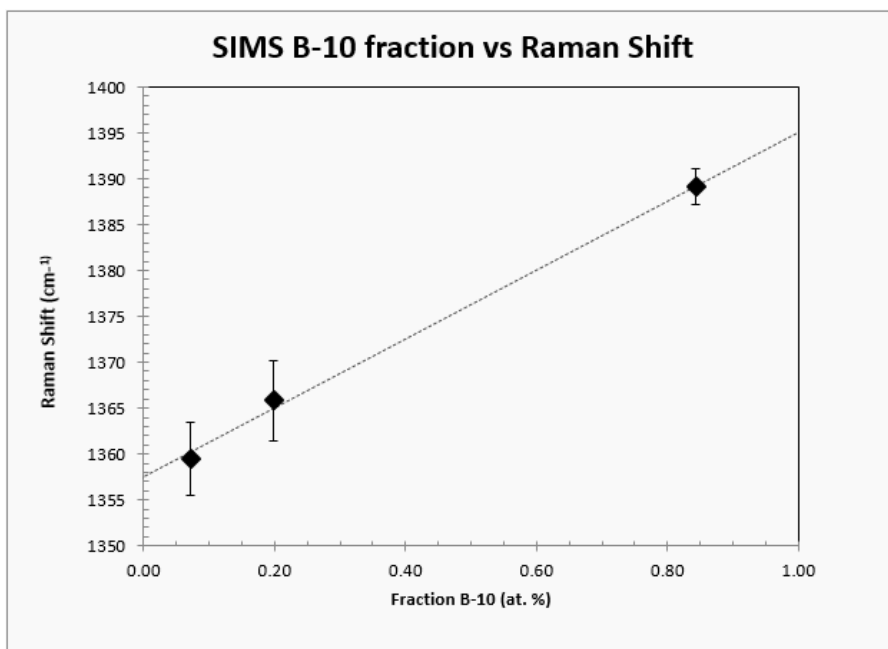


**Figure 4-7 Calibration curve relating boron enrichment to Raman shift in hBN crystals. (From Hoffman [117])**

From this curve, the percent atomic enrichment of B in hBN crystals can be estimated by the Raman shift of the sample. This can be seen by Figure 4-8, which shows the Raman spectra of

hBN crystals grown from natural abundance boron and those grown with 99%  $^{10}\text{B}$  sources. Here the blue shift of the enriched hBN crystals can be obviously seen from those of natural abundance boron. By using the quasi-calibration curve, these hBN crystals are estimated to have isotopic enrichment of 94% (green) and 96% (blue)  $^{10}\text{B}$  enrichment.

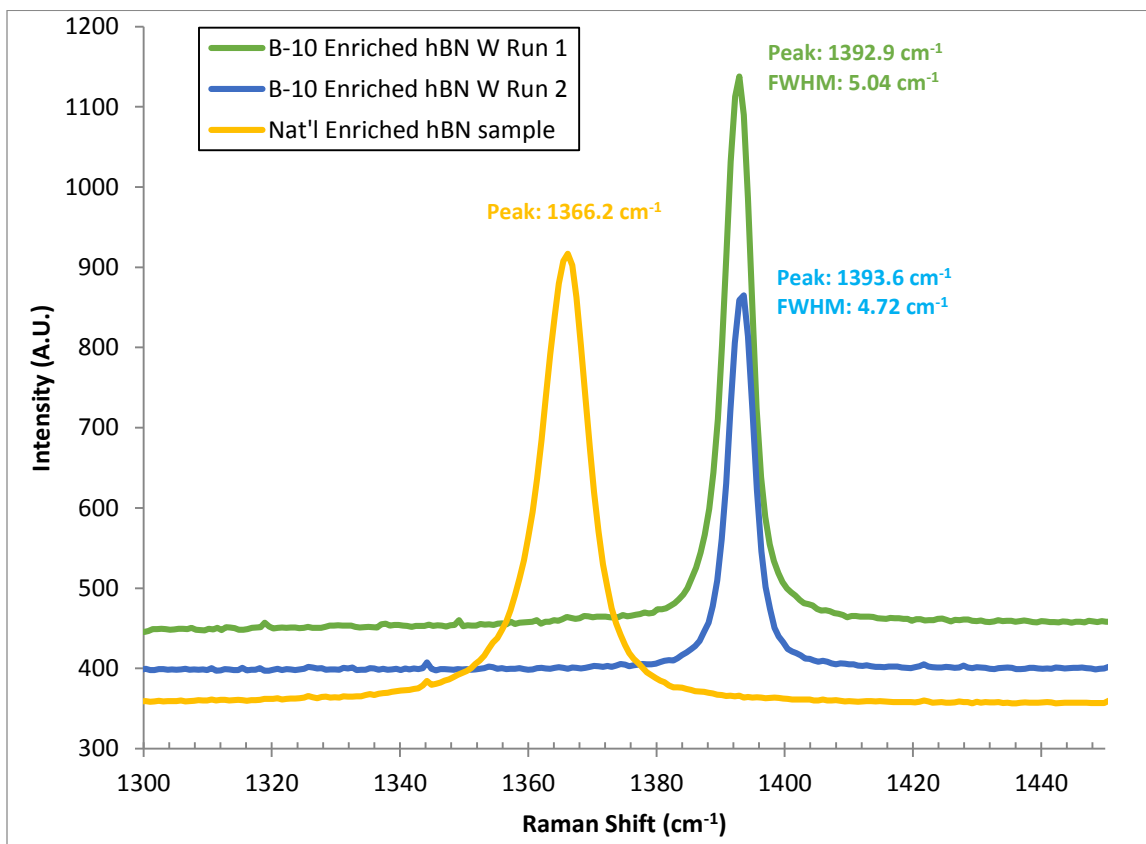


**Figure 4-8 Raman Spectra of natural abundance boron in hBN crystals compared to blue shift of  $^{10}\text{B}$  enriched hBN crystals.**

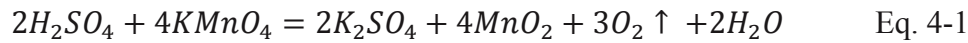
These results are a large step forward toward a handheld neutron detector. With such a high percentage of  $^{10}\text{B}$ , a crystal size capable of the proper neutron capture cross-section and electronic transport properties may currently be achievable using the Ni-Cr solution method.

### Hexagonal Boron Nitride Exfoliation

The following methods for exfoliating hBN into thin layers were tested in this project.

### Adapted Hummers' Method

The exfoliation mechanism of hBNNSs from hBN is still unclear, but it is believed that the adapted Hummers' method process (Figure 4-9) contains three steps: 1.)  $H_2SO_4$  is mixed with BN powder, then hydrogen ions intercalate into layered BN and cause the layer spacing to enlarge. 2.)  $KMnO_4$  is added and reacts with  $H_2SO_4$ , which leads to the formation of  $MnO_2$  nanoparticles. 3.) BNNSs are then exfoliated from bulk BN by the intercalation of  $MnO_2$  nanoparticles into the greater interlayer of bulk BN. Moreover,  $MnO_2$  nanoparticles play a key role in keeping the BNNSs from re-stacking (Equation (4-1) [186]).



Finally,  $MnO_2$  nanoparticles are removed by  $H_2O_2$  (Equation (4-2)) and oxygen gas generated in this reaction may contribute to a force that pushes the layers apart, which accelerates the expansion of multilayer BNNSs and results in a complete exfoliation of BNNSs [163].

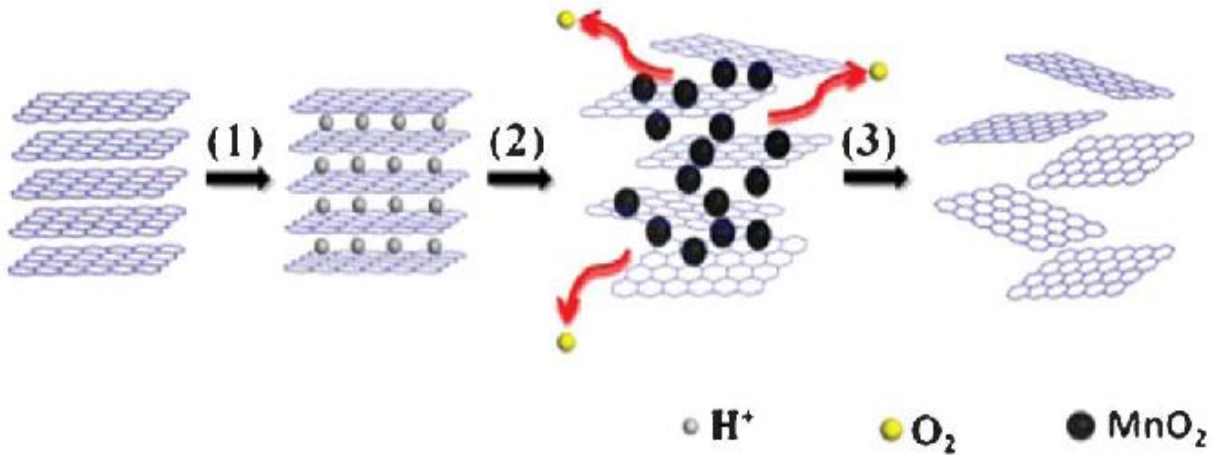


**Figure 4-9** Scheme for the exfoliation of hBN powder by modified Hummers' method. (From Du [163])

However, when tested, this method was ineffective at producing hBN nanosheets from hBN powder. Figure 4-10(a) is a good representation of the products obtained from this method.

Compared to pristine hBN powder (Figure 4-10(b)) the exfoliated hBN powder's (Figure 4-10(a)) surface was modified, its edges were blunted and rounded. The powder seems to have coagulated into a single mass and no nanosheets can be discerned from the bulk. As a result, this method was abandoned as a potential method for chemically exfoliating single crystals.

### **Adapted Hummers' Method Acid Mixture**

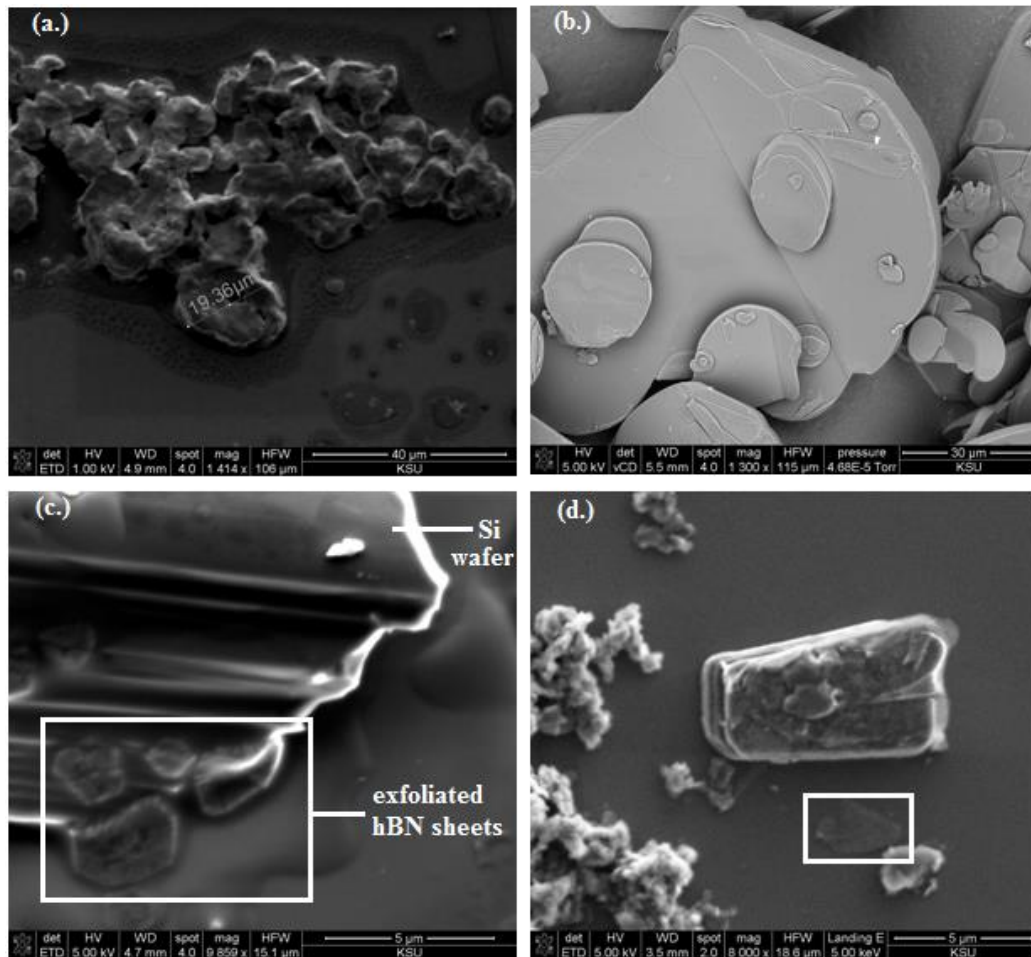
This method is effectively the same as modified Hummers' method, varying only in the mixing of  $\text{H}_3\text{PO}_4$  with  $\text{H}_2\text{SO}_4$ . Bending of hBN sheets is also observed (Figure 4-10(c)), indicating that these sheets are "peeled" from the bulk hBN material during the exfoliation process. This method was more promising for exfoliating of hBN powders to single to few-layered hBN as displayed in Figure 4-10(c). At the bottom left of the SEM image, an hBN layer is hanging from the edge of a Si wafer. These are only a few micrometers in lateral size and the number of layers cannot be determined from this figure. The surface has been attacked vigorously by the acid mixture, and, while the modification of Hummers' method with its mixture of acids seems to have been more successful than the original Hummers' method, the number of exfoliated hBN layers produced were few and far between. Additionally, with the overall goal of exfoliating hBN single crystals for use in nano-optics and nano-electronics, maintaining a pristine surface is of the utmost importance. Another negative aspect of this method was its high volume of strong acid compared to the overall yield of exfoliated sheets; and produced a large amount of waste that is environmentally unfriendly. With all of these shortcomings, this method was also abandoned.

### **Exfoliation by Methanesulfonic Acid (MSA)**

In this method, a protic sulfonic acid, methanesulfonic acid (MSA), was employed as the solvent for liquid-phase chemical exfoliation of hBN. The sonication of MSA with hBN

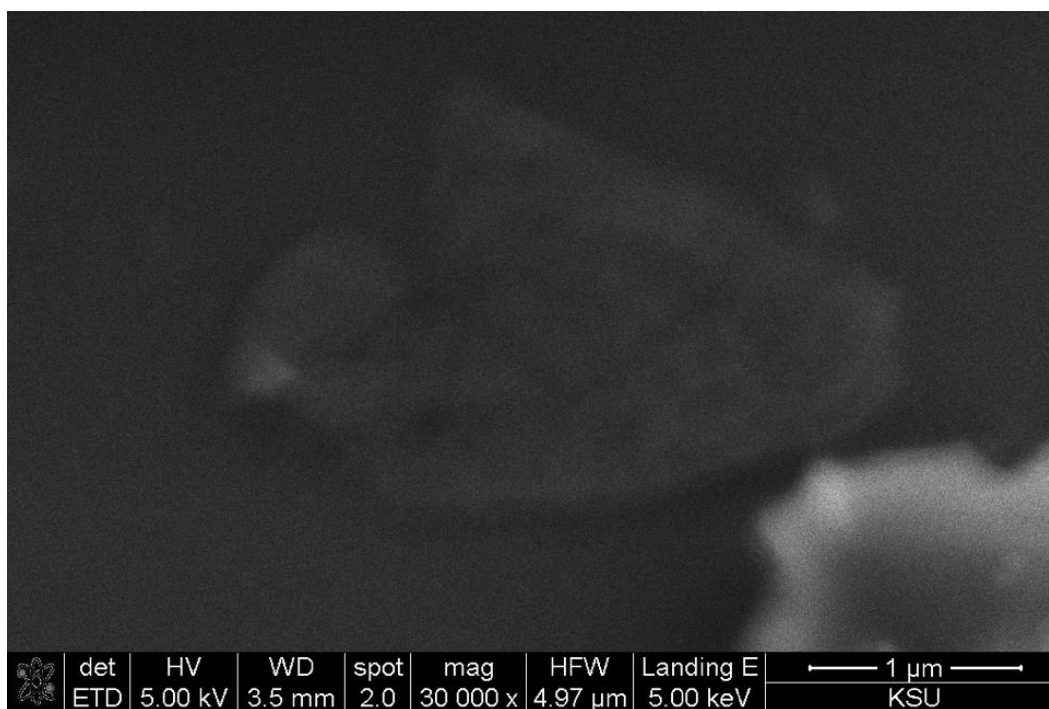
powders produced a faint orange colored solution, a consequence of the charge transfer between hBNNS and MSA molecules, as in the cases of carbon nanotubes or graphene [187-190]. In a previous study, Xie *et al.* [190] also found the interactions between amino groups and BN nanotubes (BNNT) results in a color change of the dispersion of BNNT.

Figure 4-10(d) illustrates the main features of this exfoliation method. Seen on the left side of the image, are many small platelets that have coagulated into a mass of hBN sheets, as was the case with the adapted Hummers' method. This is most likely due to the protonation of the hBN sheets by the MSA causing a static charge.



**Figure 4-10 High magnification scanning electron microscope images of (a) exfoliation by adapted Hummers' method, (b) pristine hBN, (c) exfoliation by acid adapted Hummers' method, and (d) exfoliation by MSA protonation**

These sheets are all less than 1  $\mu\text{m}$  in lateral size suggesting that the process is destructive, causing hBN layers to break apart during sonication. Seen in the center of Figure 4-10(d) is a large particle of hBN powder has not been exfoliated. This highlights one of the ineptitudes of many of the current processes for chemical exfoliation, which is a dearth of hBN nanosheets yielded. Just below this large hBN particle, what is believed to be the only exfoliated sheet of hBN in this image can be seen. A magnified view of this sheet is given in Figure 4-11. At 5 kEV landing energy, this sheet is very transparent and little can be seen of its surface to determine its usefulness as part of a nano-optics instrument or in nano-electronics. While the simplicity of the method is attractive, like the variations of Hummers methods presented, it also requires a strong acid that requires special care to deal with as well as environmentally unfriendly waste. With its low yield and dependence on strong acid this method was also discarded.



**Figure 4-11 High magnification SEM image of exfoliated hBN by MSA method.**

### **Intercalation of Water Molecules**

This method was an exciting concept because unlike previous methods for chemical exfoliation it does not require harsh chemicals. Additionally, there is no functionalization of the layers, which eliminates impurities that could be an issue with other chemical methods. Impurities must be avoided if a functioning nano-optical or nano-electronic device is desired. Another benefit of using water as an intercalating molecule is the small impact on the environment and cost associated with waste in this process.

The morphology of bulk hBN shown in Figure 4-10(b) indicates a regular shape with a smooth surface, and clean edges. However, after undergoing the freezing treatment, bulk hBN becomes out of shape, with the surface becoming rough and bumpy. Figure 4-12(a) shows the result of the water freezing method. Once again, hBN sheets have been broken into small particles and coagulated together. This is most likely due to the surface charges pulling the particles together. There is no evidence of few-to-monolayer hBN sheets present. Once again, a new method was sought out.

### **Functionalization by Octadecylamine (ODA)**

Octadecylamine was employed in the functionalization and exfoliation of hBN. This amine molecule has previously been studied for the functionalization of carbon nanotubes [191-196]. The resulting products of the reflux after sonicating in THF were colorless and transparent but with “milky” appearances. When dilute in hBN, the milkiness became less significant, and the dispersions appeared just as a clear solution without the presence of hBN. A small amount of white precipitates appeared over time. The identification of free-standing monolayered species was challenging since they made up a smaller population of overall hBN particles. There were



amorphous materials covering most of the surface of the functionalized hBN samples (Figure 4-12(b)).

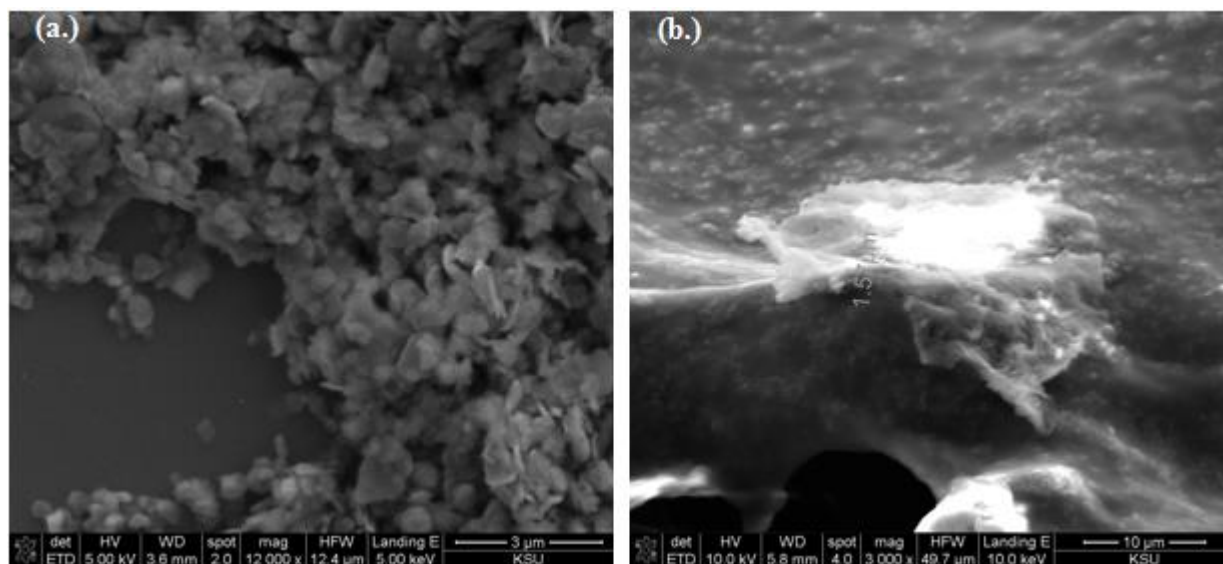


**Figure 4-12 High magnification scanning electron microscope images of (a) exfoliation by water freezing method, and (b) exfoliation by ODA functionalization.**

These materials might be attributed to the organic functionalities attached to the hBN surface. This functionalization is consistent with the proposed mechanism that there are Lewis acid-base complexations occurring between the electron-rich amine groups of ODA molecules and the electron-deficient boron atoms on the hBNNS surface. It is proposed that the amine-boron complexations allowed the attachment of the amine molecules to the hBN surface and possibly partial intercalation between the hBN layers, both of which facilitated the subsequent exfoliation of the nanosheet from the bulk hBN powder. The average lateral sizes of the functionalized hBN nanosheets were generally smaller than the original hBN sample, suggesting that the functionalization/exfoliation process induces destructive exfoliation. The wide selection of Lewis bases make this approach more versatile than those studied above. Figure 4-12(b) shows a sheet of exfoliated hBN by this process; this sheet displays many ripples and folds like those shown in previous literature. While it is almost certainly not a monolayer, its lateral size is

much larger than other methods considered here. FT-IR cannot confirm the exfoliation of hBN layers. However, it can confirm that the amine functional group is present in the samples. The FT-IR spectra of pristine hBN powder is shown in Figure 4-13(a) with characteristic peaks at  $1372\text{ cm}^{-1}$  and  $816\text{ cm}^{-1}$ . Spectroscopic signatures of hBNNSs display FT-IR characteristic peaks quite similar to those of bulk hBN crystals. The  $A_{2u}$  and  $E_{1u}$  modes are IR active, and the  $B_{1g}$  modes are optically inactive. The typical FT-IR absorption peak for hBN nanosheets is observed at  $811\text{ cm}^{-1}$  and a broad absorption band in the range of  $1350\text{-}1520\text{ cm}^{-1}$  which are ascribed to the B - N - B bending vibration mode parallel to the c-axis and B - N stretching vibration mode perpendicular to the c-axis modes of hBN, respectively [136]. Figure 4-13(b) displays the FT-IR spectra of the exfoliated hBN sheets. The characteristic peak of hBN at  $1372\text{ cm}^{-1}$  is clearly evident. The  $816\text{ cm}^{-1}$  peak is less distinguishable and most likely washed out by the strong peaks of ODA. The broad peak centered at  $3450\text{ cm}^{-1}$  can be attributed to N-H stretching of the amine, while the two peaks at  $2910\text{ cm}^{-1}$  and  $2850\text{ cm}^{-1}$  can be characterized as C-H<sub>3</sub> and C-H<sub>2</sub> bending respectively. Consequently, the presence of ODA has been confirmed. This confirms only the presence of ODA in the samples; by using XRD analysis of the samples confirmation that the amine has intercalated between the layers may be attained. Figure 4-14 is the XRD pattern of pristine hBN along with that of unexfoliated hBN that was recovered from the process. Pictured in Figure 4-15 is an unexfoliated hBN particle. A layer has begun to be exfoliated and has folded over onto itself, seen in the bottom left of the image. While it has not exfoliated, if the amine molecules were intercalated between layers, a shift of the hBN (002) XRD peak at approximately  $2\theta = 26.7^\circ$  would indicate an increase in the distance between hBN layers. Figure 4-14 does not display a shift in the (002) peak for ODA functionalized hBN, therefore it cannot be concluded that intercalation of the ammine has taken place.

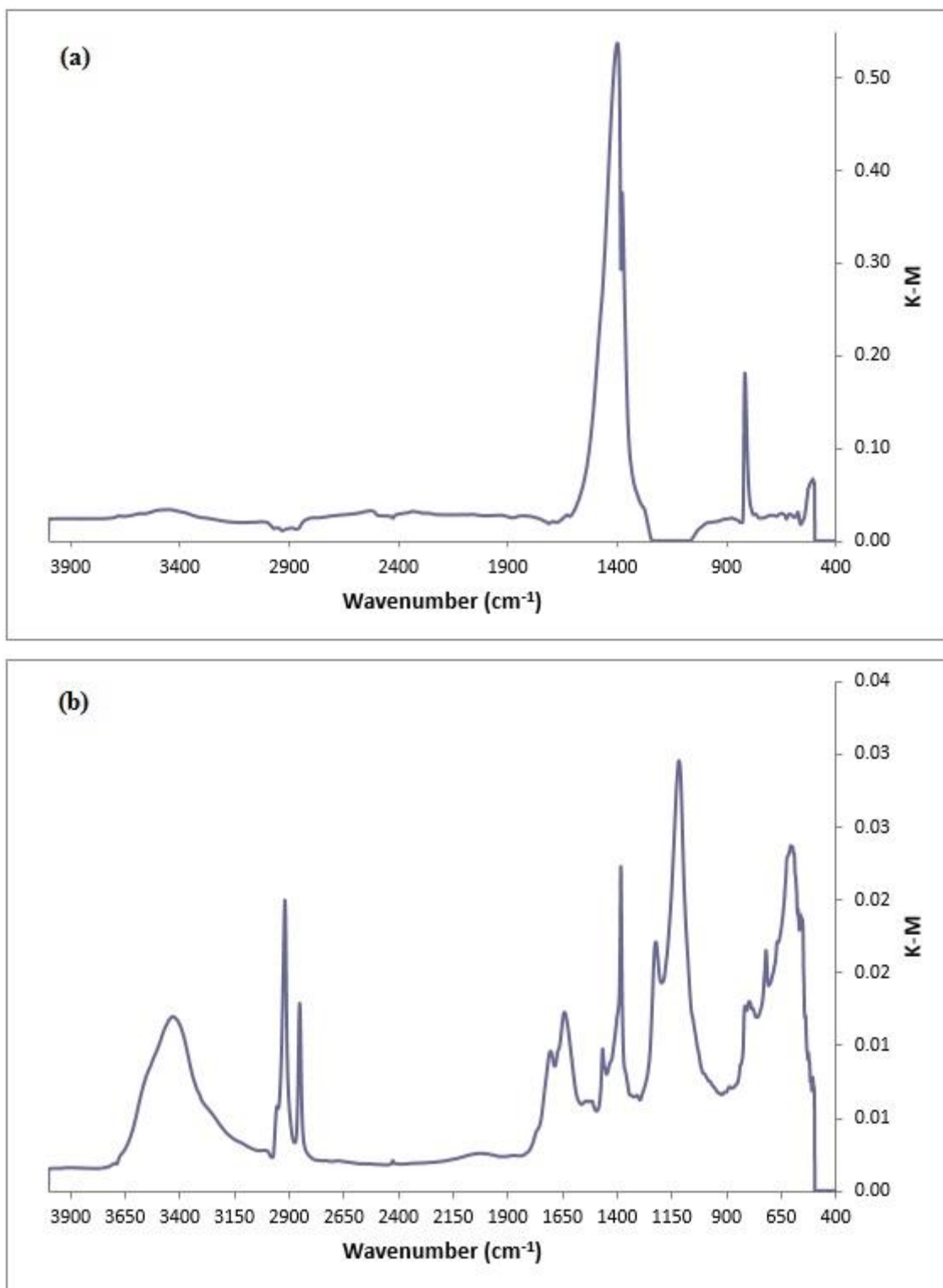


**Figure 4-13** FT-IR spectra of (a) pristine hBN powder and (b) ODA functionalized hBN powder.

The extra peaks of the ODA functionalized hBN can be attributed to ODA as seen from the XRD spectra of pure ODA (Figure 4-16).

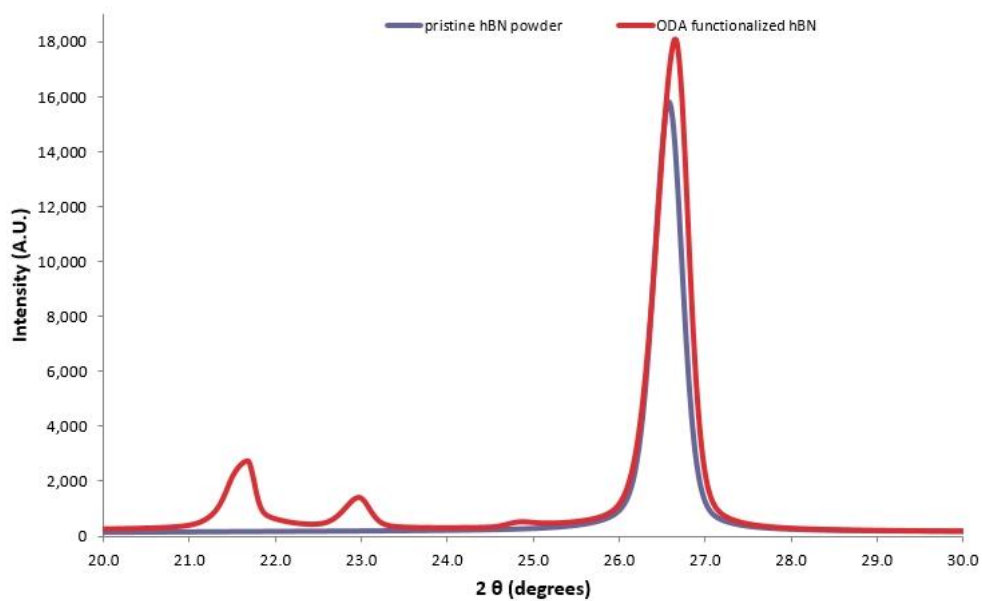


**Figure 4-14 X-ray diffraction pattern comparison of ODA functionalized hBN powder (red) and pristine hBN powder (blue) (002) peaks.**

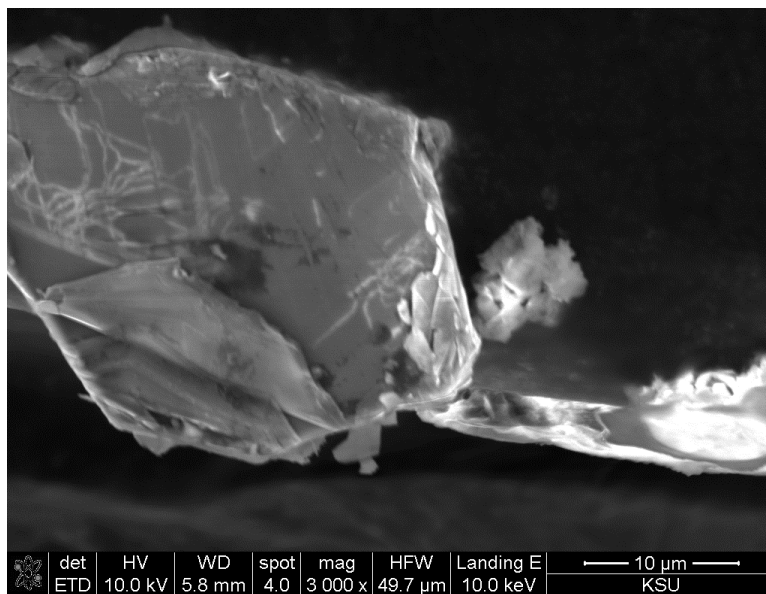


**Figure 4-15 ODA functionalized hBN that did not fully exfoliate.**

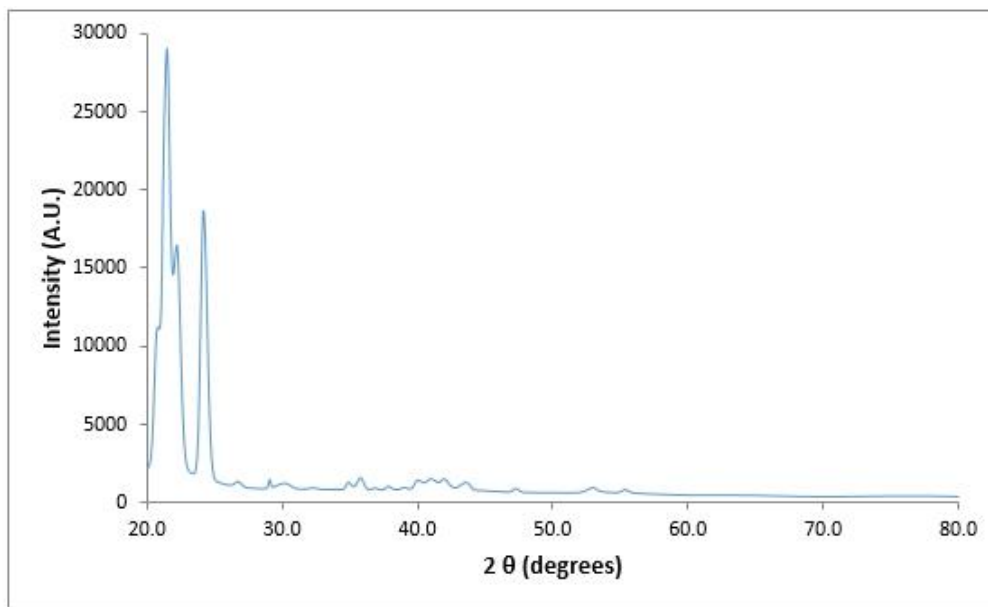


**Figure 4-16 X-ray diffraction pattern pure ODA powder.**

Although, XRD did not reveal intercalation of the ammine molecules further evidence of exfoliated hBN can be found from the Raman spectra of the sample. Multilayered hBN has a red shift while single layered nanosheets have a blue shift of approximately  $4\text{ cm}^{-1}$ , attributed to hardening of the  $E_{2g}$  phonon mode, due to slightly shorter B-N bond in the isolated monolayers. The Raman active  $E_{2g}$  mode is due to in-plane atomic displacements characterized by B and N atoms moving against each other within a plane [136, 150]. Figure 4-17 is the Raman spectra of an hBN bulk crystal at  $1367\text{ cm}^{-1}$  along with the Raman spectra of exfoliated hBN. Here can be seen a red shift as attributed to few-layered hBN at  $1348\text{ cm}^{-1}$ . This indicates that the hBN powder has been exfoliated by the chemical functionalization with ODA. Functional groups may be removed by heating in an  $N_2$  atmosphere leaving clean hBN nanosheets. Consequently, this method was found to be the most promising toward chemically exfoliating hBN single crystals into mono or few-layers.



**Figure 4-17 Raman shift of exfoliated hBN powder (blue) from bulk hBN Raman signature (orange).**

## Chapter 5 - Conclusion and Future Work

The solution growth process of producing bulk hBN crystals by Edgar *et al.* [22] employs a constant cooling rate from the saturation point to the freezing point leading to many different sized crystals. A stepped cooling process was researched in order to grow more uniform crystals with growth occurring in both the  $a$  and  $c$  directions. The set of experiments produced at least small triangular crystals which differed in the quality, quantity, and geometry of crystals. All samples exhibited pyramid-like crystal growth. The top side of the metal flux after crystal growth had mostly amorphous hBN with some flat hBN crystals of varying size on top. The pyramid-like structures primarily formed on the sides of the metal flux. The goal of producing both thick and large grain boundary single crystals was unsuccessful.

Future work in stepped temperature work requires the discovery of how crystal habit can be affected by the stepped cooling process. Specifically, step 2 of the process presented should be further studied with a slower cooling rate from between 1 and 4 °C/hr. Further understanding of how the crystal habit came to be may be informative toward the growth mechanism of hBN. Better understanding the growth mechanism will be a step toward Si type control of single crystal growth.

The solution growth method of Hoffman *et al.* [22] is effective in producing large, pristine crystals, but inevitably produces cracked crystals. A process for growing large crystals and extracting them from the solution so as to prevent cracking has been demonstrated. A set of nested crucibles were designed in which hBN crystals were grown and extracted from the metal flux *in situ*; the inner crucible was raised and the melt, still in liquid phase, were drained away from the crystals into the outer crucible. This process has proven promising in the extraction of

crystals from the metal solvent and it eliminates the problem of mechanical breakage by the cooling metal or by extraction with thermal release tape.

Future work in this area requires tuning process variables so as to allow for larger crystal growth as well as refining the crucible design for better control of the melt (i.e. draining properly). Currently, a derivative of this process for extraction of crystals from the metal solution is planned by this group. This will involve a tilting horizontal tube furnace and a specialized crucible for growing crystals, tilting the furnace to separate the crystals and the liquid metal at opposite ends of the crucible. If successful, device fabrication will be much easier due to dealing with larger, more pristine crystals.

Isotopically enriched hBN from  $^{10}\text{B}$  and  $^{11}\text{B}$  can give special properties to hBN crystals where  $^{10}\text{B}$  enriched hBN may be utilized as a thermal neutron detector. The typical process used to grow hBN crystals utilizes hot pressed boron nitride as a crucible. To control the enriched boron content different materials were tested as crucibles for enriched growth. Materials tested were yttria, yttria-stabilized zirconia, and alumina. Raman spectra revealed that alumina and yttria did not affect the boron composition. hBN crystals have been produced with  $\text{B}^{10}$  and  $\text{B}^{11}$  enrichment above 94% according to Raman spectroscopy measurements. By increasing the amount of  $^{10}\text{B}$  isotope in hBN single crystals, the efficiency of hBN as a neutron detector is increased.

Future work in this area requires larger crystals. The crystal grain boundaries may be increased by raising the soak temperature of the furnace [22]. The bulk growth of enriched hBN crystals can also benefit from optimization of the composition of the flux from which it is grown, specifically determination of the appropriate ratio of isotopically enriched B powder in the flux to  $\text{N}_2$  dissolved. Also, a method to facilitate mixing in the flux might be beneficial. Once



appropriately sized crystals are produced, work can progress toward crystal processing and device fabrication.

Testing of exfoliation methods for hBN powder was undertaken towards finding an appropriate method with which to exfoliate large single crystal hBN for use as nano-optics and nano-electronics. The methods tested were: an oxidation reaction based on Hummers' method for exfoliating graphene, a modification of Hummers' method which eliminates large exotherms and toxic gases, the functionalization and solvation of hBN layers by an organic acid, a water freezing and thawing method to intercalate water molecules between hBN layers, and the functionalization and subsequent intercalation of hBN by a long chain amine, ODA. The most successful of these methods was functionalization with ODA. Other methods displayed exfoliation of hBN layers, however when functionalized and exfoliated by ODA, hBN powder was exfoliated to fewer layers and maintained larger lateral dimensions. Exfoliation was determined through several qualitative techniques. Infrared spectroscopy of exfoliated hBN showed that the functional group was present in the exfoliated hBN. Raman spectroscopy showed a red-shift of the  $E_{2g}$  band indicating hBN had been exfoliated to only a few layers. A common theme seen in all the methods tested was the distortion and destruction of hBN layers as a result of the exfoliation as compared to the pristine hBN powders before exfoliation. Another common issue with each method was the conglomeration of exfoliated hBN, making it difficult to manipulate and locate monolayers.

Future work is required to adapt this process to functionalize and exfoliate large, highly ordered hBN crystals into a 2-D material. The key to this will be to understand how the crystal is functionalized, as well as the forces available through this method as compared to those forces necessary to separate hBN layers. *In-situ* XRD, Raman, and FT-IR measurements could supply

the answers. To determine the forces available for exfoliation, one could study the solvent interactions between solvents and amine functional groups as well as sonication forces. These methods may not be appropriate for hBNNSs in nano-electronic and nano-optic applications due to physical abuse and defects created by the exfoliation process; modifications of the methods tested to eliminate these issues or an alternative method is needed. Additionally, avoiding conglomeration of the hBNNSs must be solved. A single crystal, monolayer would be an amazing first step in the creation of nan-optics and nano-electronics.

## References

- [1] H.O. Pierson, *J. Composite Mater.* 9 (1975) 228.
- [2] A.S. Rozenberg, Y.A. Sinenko, N.V. Chukanov, *J. Mater. Sci.* 28 (1993) 5528.
- [3] S. Middleman, *Materials Science and Engineering: A* 163 (1993) 135.
- [4] Y. Shi, C. Hamsen, X. Jia, K.K. Kim, A. Reina, M. Hofmann, A.L. Hsu, K. Zhang, H. Li, Z. Juang, M.S. Dresselhaus, L. Li, J. Kong, *Nano Lett.* 10 (2010) 4134.
- [5] K. Kim, S. Kim, Y. Lee, *Journal of the Korean Physical Society* 64 (2014) 1605.
- [6] J.H. Boo, S.B. Lee, K.S. Yu, Y.S. Kim, Y.S. Kim, J.T. Park, *J.Korean Phys.Soc.* 34 (1999) 532.
- [7] A.W. Moore, S.L. Strong, (2008) 846.
- [8] T. Ishii, T. Sato, *J. Cryst. Growth* 61 (1983) 689.
- [9] M. Hubacek, T. Sato, *J. Mater. Sci.* 32 (1997) 3293.
- [10] Y. Gu, M. Zheng, Y. Liu, Z. Xu, *J Am Ceram Soc* 90 (2007) 1589.
- [11] B.N. Feigelson, R.M. Frazier, M. Twigg, *J. Cryst. Growth* 305 (2007) 399.
- [12] T. Taniguchi, *NEW DIAMOND AND FRONTIER CARBON TECHNOLOGY* 14 (2004) 289.
- [13] R. WENTORF, *JOURNAL OF CHEMICAL PHYSICS* 34 (1961) 809.
- [14] T. Taniguchi, K. Watanabe, *Journal of Crystal Growth* 303 (2007) 525.
- [15] Y. Kubota, K. Watanabe, O. Tsuda, T. Taniguchi, *Chem. Mater.* 20 (2008) 1661.
- [16] R.F. Abdulrahman, A. Hendry, *Metallurgical and Materials Transactions B* 32 (2001) 1103.
- [17] J.H. Edgar, T.B. Hoffman, B. Clubine, M. Currie, X.Z. Du, J.Y. Lin, H.X. Jiang, *J. Cryst. Growth* 403 (2014) 110.

- [18] D.S. McGregor, T.C. Unruh, W.J. McNeil, Nuclear Instruments and Methods in Physics Research Section A: Accelerators, Spectrometers, Detectors and Associated Equipment 591 (2008) 530.
- [19] J. Li, R. Dahal, S. Majety, J.Y. Lin, H.X. Jiang, Nuclear Instruments and Methods in Physics Research Section A: Accelerators, Spectrometers, Detectors and Associated Equipment 654 (2011) 417.
- [20] K. Watanabe, T. Taniguchi, H. Kanda, NATURE MATERIALS 3 (2004) 404.
- [21] S. Majety, X.K. Cao, J. Li, R. Dahal, J.Y. Lin, H.X. Jiang, Appl. Phys. Lett. 101 (2012) .
- [22] T.B. Hoffman, B. Clubine, Y. Zhang, K. Snow, J.H. Edgar, J. Cryst. Growth 393 (2014) 114.
- [23] B. Clubine, (2012) .
- [24] K.S. Novoselov, A.K. Geim, S.V. Morozov, D. Jiang, Y. Zhang, S.V. Dubonos, I.V. Crigorieva, A.A. Firsov, Science 306 (2004) 666.
- [25] A.C. Adams, J. Electrochem. Soc. 128 (1981) 1378.
- [26] W. Auwarter, H.U. Suter, H. Sachdev, T. Greber, Chem. Mater. 16 (2004) 343.
- [27] F. Muller, K. Stowe, H. Sachdev, Chemistry of Materials 17 (2005) 3464.
- [28] G. Lian, X. Zhang, M. Tan, S. Zhang, D. Cui, Q. Wang, J. Mater. Chem. 21 (2011) 9201.
- [29] X. Wang, C. Zhi, L. Li, H. Zeng, C. Li, M. Mitome, D. Golberg, Y. Bando, Adv Mater 23 (2011) 4072.
- [30] X. Wang, A. Pakdel, C. Zhi, K. Watanabe, T. Sekiguchi, D. Golberg, Y. Bando, J. Phys. Condens Matter 24 (2012) 314205.
- [31] W. Han, H. Yu, Z. Liu, Appl. Phys. Lett. 98 (2011) 203112.
- [32] C. Jin, F. Lin, K. Suenaga, S. Iijima, Phys. Rev. Lett. 102 (2009) 195505.

- [33] J.C. Meyer, A. Chuvilin, G. Algara-Siller, J. Biskupek, U. Kaiser, *Nano Lett.* 9 (2009) 2683.
- [34] D. Pacilé, J.C. Meyer, ÇÖ Girit, A. Zettl, *Appl. Phys. Lett.* 92 (2008) 133107.
- [35] R.V. Gorbachev, I. Riaz, R.R. Nair, R. Jalil, L. Britnell, B.D. Belle, E.W. Hill, K.S. Novoselov, K. Watanabe, T. Taniguchi, A.K. Geim, P. Blake, *Small* 7 (2011) 465.
- [36] W.H. Balmain, *Journal für Praktische Chemie* 27 (1842) 422.
- [37] R. Haubner, M. Wilhelm, R. Weissenbacher, B. Lux, in: M. Jansen (Ed.), *High Performance Non-oxide Ceramics II*, Springer Berlin Heidelberg, 2002, p. 1.
- [38] A. Lipp, K.A. Schwetz, K. Hunold, *Journal of the European Ceramic Society* 5 (1989) 3.
- [39] <http://panadyneabrasives.com/> 2016 (2016) 2.
- [40] D. Singh, *Mechanical Properties and Performance of Engineering Ceramics and Composites VI Ceramic Engineering and Science Proceedings*, Hoboken : Wiley, Hoboken, 2011.
- [41] N.C. Calkins, (2007) .
- [42] K. Watanabe, T. Taniguchi, H. Kanda, *Nat Mater* 3 (2004) 404.
- [43] Dean C. R., Young A. F., Meric I., Lee C., Wang L., Sorgenfrei S., Watanabe K., Taniguchi T., Kim P., Shepard K. L., Hone J., *Nat Nano* 5 (2010) 722.
- [44] Han Wang, T. Taychatanapat, A. Hsu, K. Watanabe, T. Taniguchi, P. Jarillo-Herrero, T. Palacios, *Electron Device Letters, IEEE* 32 (2011) 1209.
- [45] R.F. Davis, *Proceedings of the IEEE* 79 (1991) 702.
- [46] W. Gannett, W. Regan, K. Watanabe, T. Taniguchi, M.F. Crommie, A. Zettl, *Appl. Phys. Lett.* 98 (2011) .
- [47] A.K. Geim, K.S. Novoselov, *Nat Mater* 6 (2007) 183.
- [48] T. Ando, *J. Phys. Soc. Jpn.* 75 (2006) 074716.
- [49] K. Nomura, A.H. MacDonald, *Phys. Rev. Lett.* 98 (2007) 076602.

- [50] E.H. Hwang, S. Adam, S.D. Sarma, Phys. Rev. Lett. 98 (2007) 186806.
- [51] S. Fratini, F. Guinea, Phys.Rev.B 77 (2008) 195415.
- [52] J. Chen, C. Jang, S. Xiao, M. Ishigami, M.S. Fuhrer, Nat Nano 3 (2008) 206.
- [53] M. Ishigami, J.H. Chen, W.G. Cullen, M.S. Fuhrer, E.D. Williams, Nano Lett. 7 (2007) 1643.
- [54] M.I. Katsnelson, A.K. Geim, Philosophical Transactions of the Royal Society of London A: Mathematical, Physical and Engineering Sciences 366 (2008) 195.
- [55] S.V. Morozov, K.S. Novoselov, M.I. Katsnelson, F. Schedin, D.C. Elias, J.A. Jaszczak, A.K. Geim, Phys. Rev. Lett. 100 (2008) 016602.
- [56] J. Martin, N. Akerman, G. Ulbricht, T. Lohmann, J.H. Smet, K. von Klitzing, A. Yacoby, Nat Phys 4 (2008) 144.
- [57] L.A. Ponomarenko, R. Yang, T.M. Mohiuddin, M.I. Katsnelson, K.S. Novoselov, S.V. Morozov, A.A. Zhukov, F. Schedin, E.W. Hill, A.K. Geim, Phys. Rev. Lett. 102 (2009) 206603.
- [58] M. Lafkioti, B. Krauss, T. Lohmann, U. Zschieschang, H. Klauk, K.v. Klitzing, J.H. Smet, Nano Letters 10 (2010) 1149.
- [59] C.H. Lui, L. Liu, K.F. Mak, G.W. Flynn, T.F. Heinz, Nature 462 (2009) 339.
- [60] A. Reina, X. Jia, J. Ho, D. Nezich, H. Son, V. Bulovic, M.S. Dresselhaus, J. Kong, Nano Lett. 9 (2009) 30.
- [61] G. Giovannetti, P.A. Khomyakov, G. Brocks, P.J. Kelly, J. van den Brink, Phys.Rev.B 76 (2007) 073103.
- [62] A.F. Young, C.R. Dean, I. Meric, S. Sorgenfrei, H. Ren, K. Watanabe, T. Taniguchi, J. Hone, K.L. Shepard, P. Kim, Phys.Rev.B 85 (2012) 235458.
- [63] X. Hong, K. Zou, J. Zhu, Phys.Rev.B 80 (2009) 241415.

- [64] Dean C. R., Young A. F., Meric I., Lee C., Wang L., Sorgenfrei S., Watanabe K., Taniguchi T., Kim P., Shepard K. L., Hone J., Nat Nano 5 (2010) 722.
- [65] J. Xue, J. Sanchez-Yamagishi, D. Bulmash, P. Jacquod, A. Deshpande, K. Watanabe, T. Taniguchi, P. Jarillo-Herrero, B.J. LeRoy, Nat Mater 10 (2011) 282.
- [66] R. Decker, Y. Wang, V.W. Brar, W. Regan, H. Tsai, Q. Wu, W. Gannett, A. Zettl, M.F. Crommie, Nano Lett. 11 (2011) 2291.
- [67] A.S. Mayorov, R.V. Gorbachev, S.V. Morozov, L. Britnell, R. Jalil, L.A. Ponomarenko, P. Blake, K.S. Novoselov, K. Watanabe, T. Taniguchi, A.K. Geim, Nano Lett. 11 (2011) 2396.
- [68] G. Lee, Y. Yu, C. Lee, C. Dean, K. Shepard, P. Kim, J. Hone, Appl. Phys. Lett. 99 (2011) 243114.
- [69] L. Britnell, R.V. Gorbachev, R. Jalil, B.D. Belle, F. Schedin, M.I. Katsnelson, L. Eaves, S.V. Morozov, A.S. Mayorov, N.M.R. Peres, A.H. Castro Neto, J. Leist, A.K. Geim, L.A. Ponomarenko, K.S. Novoselov, Nano Lett. 12 (2012) 1707.
- [70] L. Britnell, R.V. Gorbachev, R. Jalil, B.D. Belle, F. Schedin, A. Mishchenko, T. Georgiou, M.I. Katsnelson, L. Eaves, S.V. Morozov, N.M.R. Peres, J. Leist, A.K. Geim, K.S. Novoselov, L.A. Ponomarenko, Science 335 (2012) 947.
- [71] Y. Zhang, Z. Jiang, J.P. Small, M.S. Purewal, Y.-. Tan, M. Fazlollahi, J.D. Chudow, J.A. Jaszczak, H.L. Stormer, P. Kim, Phys. Rev. Lett. 96 (2006) 136806.
- [72] K. Watanabe, T. Taniguchi, T. Niiyama, K. Miya, M. Taniguchi, Nat Photon 3 (2009) 591.
- [73] A.H. Castro Neto, F. Guinea, N.M.R. Peres, K.S. Novoselov, A.K. Geim, Rev.Mod.Phys. 81 (2009) 109.
- [74] M. Kalbac, O. Frank, J. Kong, J. Sanchez-Yamagishi, K. Watanabe, T. Taniguchi, P. Jarillo-Herrero, M.S. Dresselhaus, The Journal of Physical Chemistry Letters 3 (2012) 796.

- [75] F.P. Bundy, R.H. Wentorf, J. Chem. Phys. 38 (1963) 1144.
- [76] F.R. Corrigan, F.P. Bundy, J. Chem. Phys. 63 (1975) 3812.
- [77] V.L. Solozhenko, V.Z. Turkevich, W.B. Holzapfel, J Phys Chem B 103 (1999) 2903.
- [78] G. Will, G. Nover, J. von der Gönna, Journal of Solid State Chemistry 154 (2000) 280.
- [79] M. Halo, C. Pisani, L. Maschio, S. Casassa, M. Sch $\tilde{A}$ tz, D. Usvyat, Phys. Rev. B 83 (2011) 035117.
- [80] J. Furthmuller, J. Hafner, G. Kresse, Phys. Rev. B: Condens. Matter 50 (1994) 15606.
- [81] K. Albe, Phys. Rev. B 55 (1997) 6203.
- [82] G. Kern, G. Kresse, J. Hafner, Phys. Rev. B 59 (1999) 8551.
- [83] T.E. Mosuang, J.E. Lowther, Journal of Physics and Chemistry of Solids 63 (2002) 363.
- [84] W.J. Yu, W.M. Lau, S.P. Chan, Z.F. Liu, Q.Q. Zheng, Phys. Rev. B 67 (2003) 014108.
- [85] M. Topsakal, E. Akturk, S. Ciraci, Phys. Rev. B 79 (2009) 115442.
- [86] R. Ahmed, Fazal-e-Aleem, S.J. Hashemifar, H. Akbarzadeh, Physica B: Condensed Matter 400 (2007) 297.
- [87] Y. Xu, W.Y. Ching, Phys. Rev. B 44 (1991) 7787.
- [88] L.M. Caroline, Bharath University (2010) .
- [89] J. Wang, G. Zhang, H. Yu, Y. Wang, C. Chen, in: P. Rudolph (Ed.), Handbook of Crystal Growth (Second Edition), Elsevier, Boston, 2015, p. 169.
- [90] M. Jurisch, S. Eichler, M. Bruder, in: P. Rudolph (Ed.), Handbook of Crystal Growth (Second Edition), Elsevier, Boston, 2015, p. 331.
- [91] Z. Galazka, in: P. Rudolph (Ed.), Handbook of Crystal Growth (Second Edition), Elsevier, Boston, 2015, p. 209.
- [92] V.L. Vinogradov, A.V. Kostanovskij, Teplofizika Vysokikh Temperatur 29 (1991) 1112.



- [93] K.K. Kim, A. Hsu, X. Jia, S.M. Kim, Y. Shi, M. Hofmann, D. Nezich, J.F. Rodriguez-Nieva, M. Dresselhaus, T. Palacios, J. Kong, *Nano Lett.* 12 (2012) 161.
- [94] F. Abbona, D. Aquilano, (2010) 53.
- [95] M. Yano, Y. Yap, M. Okamoto, M. Onda, M. Yoshimura, Y. Mori, T. Sasaki, *JAPANESE JOURNAL OF APPLIED PHYSICS PART 2-LETTERS* 39 (2000) 300.
- [96] Y. Gu, M. Zheng, Y. Liu, Z. Xu, *J Am Ceram Soc* 90 (2007) 1589.
- [97] L. Liu, Y.P. Feng, Z.X. Shen, *Phys. Rev. B* 68 (2003) 104102.
- [98] C. Kowanda, M. Speidel, *Scripta Materialia* 48 (2003) 1073.
- [99] Y. Kubota, K. Watanabe, O. Tsuda, T. Taniguchi, *Science* 317 (2007) 932.
- [100] R. Roy, W.B. White, *J. Cryst. Growth* 3–4 (1968) 33.
- [101] H.J. Scheel, D. Elwell, *J. Cryst. Growth* 12 (1972) 153.
- [102] J.J.(J. Gilman, *The art and science of growing crystals*, New York, Wiley, New York, 1963.
- [103] Y. Liu, S. Bhowmick, B.I. Yakobson, *Nano Letters* 11 (2011) 3113.
- [104] W.H. Grodkiewicz, E.F. Dearborn, L.G. Van Uitert, in: H.S.(S. Peiser, *Air Force Cambridge Research Laboratories (U.S.) and International Union of Pure and Applied Physics. Commission on the Solid State (Eds.), Crystal growth*, Oxford, New York, Symposium Publications Division, Pergamon Press, Oxford, New York, 1967, p. 441.
- [105] G.A. Bennett, *J. Cryst. Growth* 3–4 (1968) 458.
- [106] W. Tolksdorf, *J. Cryst. Growth* 3–4 (1968) 463.
- [107] K. Kawabe, S. Sawada, *Journal of the Physical Society of Japan* 12 (1957) 218.
- [108] N.D. Zhigadlo, *J. Cryst. Growth* 402 (2014) 308.

- [109] T.W. Crane, M.P. Baker, Passive Nondestructive Assay of Nuclear Materials NUREG/CR-5550 (1991) 379.
- [110] J.E. Estevez, M. Ghazizadeh, J.G. Ryan, A.D. Kelkar, International Journal of Chemical, Molecular, Nuclear, Materials and Metallurgical Engineering 8 (2014) 61.
- [111] M. Rockwell, gsnmagazine.com/node/24945 2015 (2011) .
- [112] Sandia National Laboratories, United States, United States, Advanced digital detectors for neutron imaging, United States. Dept. of Energy. ;Oak Ridge, Tenn., Washington, D.C., 2003, p. 24.
- [113] H. Kitaguchi, H. Miyai, S. Izumi, A. Kaihara, in: Anonymous , Silicon semiconductor detectors for various nuclear radiations, Nuclear Science Symposium and Medical Imaging Conference Record, 1995., 1995 IEEE, Oct, 1995, p. 828.
- [114] R.J. Nikolic, A.M. Conway, C.E. Reinhardt, R.T. Graff, Tzu Fang Wang, N. Deo, C.L. Cheung, in: Anonymous , Fabrication of Pillar-structured thermal neutron detectors, Nuclear Science Symposium Conference Record, 2007. NSS '07. IEEE, Oct, 2007, p. 1577.
- [115] B.W. Robertson, S. Adenwalla, A. Harken, P. Welsch, J.I. Brand, P.A. Dowben, J.P. Claassen, Appl. Phys. Lett. 80 (2002) 3644.
- [116] Y. Kumashiro, K. Kudo, K. Matsumoto, Y. Okada, T. Koshiro, Journal of the Less Common Metals 143 (1988) 71.
- [117] T.B. Hoffman, Y. Zhang, J.H. Edgar, D.K. Gaskill, in: Anonymous , Growth of hBN Using Metallic Boron: Isotopically Enriched h10BN and h11BN, Symposium T – Compound Semiconductor Materials and Devices, 2014, p. 35.
- [118] D. Golberg, Y. Bando, Y. Huang, T. Terao, M. Mitome, C. Tang, C. Zhi, ACS Nano 4 (2010) 2979.

- [119] M. Corso, W. Auwärter, M. Muntwiler, A. Tamai, T. Greber, J. Osterwalder, *Science* 303 (2004) 217.
- [120] K.S. Novoselov, D. Jiang, F. Schedin, T.J. Booth, V.V. Khotkevich, S.V. Morozov, A.K. Geim, *Proc. Natl. Acad. Sci. U. S. A.* 102 (2005) 10451.
- [121] Z. Chen, J. Zou, G. Liu, F. Li, Y. Wang, L. Wang, X. Yuan, T. Sekiguchi, H. Cheng, G.Q. Lu, *ACS Nano* 2 (2008) 2183.
- [122] D. Cho, J. Kim, S. Kwon, C. Lee, Y. Lee, *Wear* 302 (2013) 981.
- [123] E. Husain, T.N. Narayanan, J. Taha-Tijerina, S. Vinod, R. Vajtai, P.M. Ajayan, *ACS Appl. Mater. Interfaces* 5 (2013) 4129.
- [124] K.S.F. Novoselov, *Nature* 490 (2012) 192.
- [125] S. Li, Z. Ren, J. Zheng, Y. Zhou, Y. Wan, L. Hao, *J. Appl. Phys.* 113 (2013) 033703.
- [126] H. Neumann, *Crystal Research and Technology* 30 (1995) 910.
- [127] J.A. Jaszczak, <http://www.phy.mtu.edu/~jaszczak/graphprop.html> 2014 (1998) .
- [128] X. Blase, A. De Vita, J.-. Charlier, R. Car, *Phys. Rev. Lett.* 80 (1998) 1666.
- [129] A. Pakdel, Y. Bando, D. Golberg, *Chem. Soc. Rev.* 43 (2014) 934.
- [130] J.-. Charlier, X. Blase, A. De Vita, R. Car, *Appl. Phys. A* 68 (1999) 267.
- [131] D. Golberg, Y. Bando, *Appl. Phys. Lett.* 79 (2001) 415.
- [132] M. Buongiorno Nardelli, C. Brabec, A. Maiti, C. Roland, J. Bernholc, *Phys. Rev. Lett.* 80 (1998) 313.
- [133] N. Alem, Q.M. Ramasse, C.R. Seabourne, O.V. Yazyev, K. Erickson, M.C. Sarahan, C. Kisielowski, A.J. Scott, S.G. Louie, A. Zettl, *Phys. Rev. Lett.* 109 (2012) 205502.
- [134] N. Marom, J. Bernstein, J. Garel, A. Tkatchenko, E. Joselevich, L. Kronik, O. Hod, *Phys. Rev. Lett.* 105 (2010) 046801.

- [135] A. Pakdel, Y. Bando, D. Golberg, *Langmuir* 29 (2013) 7529.
- [136] J. Yu, L. Qin, Y. Hao, S. Kuang, X. Bai, Y. Chong, W. Zhang, E. Wang, *ACS Nano* 4 (2010) 414.
- [137] A. Pakdel, X. Wang, Y. Bando, D. Golberg, *Acta Materialia* 61 (2013) 1266.
- [138] T. Kuzuba, Y. Sato, S. Yamaoka, K. Era, *Phys. Rev. B* 18 (1978) 4440.
- [139] H. Cho, Y. Tokoi, S. Tanaka, H. Suematsu, T. Suzuki, W. Jiang, K. Niihara, T. Nakayama, *Composites Sci. Technol.* 71 (2011) 1046.
- [140] W.L. Song, P. Wang, L. Cao, A. Anderson, M.J. Mezziani, A.J. Farr, Y.P. Sun, *Angew. Chem. Int. Ed Engl.* 51 (2012) 6498.
- [141] J. Yu, X. Huang, C. Wu, X. Wu, G. Wang, P. Jiang, *Polymer* 53 (2012) 471.
- [142] L. Lindsay, D.A. Broido, *Phys. Rev. B* 85 (2012) 035436.
- [143] L.J. Romasanta, M. Hernandez, M.A. Lopez-Manchado, R. Verdejo, *Nanoscale Res. Lett.* 6 (2011) 508.
- [144] J. Taha-Tijerina, T.N. Narayanan, G. Gao, M. Rohde, D.A. Tsentalovich, M. Pasquali, P.M. Ajayan, *ACS Nano* 6 (2012) 1214.
- [145] Y. Lin, J.W. Connell, *Nanoscale* 4 (2012) 6908.
- [146] J. Zhou, Q. Wang, Q. Sun, P. Jena, *Phys. Rev. B* 81 (2010) 085442.
- [147] M.S. Si, D.S. Xue, *Phys. Rev. B* 75 (2007) 193409.
- [148] J. Yang, D. Kim, J. Hong, X. Qian, *Surf. Sci.* 604 (2010) 1603.
- [149] H.S. Lim, J.W. Oh, S.Y. Kim, M. Yoo, S. Park, W.S. Lee, *Chem. Mater.* 25 (2013) 3315.
- [150] A. Pakdel, C. Zhi, Y. Bando, T. Nakayama, D. Golberg, *ACS Nano* 5 (2011) 6507.
- [151] C.H. Lee, J. Drelich, Y.K. Yap, *Langmuir* 25 (2009) 4853.
- [152] L.H. Li, Y. Chen, *Langmuir* 26 (2010) 5135.

- [153] M. Gao, A. Lyalin, T. Taketsugu, *J. Phys. Chem. C* 116 (2012) 9054.
- [154] L. Lin, Z. Li, Y. Zheng, K. Wei, *J Am Ceram Soc* 92 (2009) 1347.
- [155] W. Lei, D. Portehault, D. Liu, S. Qin, Y. Chen, *Nat. Commun.* 4 (2013) 1777.
- [156] F. Zhang, X. Chen, R.A. Boulos, F. Md Yasin, H. Lu, C. Raston, H. Zhang, *Chem. Commun.* 49 (2013) 4845.
- [157] J. Welser, S. Wolf, P. Avouris, T. Theis, *1* (2011) 375.
- [158] H. Kostal, *EDU. photonics* 2015 (2015) .
- [159] Y. - Lin, J.W. - Connell, - *Nanoscale* - 6908.
- [160] L. Song, L. Ci, H. Lu, P.B. Sorokin, C. Jin, J. Ni, A.G. Kvashnin, D.G. Kvashnin, J. Lou, B.I. Yakobson, P.M. Ajayan, *Nano Lett.* 10 (2010) 3209.
- [161] J.N. Coleman, M. Lotya, A. O'G'Connell, S.D. Bergin, P.J. King, U. Khan, K. Young, A. Gaucher, S. De, R.J. Smith, I.V. Shvets, S.K. Arora, G. Stanton, H. Kim, K. Lee, G.T. Kim, G.S. Duesberg, T. Hallam, J.J. Boland, J.J. Wang, J.F. Donegan, J.C. Grunlan, G. Moriarty, A. Shmeliov, R.J. Nicholls, J.M. Perkins, E.M. Grieveson, K. Theuwissen, D.W. McComb, P.D. Nellist, V. Nicolosi, *Science* 331 (2011) 568.
- [162] A. Pakdel, X. Wang, C. Zhi, Y. Bando, K. Watanabe, T. Sekiguchi, T. Nakayama, D. Golberg, *J. Mater. Chem.* 22 (2012) 4818.
- [163] M. Du, Y. Wu, X. Hao, *CrystEngComm* 15 (2013) 1782.
- [164] G.R. Bhimanapati, D. Kozuch, J.A. Robinson, *Nanoscale* 6 (2014) 11671.
- [165] X. Wang, A. Pakdel, J. Zhang, Q. Weng, T. Zhai, C. Zhi, D. Golberg, Y. Bando, *Nanoscale Res. Lett.* 7 (2012) 662.
- [166] C. Li, T. Wang, Y. Wu, F. Ma, G. Zhao, X. Hao, *Nanotechnology* 25 (2014) 495302.
- [167] Y. Lin, T.V. Williams, J.W. Connell, *J. Phys. Chem. Lett.* 1 (2010) 277.

- [168] A. Pakdel, C. Zhi, Y. Bando, D. Golberg, *Materials Today* 15 (2012) 256.
- [169] L.H. Li, Y. Chen, G. Behan, H. Zhang, M. Petracic, A.M. Glushenkov, *J. Mater. Chem.* 21 (2011) 11862.
- [170] H. Yurdakul, Y. Göncü, O. Durukan, A. Akay, A.T. Seyhan, N. Ay, S. Turan, *Ceram. Int.* 38 (2012) 2187.
- [171] M. Basche, Patent 3,152,006 (1964) .
- [172] M.J. Rand, J.F. Roberts, *J. Electrochem. Soc.* 115 (1968) 423.
- [173] M.T. Paffett, R.J. Simonson, P. Papin, R.T. Paine, *Surf. Sci.* 232 (1990) 286.
- [174] Jiao, LiyingZhang, LiWang, XinranDiankov,GeorgiDai, Hongjie, *Nature* 458 (2009) 877.
- [175] H. Zeng, C. Zhi, Z. Zhang, X. Wei, X. Wang, W. Guo, Y. Bando, D. Golberg, *Nano Lett.* 10 (2010) 5049.
- [176] W. Han, L. Wu, Y. Zhu, K. Watanabe, T. Taniguchi, *Appl. Phys. Lett.* 93 (2008) .
- [177] J.H. Warner, M.H. Rummeli, A. Bachmatiuk, B. Buchner, *ACS Nano* 4 (2010) 1299.
- [178] X. Li, X. Hao, M. Zhao, Y. Wu, J. Yang, Y. Tian, G. Qian, *Adv Mater* 25 (2013) 2200.
- [179] W.S.H. Jr., R.E. Offeman, *J. Am. Chem. Soc.* 80 (1958) 1339.
- [180] D.C. Marcano, D.V. Kosynkin, J.M. Berlin, A. Sinitskii, Z. Sun, A. Slesarev, L.B. Alemany, W. Lu, J.M. Tour, *ACS nano* 4 (2010) 4806.
- [181] Y. Wang, Z. Shi, J. Yin, *J. Mater. Chem.* 21 (2011) 11371.
- [182] Y. Lin, T.V. Williams, W. Cao, H. Elsayed-Ali, J.W. Connell, *J. Phys. Chem. C* 114 (2010) 17434.
- [183] R.R. Schroder, M. Muller, in: J.H. Moore and N.D. Spencer (Eds.), *Encyclopedia of Chemical Physics and Physical Chemistry*, Vol II, Institute of Physics, 2001, p. 1.
- [184] P. Paufler, *Crystal Research and Technology* 30 (1995) 316.

- [185] D.A. Skoog, F.J. Holler, S.R. Crouch, in: M.A. Short (Ed.), Principles of Instrumental Analysis, Brooks/Cole, Canada, 2007, p. 143.
- [186] Z. Wu, W. Ren, L. Wen, L. Gao, J. Zhao, Z. Chen, G. Zhou, F. Li, H. Cheng, ACS Nano 4 (2010) 3187.
- [187] Y. Wang, Z. Shi, J. Fang, H. Xu, X. Ma, J. Yin, J.Mater.Chem. 21 (2011) 505.
- [188] S. Ramesh, L.M. Ericson, V.A. Davis, R.K. Saini, C. Kittrell, M. Pasquali, W.E. Billups, W.W. Adams, R.H. Hauge, R.E. Smalley, Journal of Phys. Chem. B 108 (2004) 8794.
- [189] V.A. Davis, N.G. Parra-Vasquez, M.J. Green, P.K. Rai, N. Behabtu, V. Prieto, R.D. Booker, J. Schmidt, E. Kesselman, W. Zhou, H. Fan, W.W. Adams, R.H. Hauge, J.E. Fischer, Y. Cohen, Y. Talmon, R.E. Smalley, M. Pasquali, Nat Nano 4 (2009) 830.
- [190] N. Behabtu, J.R. Lomeda, M.J. Green, A.L. Higginbotham, A. Sinitskii, D.V. Kosynkin, D. Tsentelovich, A. Parra-Vasquez, J. Schmidt, E. Kesselman, Y. Cohen, Y. Talmon, J.M. Tour, M. Pasquali, Nat Nano 5 (2010) 406.
- [191] J. Chen, M.A. Hamon, H. Hu, Y. Chen, A.M. Rao, P.C. Eklund, R.C. Haddon, Science 282 (1998) 95.
- [192] W. Huang, S. Fernando, L.F. Allard, Y. Sun, Nano Lett. 3 (2003) 565.
- [193] K.A. Fernando, Y. Lin, Y.P. Sun, Langmuir 20 (2004) 4777.
- [194] D. Tasis, N. Tagmatarchis, A. Bianco, M. Prato, Chem. Rev. 106 (2006) 1105.
- [195] S. Niyogi, M. A. Hamon, H. Hu, B. Zhao, P. Bhowmik, R. Sen, M. E. Itkis, and R. C. Haddon\*, Acc. Chem. Res. 35 (2002) 1105.
- [196] Y. Lin, S. Taylor, H. Li, K.A.S. Fernando, L. Qu, W. Wang, L. Gu, B. Zhou, Y. Sun, J.Mater.Chem. 14 (2004) 527.